A Finite Element Analysis and Redesign of the Draftsill Casting on a Railroad Hopper Car

by

Douglas Kevin Roach

Thesis submitted to the Faculty of the
Virginia Polytechnic Institute and State University
in partial fulfillment of the requirements for the degree of
Master of Science
in
Mechanical Engineering

APPROVED:

Dr. Charles E. Knight, Chairman

Dr. Robert H. Fries

Dr. Reginald G. Mitchiner

January, 1987

Blacksburg, Virginia

A Finite Element Analysis and Redesign of the Draftsill Casting on a Railroad Hopper Car

by

Douglas Kevin Roach

Dr. Charles E. Knight, Chairman

Mechanical Engineering

(ABSTRACT)

This paper presents a static three-dimensional finite element analysis and redesign of a railroad hopper car draftsill. The purpose of the work was to modify the current draftsill structure to minimize its weight without compromising its current capabilities and foundry production specifications. The intuitive optimization procedure used both linear and parabolic isoparametric solid finite element models to check for solution convergence. In order to intuitively optimize the models, a composite plotting program was developed to display only the highest stresses at each node from all loading cases. This allowed for an overall visualization of low stressed regions for potential weight reduction.

An additional study investigated the possibility of tapering the front and rear draftlugs for a better stress distribution in the draftsill's structure under loading. It was determined that a tapered relief of 0.025 - 0.050 in.(0.0635 - 0.127 cm) from the center of the draftlug to its outer edge would more effectively distribute the stresses created, and also reduce the maximum stress levels generated by at least 20 percent. All loading and geometry specifications used in this research were based on data provided by the Norfolk Southern Corporation.

If both the redesign and tapered relief are adopted, then the final redesign will produce a draftsill that is approximately 106 lb(471.5 N) or 9.6 percent lighter than its original weight with maximum stresses reduced by 20 percent.

Acknowledgements

I would like to thank for his many hours of help and guidance throughout this year and a half. He has taught me more than just engineering principles, he has taught me things about myself and for that I will always be grateful. I would also like to thank the other members of my committee, , for their time and effort during my trip down this Masters path. A special thanks goes to my long time friends , and for always being supportive and encouraging. It must also be mentioned that my newly made friends , , , , and others helped to keep me going through the tough times and late nights. To them I say thanks. An additional thanks also goes to for initially providing me the opportunity to become involved in the area of finite elements and academic research.

I would like to sincerely thank my parents for the many years of faith they kept in me and their never-ending love and support, even when I seemed to be on the wrong track. To my sister I say thank you for always caring, even when I may have appeared to be caring only for myself. To my fiancee , I dedicate this work. Knowing that she has always been patient and encouraging, gave me the inspiration to finish this degree. I love you we make a great team.

Table of Contents

List of Illustrations

List of Tables

Chapter 1

Introduction

For many years mechanical designers have used an evolutionary and conservative method for design. If a part failed, it was usually redesigned by adding more material in the area of the failure. Recently, with the advent of analysis techniques such as finite elements, it has become possible to analyze complicated structures and redesign them to help prevent failure. This technique has also provided the capability of redesigning existing components to make them more optimum from a weight standpoint. Reducing the weight of any part on a railroad car can only be helpful, as a lower weight car can then carry more load and in turn be more economically productive.

The following paper will present an analysis and suggested redesign to reduce the weight of a railroad hopper car draftsill. The draftsill is a cast steel part weighing approximately 1,100 lbs(4890 N) and measuring approximately 6 feet(1.8 m) long and 13 in.(33 cm) square. It is a unit that is attached to each end of a hopper car via a long box shaped member called a centersill which runs the under length of the car (see Appendix A, Drawing 4). The purpose of the draftsill is to transmit, to the hopper car, all loads applied by the draftgear assembly. The draftgear consists of the coupler and follower blocks and fits into the draftsill in an area called the draft pocket. The draftsill and draftgear are shown in the blueprints and detailed drawings of Appendix A.

When initially investigating this problem the approach used was as follows. First the draftsill model was to be created using the S.D.R.C. software which had the capabilities to generate three-dimensional solid finite element meshes for analysis. Next, the model was to be analyzed and the resulting Von Mises stresses were to be used as a criteria for weight reduction. An iterative process was to be incorporated into the modeling procedure to generate a solution convergence. This convergence was to be accomplished by the use of mesh refinement in the model and the technique of increased element order. In addition to redesigning the draftsill for weight reduction, an investigation into the stress distributions created by the draftgear-draftlug interface was done. The resulting redesign produced was lighter in weight and more efficient in design.

Chapter 2 discusses the previously published material in the area of manual design optimization and solution convergence. Although there was no specific literature relating to draftsill weight reduction and design, there were references relating specifically to the manual optimization incorporated into this work since the three-dimensional mesh generator was of no use. Theory of the finite elements and solution method used is contained in Chapter 3. Chapter 4 gives an explanation of the assumptions and manual techniques used in creating the original draftsill model. Modeling restraints and loads, as specified, are discussed in Chapters 5, while Chapters 6 and 7 describe the redesign iterations and the changes made in each. Chapter 8 contains all of the results as well as recommendations and conclusions drawn from this author's study of a railroad hopper car draftsill.

Chapter 2

Literature Review

At present the Norfolk Southern railroad is trying to adopt the modern tools of today's design and analysis technology to an industry that is over a century old. This idea is one that, if successfully incorporated, could substantially influence the productivity and efficiency of today's railroads. As far as actual application of modern techniques, such as finite elements, is concerned, there is much need because little analysis could be attempted in the early history of the railroad industry (1). Structural requirements were based primarily on past practice. As cars grew in size and capacity, a greater strength of steel was required and "Rules of Thumb" were replaced by design specifications (1). It is obvious that the application of the finite element method to the railroads is rather new and therefore the majority of the analysis work done is original. This is the case with this particular project. No previously published material on draftsill weight reduction and redesign or for that matter draftsills at all was found.

Two major areas of the project were covered in this literature review and they are:

1. the manual construction of the finite element model and use of increased element interpolation order as a solution convergence technique, and

2. weight reduction and redesign based on intuitive engineering judgement utilizing output stress contours, composite plots and other generated data.

Construction of the draftsill finite element model was done by manual input since a capable three-dimensional mesh generator was unavailable. Since the conversion of the real structure to a finite element model is very important and has a very strong influence on the validity and usefulness of the final solution (2) specific care had to be taken in the convergence approach used. The complexity of the draftsill model dictated that overall mesh refinement would be difficult to incorporate on an iterative basis and therefore a method of mesh refinement that did not require the total reconstruction of the model was needed. As McNally, Lee and Dehner (1) indicate, a variable order element would allow the analyst to vary the order of the polynomial which approximates the element's displacement field. This would in effect, produce results similiar to remodeling with a finer mesh (1). It is because of this refinement approximation technique that the draftsill model was constructed using linear elements originally. Once the original model was analyzed, midside nodes were added to each element in the model to increase the element order and simulate the mesh refinement.

As mentioned in the abstract, the major emphasis of this work was weight reduction. Minimizing the weight of the draftsill was an important consideration in the redesign process because it would not only save material, but also increase the load carrying capability of the hopper car. In doing so, the possibility of using a three-dimensional shape optimizer would be of great use. Since one was not readily available this was done manually. But Imam (3) shows that the capability does exist. He indicates that there are two major constraints that must be satisfied for this type design tool to be effective, and they are:

1. Stress Constraints.....(The stress at any point in the component must be less than the allowable stress based on the material properties and some failure criterion.)

2. Displacement Constraints.....(The displacement at any point must be within the prescribed limits based on the design criteria.)

For this project there were no displacement constraints (deflection limitations) which indicates that this type of optimizer might have some application if further work is to be considered.

The next and most important area of review was that of solution convergence. To begin, the question "What criteria is legitimate for solution convergence with respect to this modeling situation?" was asked. The criteria choosen was that of elemental boundary stress equality and continuity. Sussman and Bathe (4) best describe this convergence criteria as follows:

> *The stresses are discontinuous across element boundaries and the magnitude of the "jumps" between element stresses is a practical measure of how far the predicted response is from the exact solution. Similiarly, the stress boundary conditions are not satisfied to sufficient accuracy when the mesh is too coarse. As the mesh is refined, the stress jumps between the elements and the error in satisfying the stress boundary conditions become smaller until a sufficiently accurate responce is reached.*
>
> *Therefore we note that convergence of the finite element solution to the exact solution of the mechanical idealization (the solution of the problem-governing differential equations that correspond to the finite element model) can in practice be measured using the stress jumps between element boundaries and the error in satisfying the stress boundary conditions. When both these stress discontinuties are small, the analyst can expect to have obtained an acceptable solution.*

The convergence of the solution is crucial and even more so is the use of the engineering judgement that accompanies such conclusions. About this Robinson (2) writes that the subject of structural modeling and interpretation of results is not written about enough and demands a book of its own. Since this is true, it is vital to remember that the finite element results are for the approximate model and these have to be interpreted correctly to obtain results which are used for designing the real structure. Therefore, in any approximate procedure, the results are only as good as the model and the way in which they are interpreted (2).

Chapter 3

Finite Element and Solution Theory

In any finite element work, the initial step in the overall process is the selection of the proper finite element and solver to be used. The selected element must give a realistic representation of the structure's degrees of freedom without compromising any of the attributes the actual structure may have. For this reason, all models created and studied in this project were constructed with three-dimensional isoparametric solid linear and parabolic elements. The finite element solver chosen must be capable of handling the selected finite element and model size. For this project SDRC's linear solver SUPERB met the specified criteria.

The rest of this chapter is dedicated to some theoretical explanation of the three-dimensional finite elements and solver as they were applied to this research project.

3.1 *Element Development*

Figure 1 and Figure 2 show respectively the linear and parabolic elements used in this work. As mentioned, the finite element selected for this research project was the three-dimensional isoparametric solid. This element has three displacement degrees of freedom (d.o.f) per node and is a theoretical expansion of its two-dimensional parent element. Note also that the nodal rotational degrees of freedom are not active for this type of element.

Cook (5) indicates that for an element to be isoparametric, it must meet the following two conditions:

1. Nodal degrees of freedom {d} dictate displacements {u v w} of a point in the element. Symbolically this can be shown as $\{u\ v\ w\} = [N_d]\{d\}$

2. Nodal coordinates {c} define global coordinates {x y z} of a point in the element. Symbolically this can be shown as $\{x\ y\ z\} = [N_c]\{c\}$

   where: $[N_d]$ and $[N_c]$ are the shape functions specified in the natural coordinates (ξ, η, ζ).

An element is said to be isoparametric if the nodal sets of both listed conditions are the same and if the matrices $[N_d]$ and $[N_c]$ are the same. In other words, a finite element is isoparametric if the element geometry and displacements are defined by interpolating nodal coordinates and nodal displacements with the same interpolation functions $[N]$ (6).

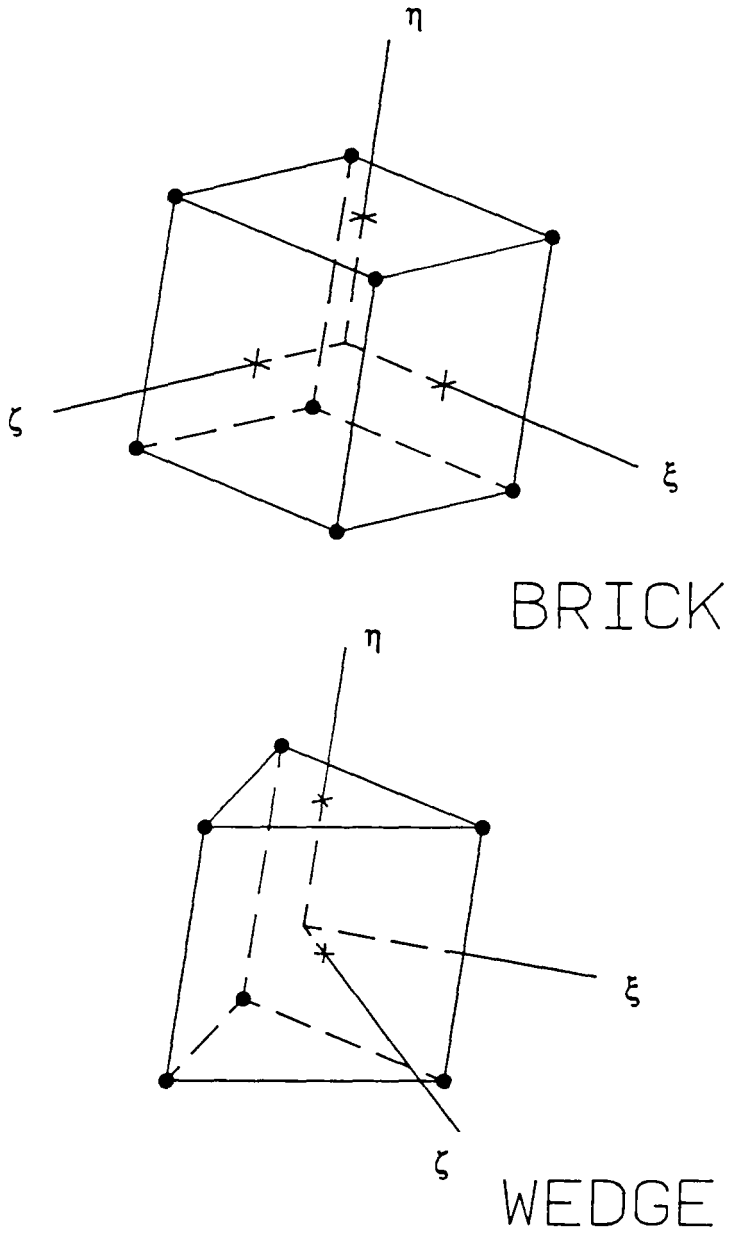

Figure 1. 3-D Isoparametric Linear Solid Finite Elements.

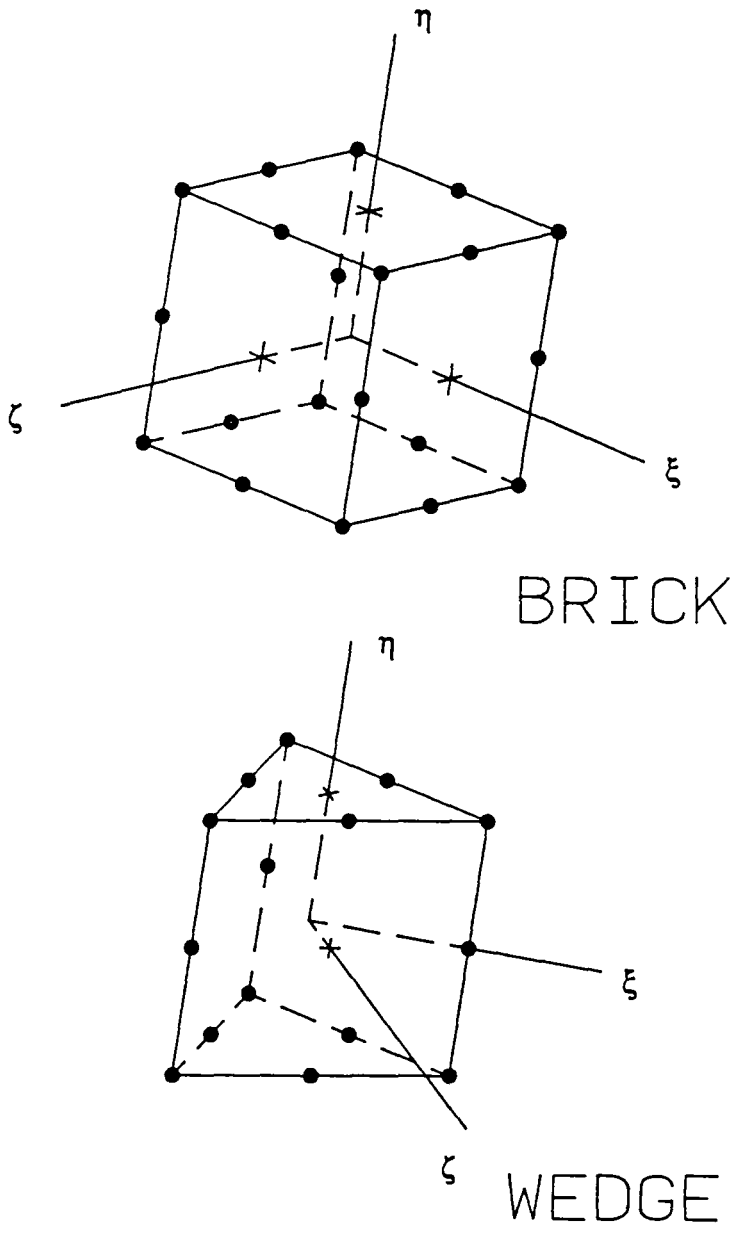

Figure 2. 3-D Isoparametric Parabolic Solid Finite Elements.

3.1.1 Eight-Noded Linear Solid Brick Element

In defining an isoparametric element, a natural or intrinsic coordinate system is applied to an element. This coordinate system is then mapped back to the actual X, Y, Z coordinate system through a transformation matrix called a Jacobian. These natural coordinates, as applied to an element, need not be orthogonal and are not usually parallel to the X, Y, Z coordinate system axes (5). The *only* criteria of the natural coordinates, is that their axes must pass through the midpoint of the planes defining each element side and that this plane-axis intersection be at ± 1 regardless of the element size in the global coordinate system. It is sometimes easier to think of the element as defined by the natural coordinates as a *unit element* having a ± 1 unit length along each axis. Figure 1 and Figure 2 show these natural coordinates as applied to the elements used in this work. The orientation of the natural coordinates with respect to the nodes on the element is dictated by the assigned node numbering of the element. There is no rule for this application it is usually code dependent.

In the development of an isoparametric element, one must first examine the criteria set in the previous section. Definition of the global coordinates and displacements for an 8-noded linear solid brick element are respectively:

$$\begin{bmatrix} x \\ y \\ z \end{bmatrix} = [N]\{c\} \qquad [3.1]$$

$$\begin{bmatrix} u \\ v \\ w \end{bmatrix} = [N]\{d\} \qquad [3.2]$$

where:

$\{d\} \equiv$ Displacements At Each Node.

$$\{d\} = \{u_1, v_1, w_1, u_2, v_2, w_2, \ldots, u_8, v_8, w_8\}$$

$$\{c\} \equiv \text{Coordinates At Each Node.}$$

$$\{c\} = \{x_1, y_1, z_1, x_2, y_2, z_2, \ldots, x_8, y_8, z_8\}$$

and

$$[N] \equiv \text{The Shape Function Matrix}$$

$$\equiv \begin{bmatrix} N_1, 0, 0, N_2, 0, 0, \ldots, N_8, 0, 0 \\ 0, N_1, 0, 0, N_2, 0, \ldots, 0, N_8, 0 \\ 0, 0, N_1, 0, 0, N_2, \ldots, 0, 0, N_8 \end{bmatrix} \quad [3.3]$$

For simplicity, the above equations 3.1 and 3.2 can be written as:

$$\begin{aligned} x &= \Sigma N_i x_i \\ y &= \Sigma N_i y_i \\ z &= \Sigma N_i z_i \end{aligned} \quad [3.4]$$

and

$$\begin{aligned} u &= \Sigma N_i u_i \\ v &= \Sigma N_i v_i \\ w &= \Sigma N_i w_i \end{aligned} \quad [3.5]$$

The shape functions used are Lagrange type and are functions based on the *unit element* and its natural coordinates (ξ, η, ζ). They are used to calculate the global coordinates and displacements of a point on an element when the natural coordinates of that point are inserted into the shape function matrix and equations respectively (5). Their displacement field origin comes from the polynomial order tetrahedron as shown by Zienkiewicz (7) in Figure 3 and are developed using a Rayliegh Ritz solution. The shape functions for a linear solid brick element (Figure 1) are:

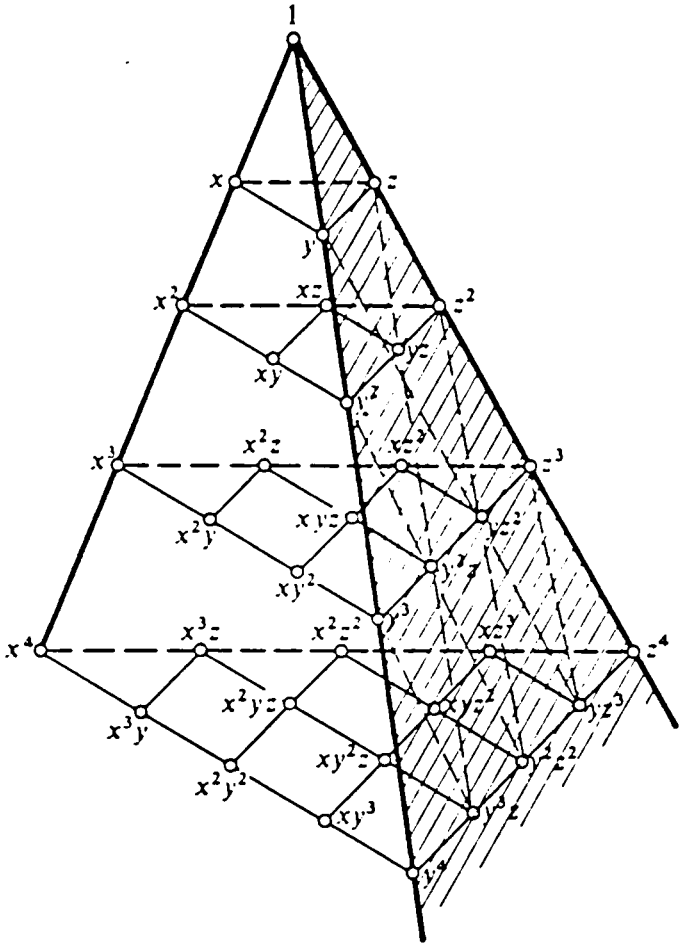

Figure 3. Polynomial Order Tetrahedron.

$$N_i = \frac{(1 + \xi\xi_i)(1 + \eta\eta_i)(1 + \zeta\zeta_i)}{8} \qquad [3.6]$$

where:

$$\xi_i, \eta_i, \zeta_i = \pm 1$$

for all nodes on the element

$$i = 1, 2, 3, 4, \ldots, 8$$

The next step in the development is to create an elemental stiffness matrix $[k]$. But as Cook (5) shows, this equation is a function of the strain-node displacement matrix $[B]$. For a typical solid element the general stiffness matrix as formulated from a minimum potential energy approach is:

$$[k] = \int_{vol}[B]^T[E][B]\,dv \qquad [3.7]$$

where:

$[E]$ = Modulus of Elasticity Matrix.

Since the stiffness matrix is a function of the unknown strain-node displacement matrix, it must be found first. To begin solving for the $[B]$ matrix, one must examine the definition of the strain within a three-dimensional solid element.

$\{\varepsilon\} \equiv$ Strain Matrix.

$$\{\varepsilon\} = \begin{bmatrix} \varepsilon_x \\ \varepsilon_y \\ \varepsilon_z \\ \tau_{xy} \\ \tau_{yz} \\ \tau_{xz} \end{bmatrix} = [H][G] \qquad [3.8]$$

where:

$$[H] = \begin{bmatrix} 1,0,0,0,0,0,0,0,0 \\ 0,0,0,0,1,0,0,0,0 \\ 0,0,0,0,0,0,0,0,1 \\ 0,1,0,1,0,0,0,0,0 \\ 0,0,0,0,0,1,0,1,0 \\ 0,0,1,0,0,0,1,0,0 \end{bmatrix} \qquad [3.8.1]$$

$$\{G\} = \begin{bmatrix} \frac{\partial u}{\partial x} \\ \frac{\partial u}{\partial y} \\ \frac{\partial u}{\partial z} \\ \frac{\partial v}{\partial x} \\ \frac{\partial v}{\partial y} \\ \frac{\partial v}{\partial z} \\ \frac{\partial w}{\partial x} \\ \frac{\partial w}{\partial y} \\ \frac{\partial w}{\partial z} \end{bmatrix} \qquad [3.8.2]$$

The strain-node displacement matrix $[B]$ will be derived from the original shape function matrix $[N]$ and once found will produce the elemental strains from the following relation.

$$\{\varepsilon\} = [B]\{d\} \qquad [3.9]$$

The $[B]$ matrix cannot be found in terms of X, Y, Z global coordinates because the shape function matrix $[N]$ on which it is based is a function of the natural coordinates (ξ, η, ζ). Therefore, a coordinate transformation must take place to allow a successful mapping of the *unit element* to the actual X, Y, Z global coordinates. It is for this reason that the Jacobian matrix is derived in terms of natural coordinates.

For simplicity, let φ be an arbitrary function of X, Y, Z, later to become a displacement u, v or w. Invoking the chain rule produces:

$$\frac{\partial \varphi}{\partial \xi} = \frac{\partial \varphi}{\partial x}\frac{\partial x}{\partial \xi} + \frac{\partial \varphi}{\partial y}\frac{\partial y}{\partial \xi} + \frac{\partial \varphi}{\partial z}\frac{\partial z}{\partial \xi}$$

$$\frac{\partial \varphi}{\partial \eta} = \frac{\partial \varphi}{\partial x}\frac{\partial x}{\partial \eta} + \frac{\partial \varphi}{\partial y}\frac{\partial y}{\partial \eta} + \frac{\partial \varphi}{\partial z}\frac{\partial z}{\partial \eta} \qquad [3.10]$$

$$\frac{\partial \varphi}{\partial \zeta} = \frac{\partial \varphi}{\partial x}\frac{\partial x}{\partial \zeta} + \frac{\partial \varphi}{\partial y}\frac{\partial y}{\partial \zeta} + \frac{\partial \varphi}{\partial z}\frac{\partial z}{\partial \zeta}$$

in matrix form the above equations are as follows

$$\begin{bmatrix} \frac{\partial \varphi}{\partial \xi} \\ \frac{\partial \varphi}{\partial \eta} \\ \frac{\partial \varphi}{\partial \zeta} \end{bmatrix} = [J] \begin{bmatrix} \frac{\partial \varphi}{\partial x} \\ \frac{\partial \varphi}{\partial y} \\ \frac{\partial \varphi}{\partial z} \end{bmatrix} \qquad [3.11]$$

where the Jacobian $[J]$ is defined as

$$[J] \equiv \begin{bmatrix} \frac{\partial x}{\partial \xi} & \frac{\partial y}{\partial \xi} & \frac{\partial z}{\partial \xi} \\ \frac{\partial x}{\partial \eta} & \frac{\partial y}{\partial \eta} & \frac{\partial z}{\partial \eta} \\ \frac{\partial x}{\partial \zeta} & \frac{\partial y}{\partial \zeta} & \frac{\partial z}{\partial \zeta} \end{bmatrix} \qquad [3.12]$$

inverting equation 3.11 produces

$$\begin{bmatrix} \frac{\partial \varphi}{\partial x} \\ \frac{\partial \varphi}{\partial y} \\ \frac{\partial \varphi}{\partial z} \end{bmatrix} = [\Gamma] \begin{bmatrix} \frac{\partial \varphi}{\partial \xi} \\ \frac{\partial \varphi}{\partial \eta} \\ \frac{\partial \varphi}{\partial \zeta} \end{bmatrix} \qquad [3.13]$$

where:

$$[\Gamma] = [J]^{-1} \qquad [3.13.1]$$

$$\begin{bmatrix} \frac{\partial \varphi}{\partial \xi} \\ \frac{\partial \varphi}{\partial \eta} \\ \frac{\partial \varphi}{\partial \zeta} \end{bmatrix} = [DN]\{d\} \qquad [3.13.2]$$

and using a different form than $[N]$

$[DN]$ = The Derivative Matrix of the Shape Functions

$$\equiv \begin{bmatrix} N_{1,\xi}, 0, 0, N_{2,\xi}, 0, 0, \ldots, N_{8,\xi}, 0, 0 \\ N_{1,\eta}, 0, 0, N_{2,\eta}, 0, 0, \ldots, N_{8,\eta}, 0, 0 \\ N_{1,\zeta}, 0, 0, N_{2,\zeta}, 0, 0, \ldots, N_{8,\zeta}, 0, 0 \\ 0, N_{1,\xi}, 0, 0, N_{2,\xi}, 0, \ldots, 0, N_{8,\xi}, 0 \\ 0, N_{1,\eta}, 0, 0, N_{2,\eta}, 0, \ldots, 0, N_{8,\eta}, 0 \\ 0, N_{1,\zeta}, 0, 0, N_{2,\zeta}, 0, \ldots, 0, N_{8,\zeta}, 0 \\ 0, 0, N_{1,\xi}, 0, 0, N_{2,\xi}, \ldots, 0, 0, N_{8,\xi} \\ 0, 0, N_{1,\eta}, 0, 0, N_{2,\eta}, \ldots, 0, 0, N_{8,\eta} \\ 0, 0, N_{1,\zeta}, 0, 0, N_{2,\zeta}, \ldots, 0, 0, N_{8,\zeta} \end{bmatrix} \qquad [3.13.3]$$

where $N_{1,\xi}$ denotes differentation of N_1 with respect to ξ, etc. It must be noted that for $X = \xi$, $Y = \eta$, and $Z = \zeta$ that $[J] = [\Gamma] = [I]$ where $[I]$ is the identity or unit matrix.

The strain-node displacement matrix $[B]$ can now be found. Starting with equation 3.8 and substituting equation 3.13 into equation 3.8.2

$$\{\varepsilon\} = [H]\{G\}$$

$$= [H][\Gamma]\begin{bmatrix} \frac{\partial \varphi}{\partial \xi} \\ \frac{\partial \varphi}{\partial \eta} \\ \frac{\partial \varphi}{\partial \zeta} \end{bmatrix}$$

now, substituting equation 3.13.2 produces

$$\{\varepsilon\} = [H][\Gamma][DN]\{d\} \qquad [3.14]$$

which simplified to the form of equation 3.9 shows

$$[B] = [H][\Gamma][DN] \qquad [3.15]$$

Having found the strain-node displacement matrix and all of its components, the elemental stiffness matrix for the isoparametric solid element can be found using equation 3.7. This equation, however, must be integrated over the natural coordinates since the $[B]$ matrix is in that form. When applying equation 3.7, it should be noted that the Jacobian determinate $|J|$ expresses the ratio of the volume element dx dy dz to $d\xi\, d\eta\, d\zeta$ and is in general a function of the natural coordinates. A more exact expression for the elemental stiffness is now shown as:

$$[k] = \int_{-1}^{1}\int_{-1}^{1}\int_{-1}^{1} [B]^T [E] [B] J \, d\xi d\eta d\zeta \qquad [3.16]$$

which defines the volumetric integration of an element with respect to its natural coordinates.

Looking at equation 3.16, one realizes that it is too complicated to be solved by hand and therefore requires a numerical integration technique. A common technique used in the finite element field is Gauss Quadrature. Because this method is integrated over a -1 to + 1 field it is very compatible to the isoparametric elements used in this work. The following equation describes mathematically the evaluation process of the Gauss Quadrature method as applied to a three-dimensional element (5):

$$I = \int_{-1}^{1}\int_{-1}^{1}\int_{-1}^{1} \varphi(\xi, \eta, \zeta)\, d\xi d\eta d\zeta \cong \sum_{i}\sum_{j}\sum_{k} W_i W_j W_k\, \varphi(\xi_i, \eta_j, \zeta_k) \qquad [3.16.1]$$

where W_i, W_j, W_k are weighting functions who's value is dependent on the number of sampling points (Gauss Points) used.

The derivation of the isoparametric linear solid brick finite element is now complete. The above equations are for one element and must now be assembled into a global matrix system with the rest of the model's elements for a global solution (6). This solution, which is discussed in detail in section 3.2, is based on the following global equation.

$$[K]\{D\} = \{F\} \qquad [3.17]$$

For stress calculations, a manipulation of Hooke's Law is done to the previously calculated strain-node displacement matrix $[B]$ and nodal degrees of freedom {d}. The stress in an element $\{\sigma\}$ can be calculated from the following general equation:

$$\{\sigma\} = [E](\{B\}\{d\} - \{\varepsilon_0\}) + \{\sigma_0\} \qquad [3.18]$$

where:

$\{\varepsilon_0\} \equiv$ The Initial Strain Matrix

$\{\sigma_0\} \equiv$ The Initial Stress Matrix

The stress is usually calculated at points in the element as specified by the Gauss Quadrature. The stress values as shown at nodes are actually an interpolation from these Gauss point values within the element.

The remaining sections will discuss the derivations of the other three elements used in this author's research, but are based on the work done above with only minor changes in the individual shape function formulations.

3.1.2 Twenty-Noded Parabolic Solid Brick Element

In finite element modeling the use of parabolic brick elements is rather common. These higher order elements generate a more accurate solution than their linear counterpart due to the parabolic displacement representation. Increasing the order of linear elements to parabolic is a common solution convergence tool.

Once the initial linear element derivation is complete, it becomes a somewhat straight forward process to increase the order of an element, that is, provided the element is to remain the same shape, i.e., rectangular. In this case, the order is to be increased from linear to parabolic which will increase the number of nodes per element from 8 to 20 as shown in Figure 1 on page 8 and Figure 2 on page 9. The major reason for creating this increase in element order is that the displacement fields on which the shape functions are based (Figure 3 on page 12) will now be of a higher order, thus, allowing a better mathematical representation throughout the element. Another reason is that a 20-noded element has approximately the same accuracy as an 8-noded element that has been refined into 8 elements (8) (see Figure 4). This increases a model's accuracy without actually subdividing the true model. These new shape functions, as applied to the parabolic brick, are shown by Newton (9) to be:

$$N_i = \frac{(1 + \xi\xi_i)(1 + \eta\eta_i)(1 + \zeta\zeta_i)(\xi\xi_i + \eta\eta_i + \zeta\zeta_i - 2)}{8} \qquad [3.19]$$

for the corner nodes i = 1, 3, 5, 7, 13, 15, 17, 19 and

$$N_i = \frac{(1 + \xi\xi_i)(1 + \eta\eta_i)(1 + \zeta\zeta_i)(1 - \xi^2\eta_i^2\zeta_i^2 - \eta^2\xi_i^2\zeta_i^2 - \zeta^2\xi_i^2\eta_i^2)}{4} \qquad [3.20]$$

for the midside nodes i = 2, 4, 6, 8, ...18, 20.

Having developed these new and more accurate elemental-shape functions the only difference in the elemental derivation is that there are more shape functions and more degrees of freedom per

PARABOLIC BRICK

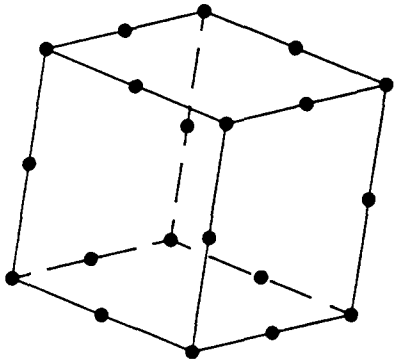

APPROXIMATELY EQUAL TO
EIGHT LINEAR
ELEMENTS IN THE
SAME GEOMETRIC SPACE

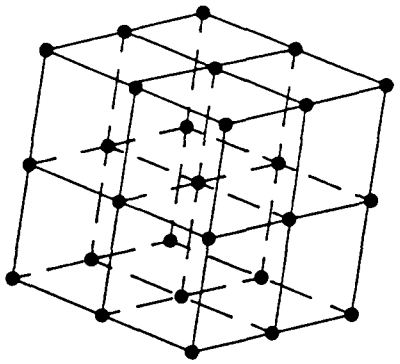

EIGHT
LINEAR BRICKS

Figure 4. Approximate Equivalence Between Linear And Parabolic Elements.

element (60 d.o.f. instead of 24 d.o.f.). Otherwise, the element formulation as discussed in the previous section will proceed in exactly the same manner.

3.1.3 Six-Noded Linear Solid Wedge

When constructing all models, linear solid elements were used. From time to time a solid wedge was used intermittantly with the solid brick. This was done because the geometry dictated places where it was not feasible to use a solid brick. In doing this, effort was made to minimize use of these wedge elements due to the fact that their origin is not of a pure triangular nature. The wedge is created by the degeneration of the linear solid brick discussed previously and shown in Figure 1 on page 8. The shape functions of the wedge are created specifically by collapsing the corner nodes of one side. This is shown in Figure 5. The collapsed nodes then take on the following shape definition.

- The shape functions of the two nodes to be collapsed are summed to form the new shape function for the collapsed node.

The shape functions for the degenerated linear wedge are:

$$N_i = \frac{(1 + \xi\xi_i)(1 + \eta\eta_i)(1 + \zeta\zeta_i)}{8} \qquad [3.21]$$

for uncollapsed nodes on the wedge i= 1, 2, 4, 5 and

$$\begin{aligned} N_6 collapsed &= N_7 + N_8 \\ N_3 collapsed &= N_3 + N_4 \end{aligned} \qquad [3.22]$$

For the new collapsed nodes N_7, N_8, N_3, N_4 are found from equation 3.21.

The stiffness matrix [k] and element development are exactly the same as that of the eight-noded linear brick, except each of the collapsed nodes now are defined by the new shape functions

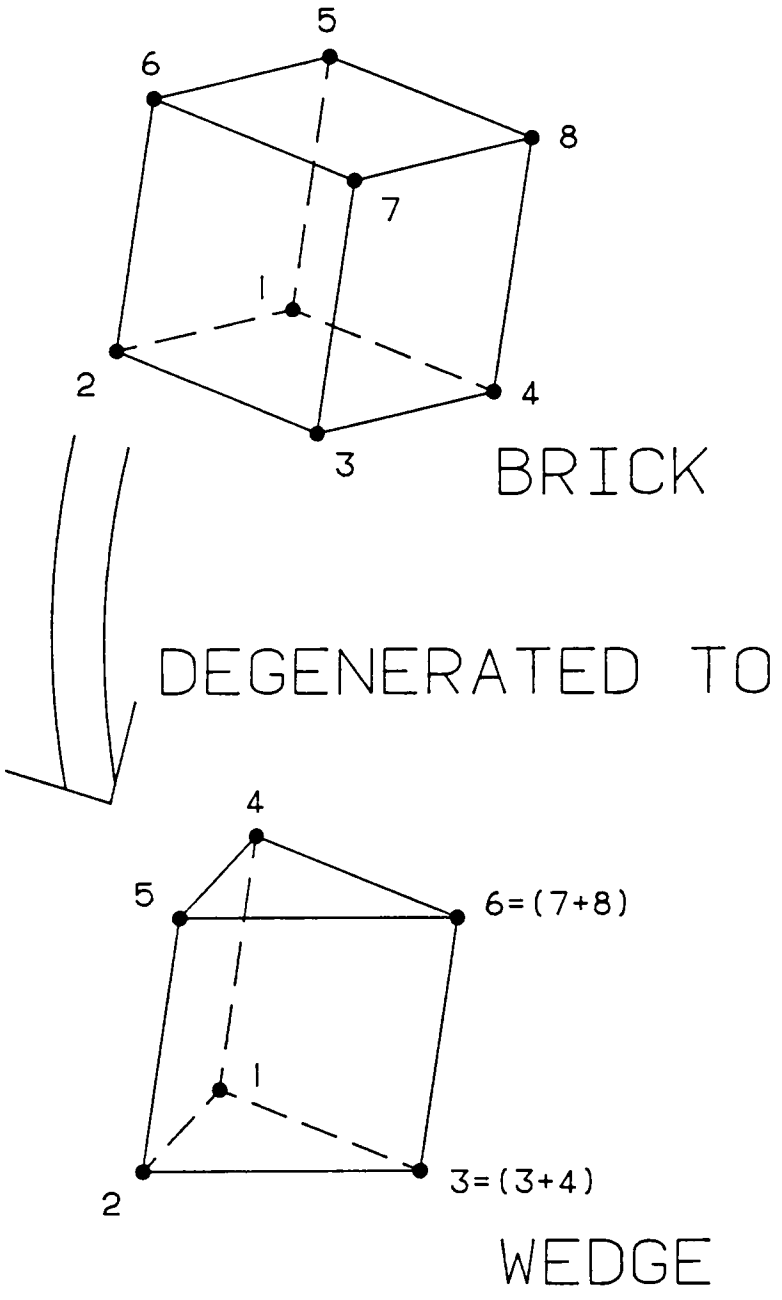

Figure 5. Degeneration of Linear Brick to Linear Wedge Element.

created in equation 3.22. There is no mathematical difference in their development, but the collapsed wedge does tend to be stiffer than a wedge derived from a triangle. This is due to the fact that when the nodes are collapsed their respective shape functions are summed. The use of this element is acceptable in a model and will not distort the results if used sparingly. Using a large number of these elements together can make the model stiffer than it actually is, therefore, distorting the results.

3.1.4 Fifteen-Noded Parabolic Solid Wedge

The construction of a degenerated parabolic element is done in almost the same way as the degeneration of a linear brick element. The only difference in procedure is that there are now midside nodes on the element that must be considered. Figure 6 shows the degeneration of a parabolic brick to a parabolic wedge. As before, the nodes on the collapsed edges sum, but in addition, there are now certain nodes on the wedge's base that take on an additional adjustment factor. Using Figure 6 Newton (9) shows the new shape functions to be:

$$
\begin{aligned}
N_3 collapsed &= N_3 + N_4 + N_5 \\
N_8 collapsed &= N_{10} + N_{11} \\
N_{12} collapsed &= N_{15} + N_{16} + N_{17} \\
N_5 collapsed &= N_7 + \Delta N_7 \\
N_1 collapsed &= N_1 + \Delta N_7 \\
N_6 collapsed &= N_8 - 2\Delta N_7 \\
N_{14} collapsed &= N_{19} + \Delta N_{19} \\
N_{10} collapsed &= N_{13} + \Delta N_{19} \\
N_{15} collapsed &= N_{20} - 2\Delta N_{19}
\end{aligned}
\qquad [3.23]
$$

where:

$$
\Delta N_7 = \frac{(1 - \xi^2)(1 - \eta^2)(1 - \zeta)}{16}
$$

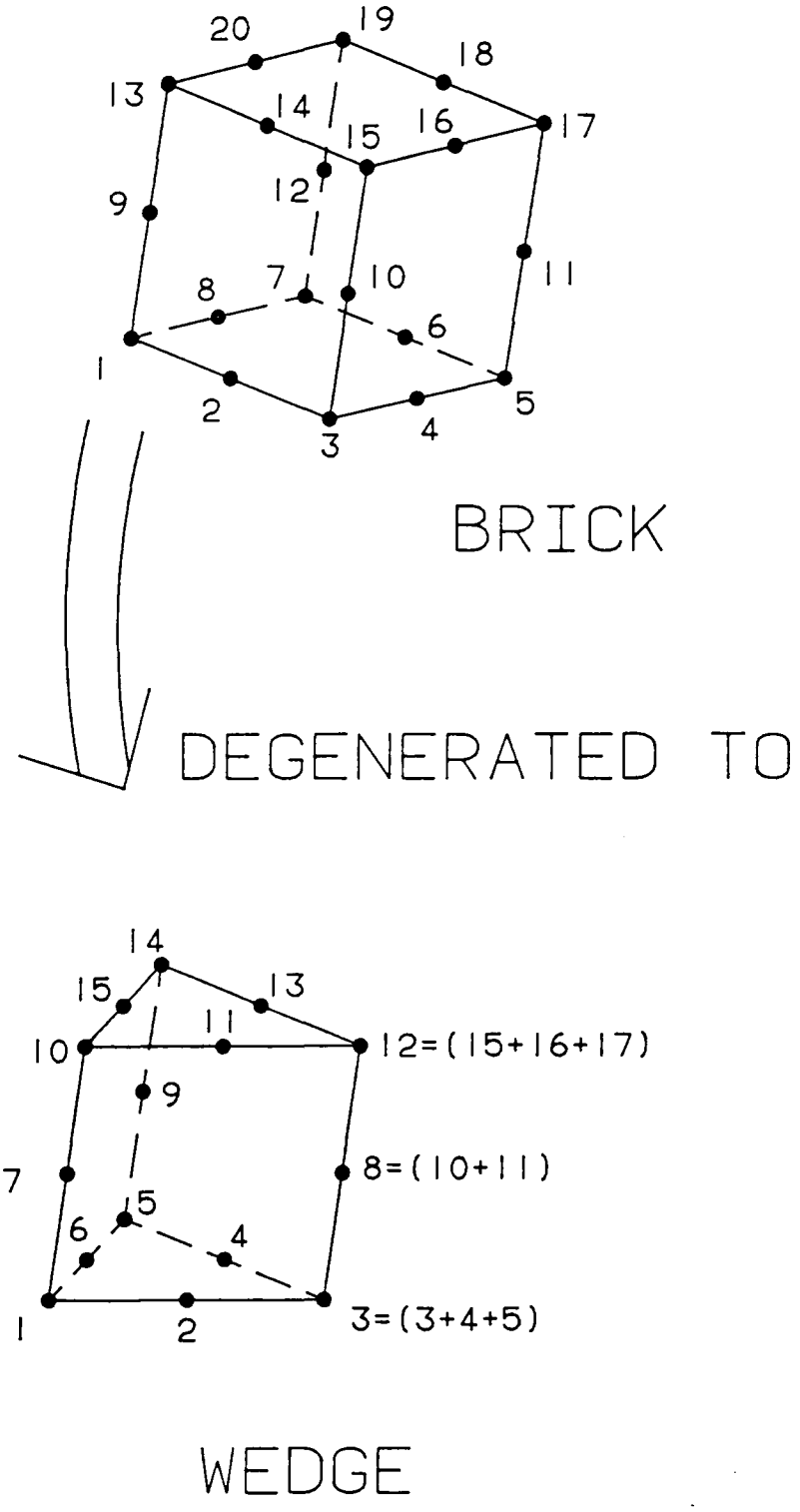

Figure 6. Degeneration of Parabolic Brick to Parabolic Wedge Element.

and

$$\Delta N_{19} = \frac{(1 - \xi^2)(1 - \eta^2)(1 + \zeta)}{16}$$

The collapsed subscript indicates nodes modified by the degeneration of the wedge. All nodes on the wedge that are not described by equation 3.23 are described by equations 3.19 and 3.20. The derivation of this element and its elemental matrices proceed just as before with only the added changes of more nodes and more degrees of freedom per element. As it was mentioned for the linear wedge, this element should also be used sparingly since it is not of pure triangular origin.

3.2 *Solution Theory*

The solution code used in this work was the linear solver SUPERB which uses a stiffness solution method. In a static model the equations created from the individual elements are solved globally for the unknown nodal displacements. The matrix form of the solution is expressed as before:

$$[K]\{D\} = \{F\} \qquad [3.24]$$

where:

$[K] \equiv$ Global Stiffness Matrix

$\{D\} \equiv$ Unknown Nodal Displacements

$\{F\} \equiv$ Externally Applied Nodal Forces

Note that the global stiffness matrix $[K]$ is created by superimposing all of the elemental stiffness matrices created in the previous sections of this chapter.

This solution method solves directly for the unknown nodal variables, which are displacements for structural analysis (6). All other solution values are then based on the calculated values for the nodal displacements.

A characteristic of the finite element method is that the fundamental unknowns (displacements) are more accurate than any of the entities derived from them. The reason for this is that most values derived from the displacements are found through the derivatives of the shape functions (6). Examples of this are the calculated stress values which were shown previously to be a function of the strain-node displacement matrix $[B]$ which is based on the derivatives of $[N]$.

When actually solving the simultaneous equations of 3.24, SUPERB uses a wavefront solution technique. By definition, the wavefront is equal to the number of equations active at any point in the solution procedure and is directly proportional to the number of active nodes at that point (6). An equation is considered active when it is pulled into the solution process and is not totally solved. That is, it still has unknown coefficients. A vital part to this solution process, is that the system of equations is taken into the solution process according to the elemental numbering scheme. An equation will remain active in the wavefront until each element associated with that equation is encountered and processed (6). In other words, the equation is not reduced out of the system until all other elements having contact with that particular element are included in the processing. It is this element numbering dependence that justifies an optimization of the numbering scheme of a model's elements before processing it in a wavefront solver.

Chapter 4

Building of Draftsill Model

The finite element model to be used was constructed using three-dimensional isoparametric solid finite elements. This type of element allowed for the most realistic representation of the draftsill possible. Although a good representation of any given structure can be made using finite elements, there were many assumptions that were made before the draftsill could be translated into this kind of computer model.

4.1 Modeling Assumptions

When creating the finite element model from the real draftsill, it was necessary to simplify certain structural characteristics. These simplifications allowed the computer model to represent the draftsill without compromising its true reaction to loading. The following is a listing of the simplifications made to create the original finite element model of the draftsill.

- Half symmetry was used since the draftsill was geometrically symmetrical with symmetric loads about its vertical centerplane along its length.

- All filets of small radius were excluded.

- All top holes were left solid.

- Side wall pads in the draft pocket were excluded.

- The 2 1/8 in.(5.4 cm) centersill weld flange connection was left out.

- The centerplate was modeled as a solid dish protruding 1 1/4 in.(3.2 cm) down from the bottom of the draftsill.

- The rear walls behind the rear lugs were not tapered inward the small degree specified in the blueprint.

- Holes in the side flange were excluded.

- The striker face end of the draftsill was modeled by an equivalent C-shaped section that had the same approximate moment of inertia as that of the real draftsill striker.

- Holes in the perpendicular rear wall were left solid.

- The thin center vertical rib connecting the centerplate and the centerpost was omitted.

- The rear centerpost was modeled as a solid post.

- The weld area between the centersill and draftsill was assumed to be a rigid connection.

- The centerplate was originally assumed to always be in contact with the truck unit.

These assumptions listed may be many, but they seem reasonable for an adequate model and are a vital part of the finite element modeling technique. Many of the items listed could have been included in the finite element model, but this would have defeated part of the purpose of the technique. This purpose being to model and analyze a particular structure in a reasonable amount of real time without compromising the solution accuracy of the model. Including all of these items in the finite element model would have increased both the complexity and creation time of the model without gaining much refined accuracy in the results.

4.2 Building Technique

Once the modeling assumptions were identified, a technique for the actual construction of the finite element model had to be decided on. It was originally thought that the model could be constructed using the ENHANCED MESH GENERATOR provided in the SDRC I-DEAS 2.5 software, but because of the complexity of the draftsill this generator in three dimensions proved useless. It was later found that this particular version of the mesh generator was not capable of handling the particular type of solid finite element this project was to use.

The alternative method was to build the finite element model by manual definition. This process was slow, but did have the advantage of allowing good control for element size and shape creation. The steps used to create the draftsill models were as follows:

1. Sketch the desired finite element model on paper to see that it meets the desired size and shape needed.

2. Identify from the draftsill blueprint the appropriate global coordinates for positions of the nodes on the model.

3. Input nodal coordinates to software.

4. Use the software to copy and translate nodes, thus creating all additional nodes needed in the model.

5. Manually use the cursor to connect appropriate nodes and construct either linear solid bricks or linear solid triangular wedges.

The completed original finite element model is shown in Figure 7, Figure 8 and Figure 9. It was composed of 628 nodes and 302 linear solid finite elements.

Once a linear finite element model had been created, a parabolic model was created by automatic addition of midside nodes to each existing linear element. This allowed all original linear elements to now function as parabolic elements with more accurately represented properties as discussed in Chapter 3. The element division in the model remained unchanged with this new increase in element order, but the number of nodes increased from 628 to 2170. The completed parabolic finite element model is in appearance the same as its linear counterpart (Figure 7 , Figure 8 and Figure 9) with the exception of the additional midside nodes that are applied to the elements. It should be noted that because of the increase in the number of nodes, the visual presentation of the model showing its nodes would be very cluttered.

4.3 Model Checking

On completion of the construction of the finite element models it could not be assumed that they were correct. It was, therefore, necessary to use the tools that could check a model for errors. The use of such tools and their feedback have allowed a feeling of confidence in the original models created. There were five major model checks done.

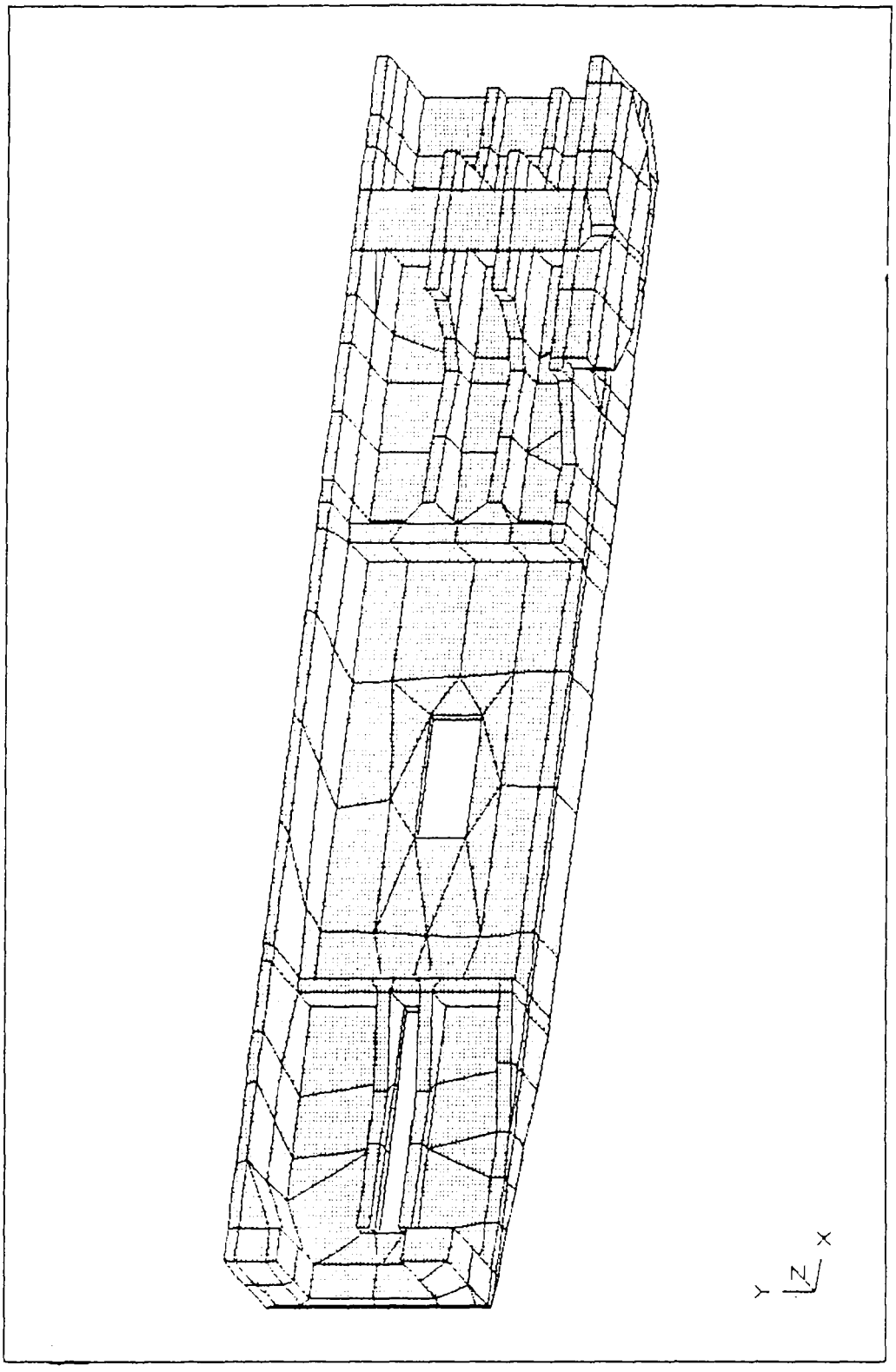

Figure 7. Original Finite Element Model (Linear)(side view).

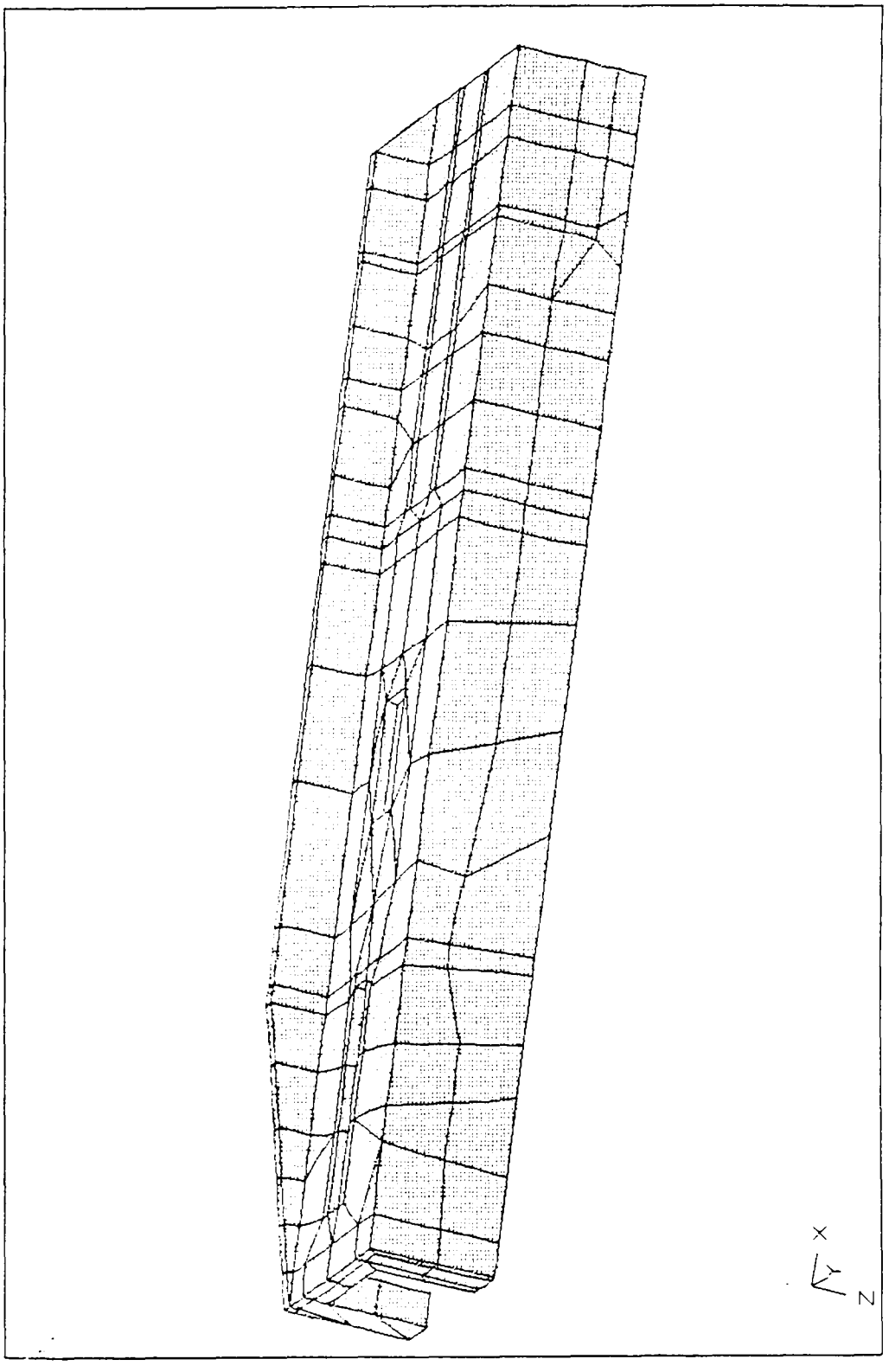

Figure 8. Original Finite Element Model (Linear)(top view).

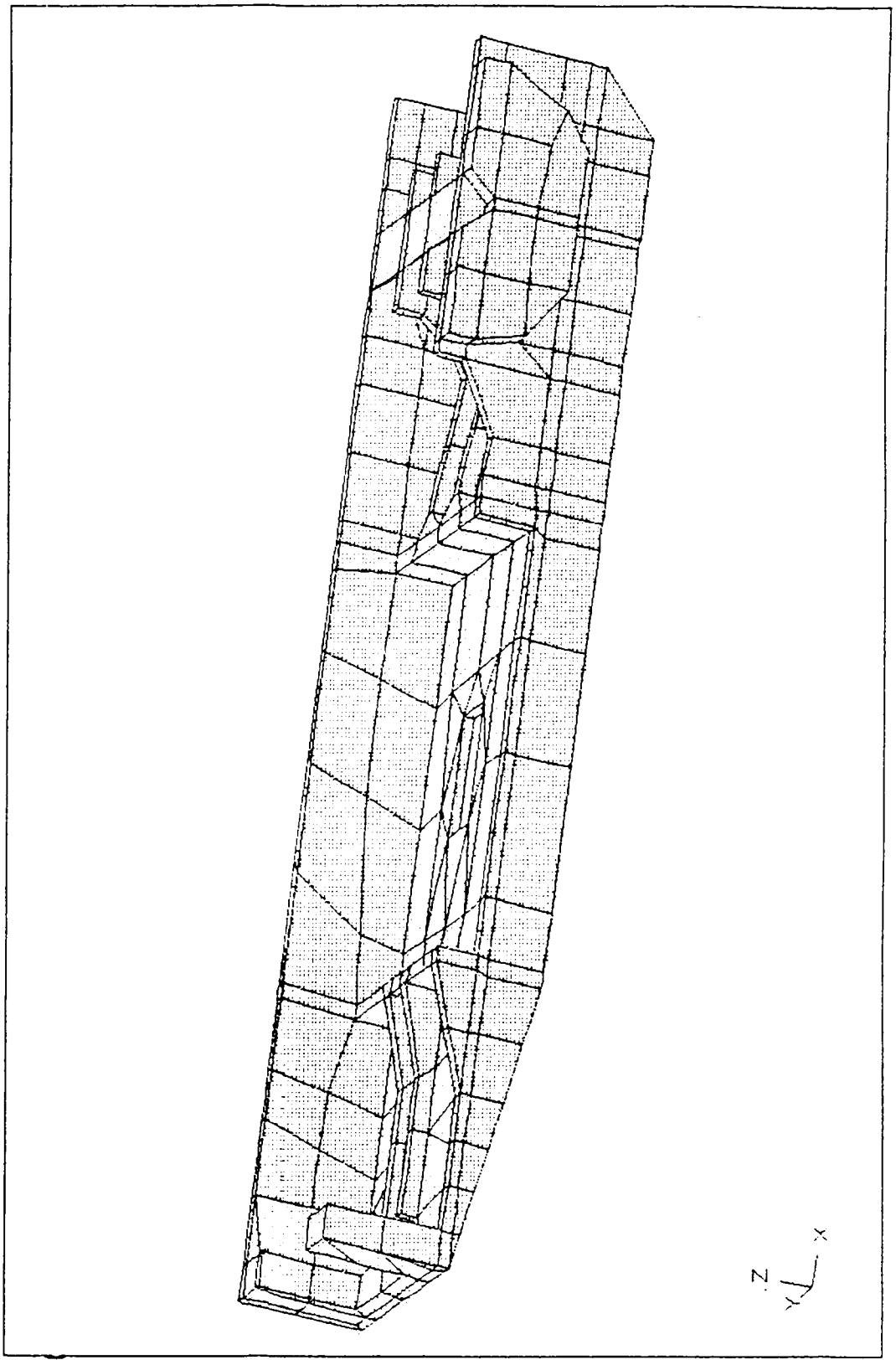

Figure 9. Original Finite Element Model (Linear)(bottom view).

Free Edge: This model check calculated and sketched all edges of any elements in the model that were not connected to another element. It was used to show whether all edge boundaries of the model were correct. This check is shown in Figures 10 and 11.

Distortion: In finite element modeling it is important that the obtained solution is an accurate, numerically-converged solution. Each finite element plays a role in the convergence of that solution. This is why element distortion is important and is always deserving of attention. Elements in a finite element model should follow these listed guidelines for best results:

- Change size from one element to the next by using a smooth transition, not sudden size changes from small to large and vise versa.

- They should not exceed a 4 to 1 geometric aspect ratio. That is, an element should not be greater in any direction than 4 times the length of any other direction on the element.

- Elements should be kept as close to square for solid bricks and equilateral for triangular wedges wherever possible.

Not following the above-mentioned guidelines can cause numerical error and inaccurate convergence of the finite element solution. Without a check for distortion, a solution will be given but confidence in that solution cannot be justified.

Mathematically, the distortion of an element was checked using the following criteria (6).

$$\text{DP} \equiv \text{Distortion Parameter}$$

$$\text{DP} = 8\left[\frac{\min|J|}{\text{VOL}}\right] \qquad [4.1]$$

where:

$$\min|J| \equiv \text{Smallest Determinant In Element Domina}$$

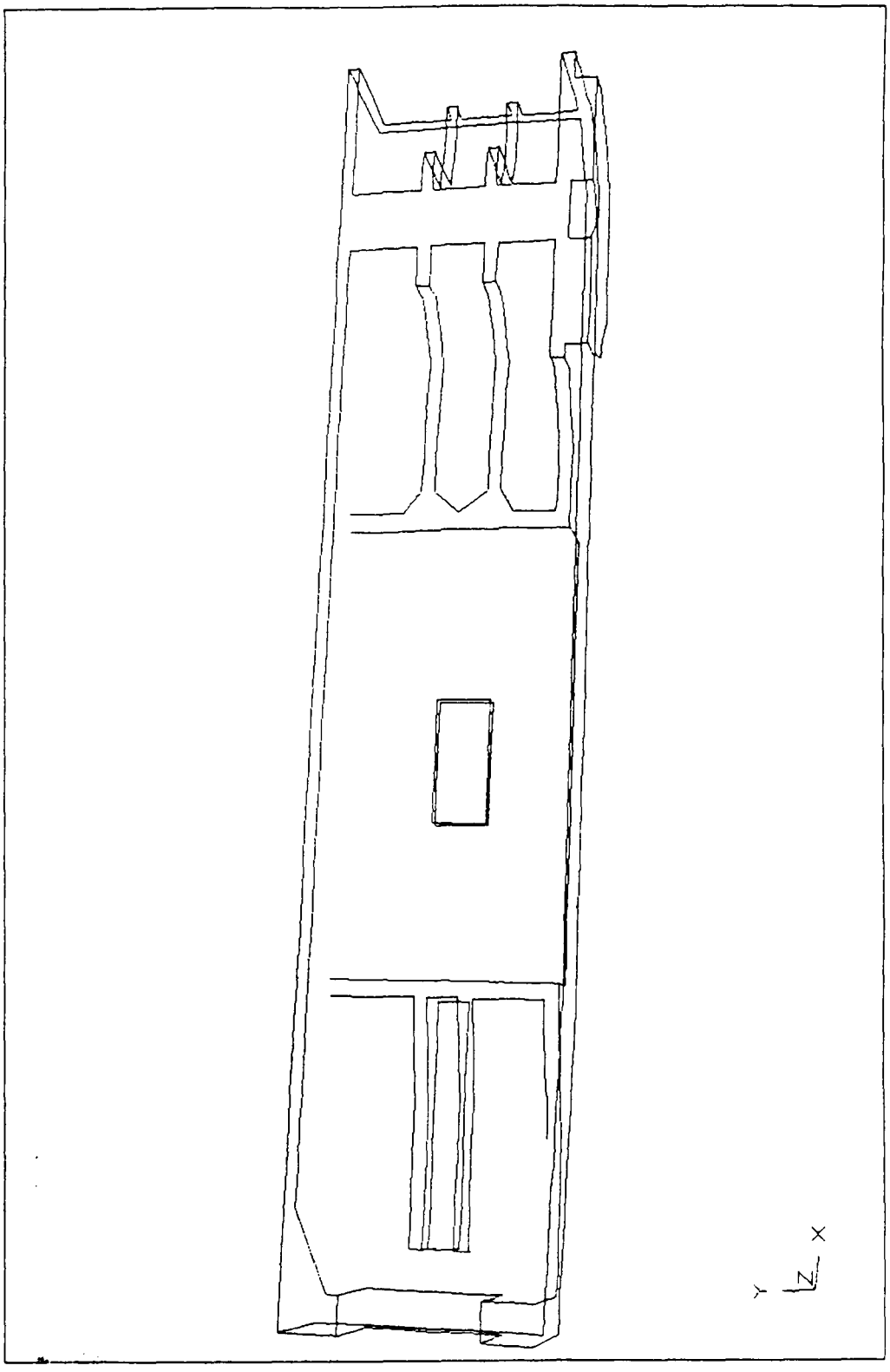

Figure 10. Free Edge Check of Finite Element Model (side view).

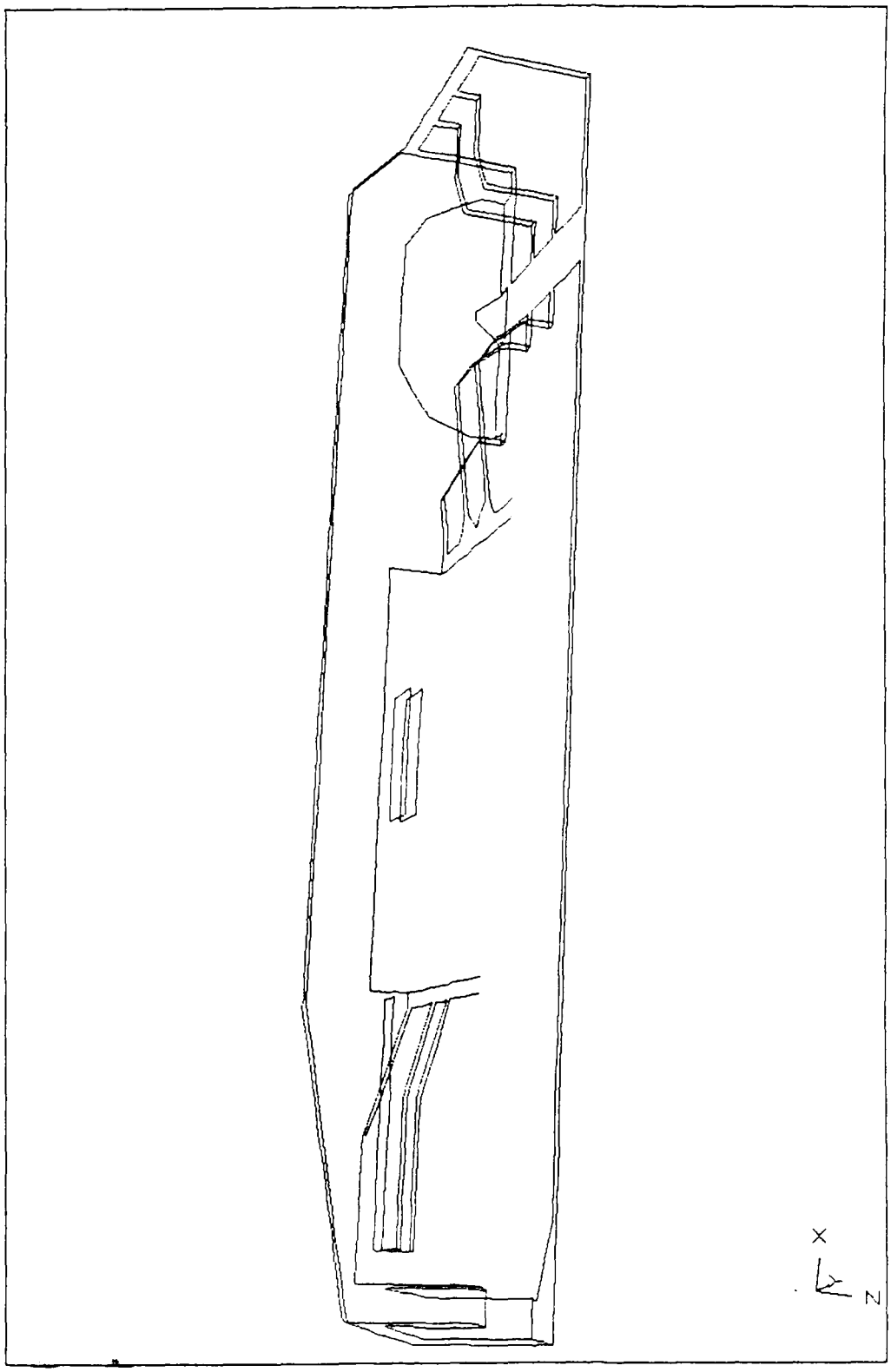

Figure 11. Free Edge Check of Finite Element Model (top view).

and

$$VOL = \int_{-1}^{1}\int_{-1}^{1}\int_{-1}^{1} |J| \, d\xi d\eta d\zeta$$

The lowest determinant value approaches zero as the element distortion increases becoming equal to zero at points of extreme distortion. The distortion parameter ranges from 0 to 1 and if found to be less than 0.2, experience shows that the element will yield poor results (6). SUPERB rejects any models with elements having a distortion parameter less than 0.2.

Weight: Another technique used to check the finite element model to see if it accurately represented the actual draftsill, was to compare the calculated weight of the computer model with that of the real draftsill. Applying an acceleration load to the model produced a weight of 464 lbs(2060 N) for the symmetrical draftsill. This means that the actual weight of the computer model was 928 lbs(4130 N). The real weight of the draftsill, as specified by Norfolk Southern, was approximately 1100 lbs(4890 N). This indicated a difference of 172 lbs(756 N) which partially could be accounted for in the modeling assumptions mentioned in the previous section. Accounting for some of these assumptions put approximately 60 to 70 lbs(267 to 311 N) on the model, thus bringing its weight up to approximately 1000 lbs(4450 N). Being this close to the approximated weight figure given generated a confidence in the model as it was initially constructed.

Wavefront: In this check the preprocessing of the model was done in such a manner that all nodes and elements were numbered in a wave form. This helped to reduce the solution wavefront and increase the solution accuracy by decreasing the number of active simultaneous equations being solved. Equations remain active in the wavefront until each element associated with that equation has been processed. After processing, equations are then reduced out of the system. In other words, the wavefront describes the size of the solution process at any given time (6), so decreasing the wavefront reduces the chance of numerical error.

Element Shrink: The purpose of this check was to determine if any voids were created during the construction of the model. When all of the finite elements were displayed it was very difficult to determine if there was any material that was actually unaccounted for by an element. For this reason the element shrink check was used. It presented a graphic image of all the finite elements that had been created where each element had been slightly decreased (shrunk) in size therefore exposing any areas that did not have an element in them.

This check was especially helpful when modifying the centerplate because of the detail and poor visibility of the elements. An example of this check as applied to the rear of the first redesigned model is shown in Figure 12.

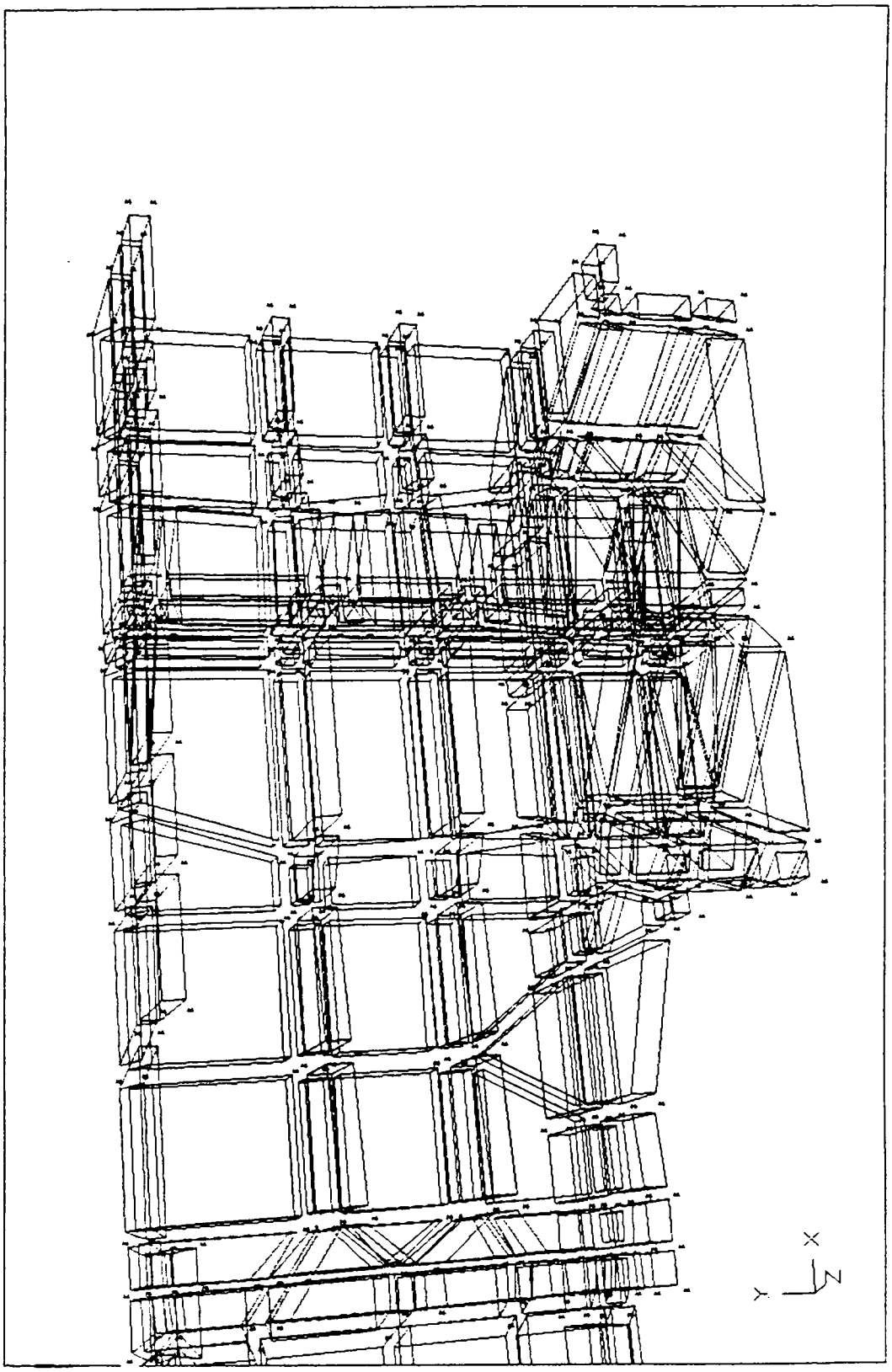

Figure 12. Element Shrink Check As Applied To The Draftsill Model.

Chapter 5

Modeling Restraints and Applied Loads

Once the finite element model was created, it was necessary to identify the proper modeling restraints that would give the model a realistic representation of its true environment. This was a step of crucial importance. An error in applying restraints can cause a model to act in a manner that is unrepresentative of its real environment, therefore, distorting all results and invalidating the finite element study.

Restraints are applied to nodes and are used to restrict any of the possible degrees of freedom for that node. The degrees of freedom for the particular kind of finite element used in this study were X, Y and Z displacements as previously discussed. Restraining any of these degrees of freedom would result in a zero displacement for the restrained direction of the node selected.

5.1 *Description of Restraints*

For this study, three major restraint planes were needed to represent the original draftsill model as it existed in its true environment. The first was that the model was symmetrical about the X-Y plane and therefore had to be restrained from any motion through that plane in the Z-direction. The second was the connection to be maintained at the centersill. Since this connection was a weld, and assumed rigid, all nodes on this Y-Z plane were restrained from any X, Y or Z motion. The third major plane of restraint was in the X-Z plane along the Y-direction where the centerplate met the truck unit. This surface for the original model was assumed to always remain in a situation of constant contact, thus justifing this restraint condition.

It should be mentioned that these same restraint conditions were applied to all of the parabolic models where each of the new midside nodes that corresponded to any of these restraint conditions were likewise restrained. In theory it appears easy, but when the parabolic model has 2170 nodes it is not very efficient to try and select each node to be restrained from the screen. For this reason a RESTRAINT CREATION program (see Appendix B) was developed to search the model's nodal coordinate data for those nodes that have global coordinates on the planes of restraint. The program was used on all of the parabolic models and later applied to the linear models to be used as a restraint checking device. For the original parabolic model there were approximately 450 nodes identified to be on the restraint planes.

5.2 *Description of Applied Loads*

In this project the load cases to be applied to the draftsill model were specified by Norfolk Southern Corporation. There were five prescribed load cases. These load cases were:

1. Draft Load -- Representing the load generated when the hopper car is being pulled by another car.

2. Compressive End Load -- Representing a load generated by another car pushing against the hopper car.

3. Vertical Load -- Representing the structural weight of the hopper car as it is applied to the draftsill through the bolster beam.

4. Carbody Lift -- Representing the lifting of a car using the coupler as the point of lift.

5. Downward Vertical Load -- Representing the load created if the draftgear does not meet the connecting car coupler correctly and is forced downward.

These five load cases as applied to the draftsill are represented more clearly in Figure 13. This figure presents a general overview as to how each load case was applied to the draftsill.

The load magnitudes specified in this report are for the symmetrical finite element model and therefore are 1/2 the true magnitude that would be applied to the whole draftsill model. Also, all loadings were applied as pressures to the element faces. Applying loads as pressures allowed the analysis program to calculate and properly load each node on the element face with the appropriate nodal force value that was to be inserted into the force matrix used in the solution method discussed in Chapter 3. This type of load application was done for both the linear and parabolic finite element models created. The following is a detailed explanation of each applied load case and its specified application criteria.

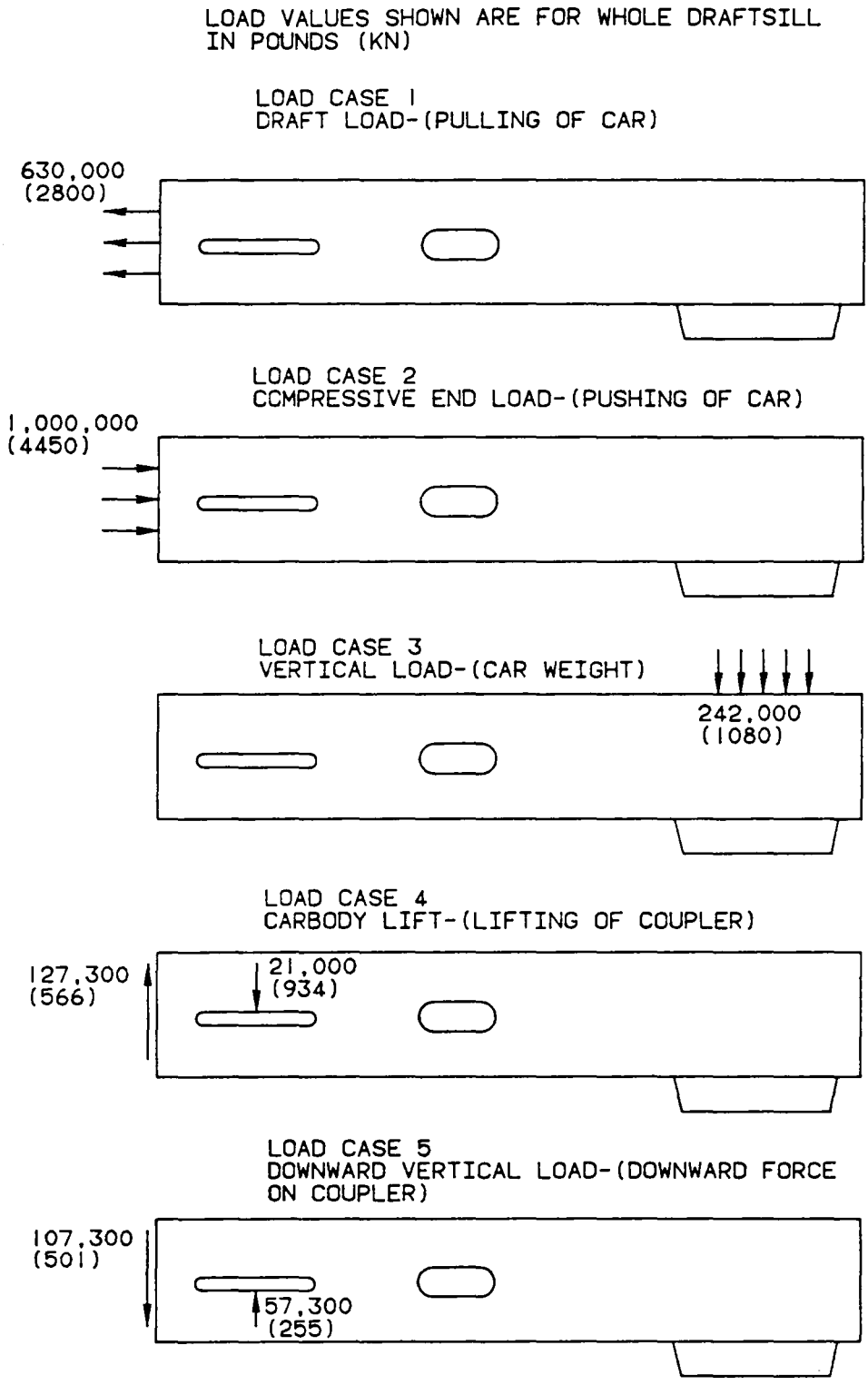

Figure 13. Overview of Loading to Draftsill.

5.2.1 Draft Load

This load case simulated the pulling or tensile load created by another car and was specified as follows:

- Apply 315,000 lbs(1400 kN) to the front draftlugs. (630,000 lbs(2800 kN) total)
- Restrain the draftsill at the centersill weld attachment.
- Apply the load to the draftlug according to the draftgear follower block contact area. (see Appendix A, Drawing 3)

When this load case was applied, it was decided that a uniform pressure of 11,030 psi(76 MPa) be applied from the top to the bottom of the draftlug. This load case is shown in Figure 14 which presents a visualization of the pressures and their application to the front draftlug. The pressures are represented by arrows that are shown normal to the face of the element to which they are applied. A more refined study of the pressure distributions, applications and recommedations is shown in Chapter 8.

5.2.2 Compressive End Load

This load case was representative of another car pushing or compressively "bumping" the hopper car. The load case was specified as follows:

- Apply 500,000 lbs(2220 kN) to the rear draftlugs of the draftsill. (1,000,000 lbs(4450 kN) total)
- Restrain the draftsill at the centersill weld attachment.

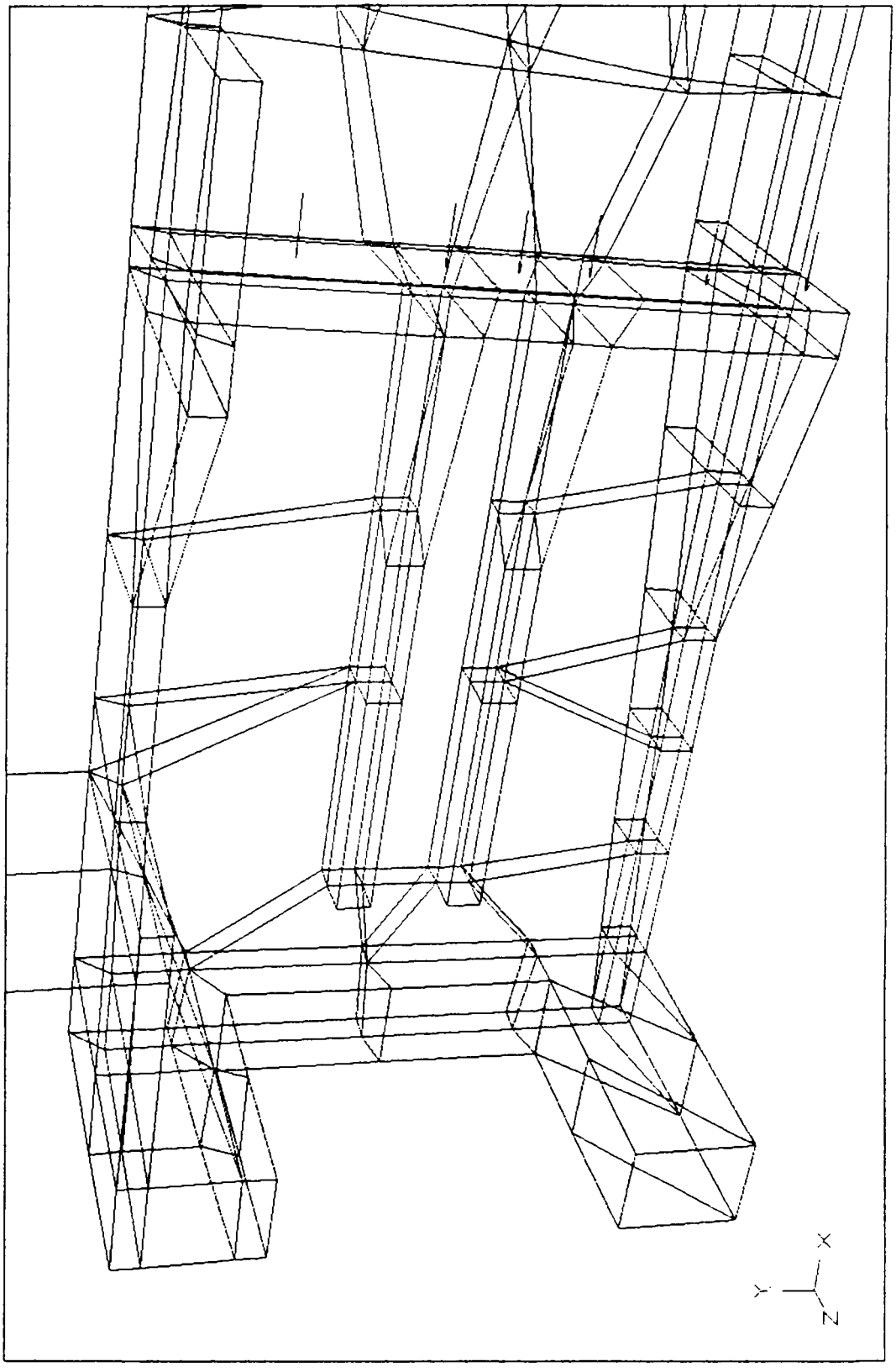

Figure 14. Draft Load as Applied to Model.

- Apply the load to the rear draftlug according to the draftgear follower block contact area. (see Appendix A, Drawing 3)

This load case was applied as a pressure of 16,630 psi(115 MPa) over the appropriate contact area specified by the draftgear follower. The application of this load case is shown in Figure 15. Here the pressure, represented by the arrows, has been confined to the actual area of application unlike load case 1.

5.2.3 Vertical Load

This load case was the most difficult to apply to the model. Only after redesign iterations did it become apparent as to the proper way to represent this load. The specified load was:

- 121,000 lbs(538 kN) were to be applied to the top of the draftsill. The load was to be located above the centerplate and distributed over the body bolster beam contact area. (242,000 lbs(1080 kN) total)

The load was applied as a pressure of 1,947 psi(13 MPa) to the top surface of the draftsill. Although this was an incorrect application of the load, it provided an approximate magnitude of the stress levels in the original model. For the final model created, this load case was applied simultaneously with each load case 1, 2, 4, 5. It was applied by adding elements to the top of the draftsill which represented the bolster beam and the cover plate. The applied load is shown in Figure 16.

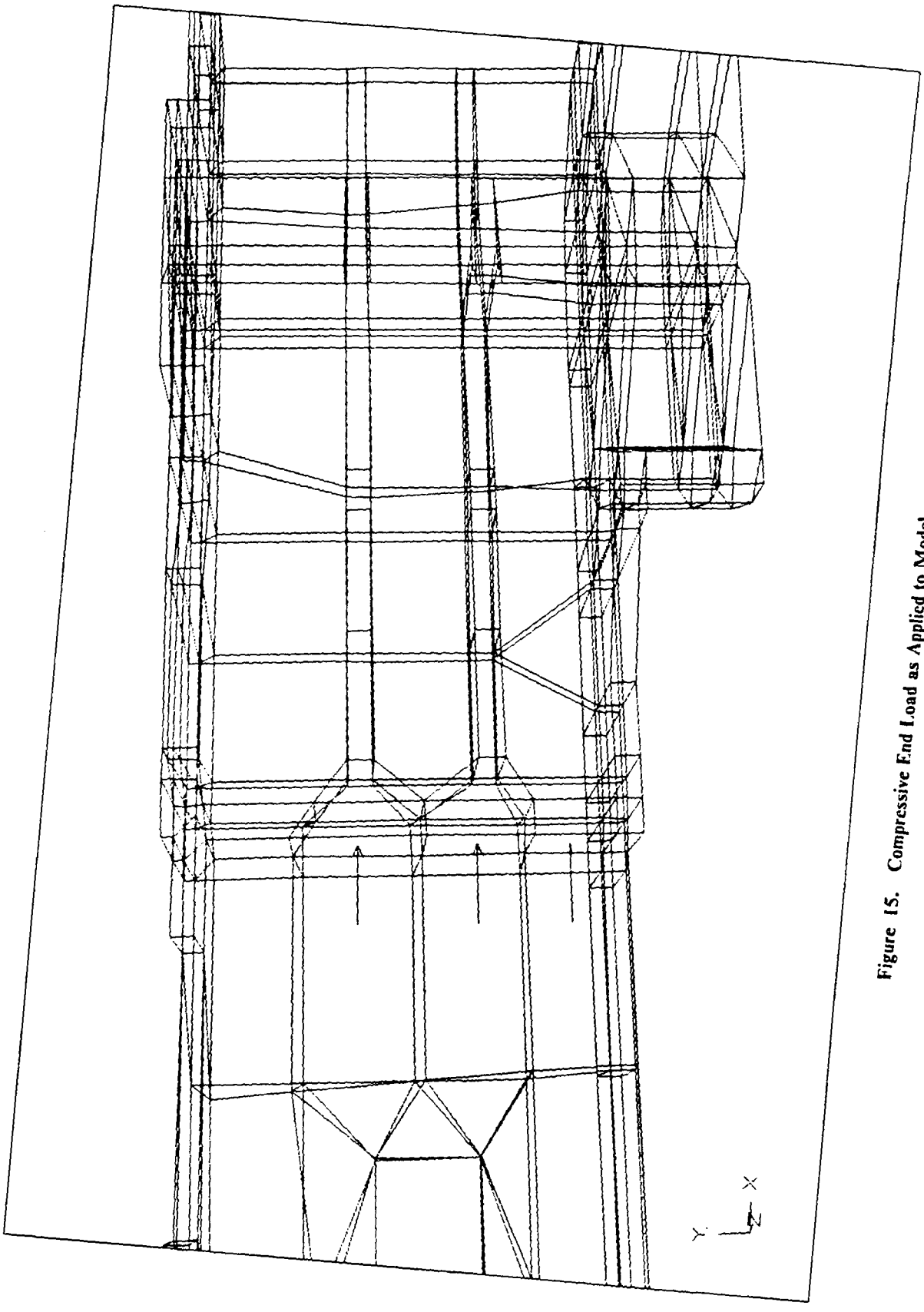

Figure 15. Compressive End Load as Applied to Model.

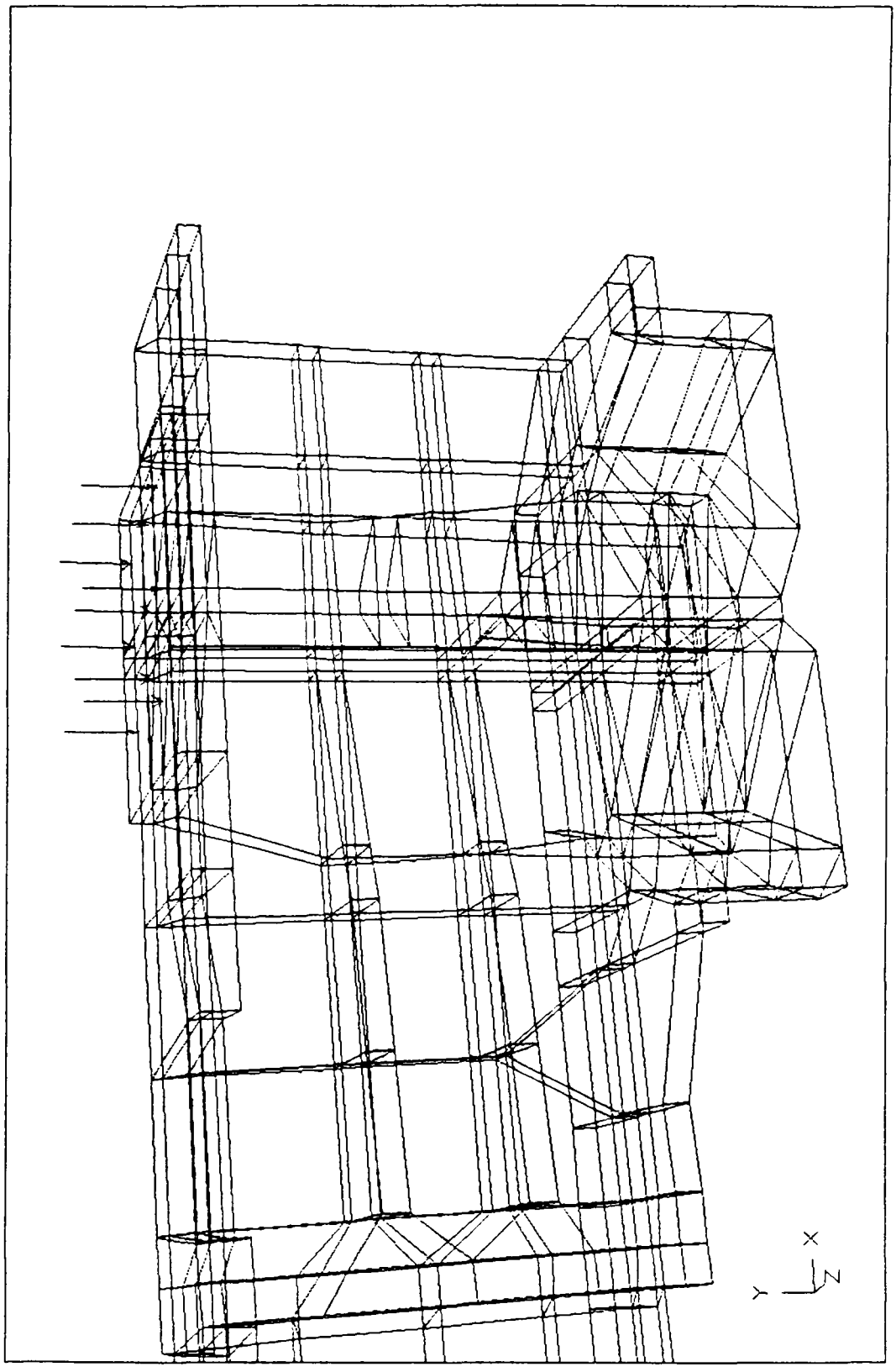

Figure 16. Vertical Load as Applied to Model.

5.2.4 Carbody Lift

This load case was representative of a lifting force applied to the striker face of the car. The load case was specified as follows:

- Apply 63,650 lbs(283 kN) vertically upward on the striker face. Distribute the load over a 3 in.(7.6 cm) width and 1 in.(2.5 cm) depth from the plane of symmetry. (127,300 lbs(566 kN) total)

- Simultaneously apply 10,500 lbs(467 kN) downward on the keyslot. Distribute the load from a point 13 3/4 in.(34 cm) back from the striker to a point 7 3/4 in.(20 cm) back from the striker. (21,000 lbs(934 kN) total)

- Restrain the draftsill at the centerplate.

- Restrain the draftsill at the weld attachment to the centersill.

The load was applied as a pressure of 10,610 psi(73 MPa) upward on the striker and a pressure of 664 psi(5 MPa) downward on the keyslot. This load case application is shown in Figure 17.

5.2.5 Downward Vertical Load

This load case simulated a large downward force on the coupler. The specified load was as follows:

- Apply 56,350 lbs(250 kN) downward to the top surface of the coupler carrier. Distribute the load over a width of 3 in.(7.6 cm). (107,300 lbs(501 kN) total)

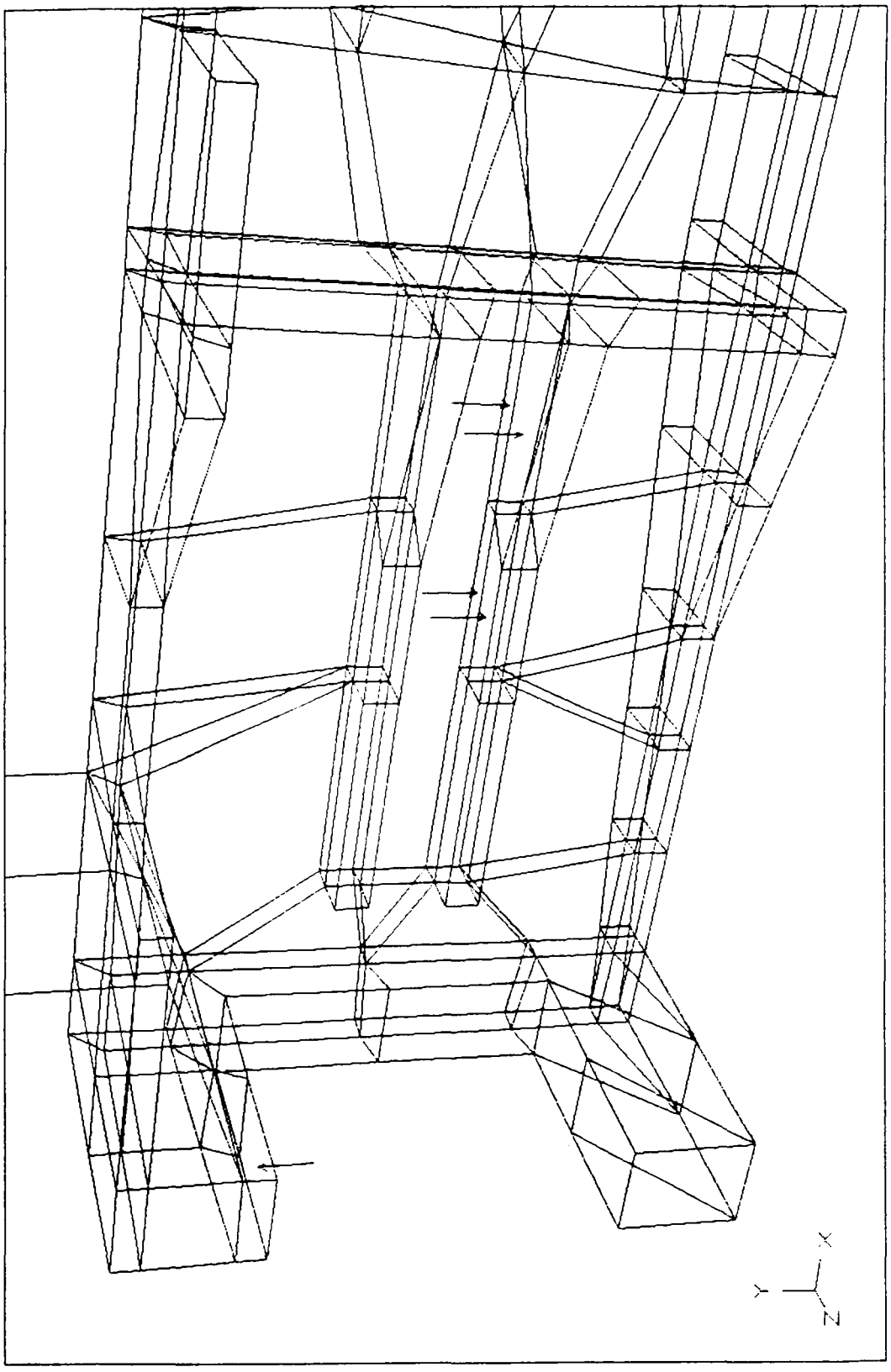

Figure 17. Carbody Lift as Applied to Model.

- Simultaneously apply 28,650 lbs(127 kN) upward to the keyslot from a point 13 3/4 in.(34 cm) back of the striker to a point 7 3/4 in.(20 cm) back from the striker. (57,300 lbs(255 kN) total)

- Restrain the draftsill at the centerplate.

- Restrain the draftsill at the weld attachment to the centersill.

The load was applied as a pressure of 8,942 psi(61 MPa) downward on the coupler carrier and a pressure of 1,811 psi(12 MPa) applied upward on the keyslot. This load case, as applied, is shown in Figure 18.

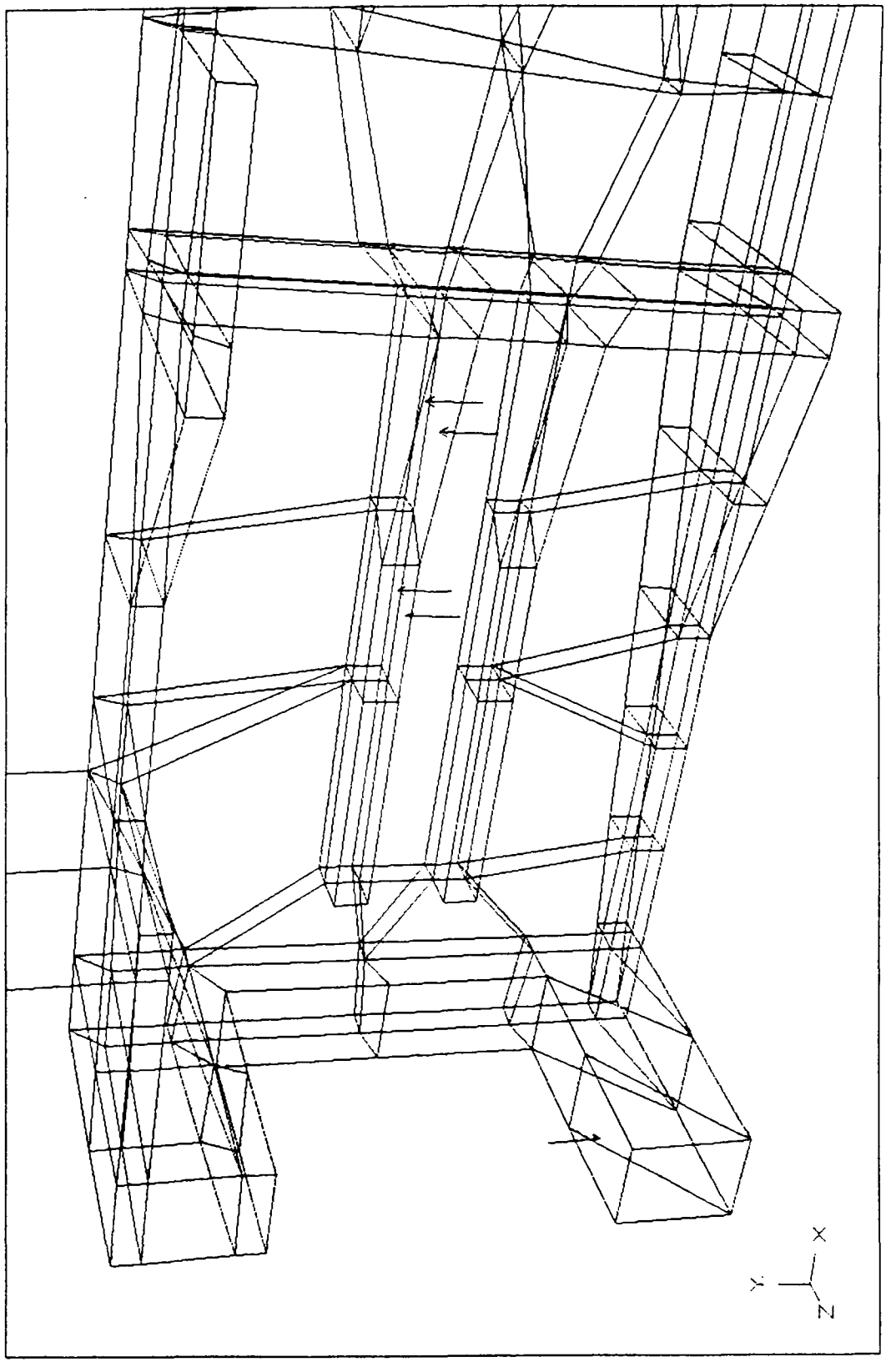

Figure 18. Downward Vertical Load as Applied to Model.

Chapter 6

First Analysis Iteration

Once the original draftsill model was completed, loaded, constrained, and analyzed, the first iteration step in the convergence of a solution was taken. This step was to make changes in the original finite element model that would make it more representative of the actual environment in which it exists, while simultaneously making redesign improvements. Any design changes to be made were in areas where the solution values showed no critical concern. That is, the stress levels were low enough to warrant any redesigns done to a particular area of the draftsill casting. The rest of this chapter will discuss the redesign improvements made to the original finite element model and will specifically list the changes made to increase the models realism with respect to its environment. At this point it should be noted that all modeling results will be discussed, in full, in Chapter 8 after all models and their modifications have been presented.

6.1 Changes Made to the Original Model

The original model of the draftsill was a good starting point for analysis, but certain characteristics of the draftsill's actual environment on the hopper car were shown to play more of a role than was originally modeled. The following is a listing of the changes that were made to make the original finite element model more realistic.

- Three linear spring finite elements were applied to the top of the draftsill to represent the load absorption capabilities of the angle iron cross member (not bolster beam) that rests on top of the draftsill just above the keyslot. The stiffness of these elements was calculated from a total hopper car model and found to be 939 lbs/in.(1640 N/cm).

- The centerplate dish which was originally modeled as a 1 1/4 in.(3.2 cm) solid on the bottom of the draftsill was remodeled. This remodeling included the 45 degree ribs inside of the dish and also its true height down from the bottom of the draftsill. The new depth of the centerplate was 3 5/16 in.(8.4 cm) as specified on the blueprints. (see Appendix A)

- The holes in the top of the draftsill were included, but were also enlarged since the stresses initially appeared to be low in those areas. Only the front hole was not made larger than was specified.

These changes mentioned allowed the model to more accurately represent the draftsill as it exists on the hopper car.

Other additional changes were also incorporated into this first iteration step, except they were done with the intention of redesigning the draftsill. These changes were:

- As mentioned, the top holes were included and opened up larger than they actually were. They were made approximately 3.5 times larger than previously specified. This was done to help

reduce the weight of the draftsill. The remaining center piece of metal between the two holes on the top of the draft pocket was left there due to foundry specifications.

- Another modification made was the deletion of some of the rear ribs. The ribs deleted were those ribs that were perpendicular to the vertical wall which contained the rear centerpost. There were ribs on both sides of the centerpost and, therefore, all were deleted.

All of the modifications made, be they for the purpose of increasing the realism of the model or redesigning it, can be seen in Figure 19, Figure 20 and Figure 21. These figures show the side, top and bottom views of this first iterative model. It can be compared to the original model shown in Figure 7 on page 31, Figure 8 on page 32 and Figure 9 on page 33 to see the changes made more vividly.

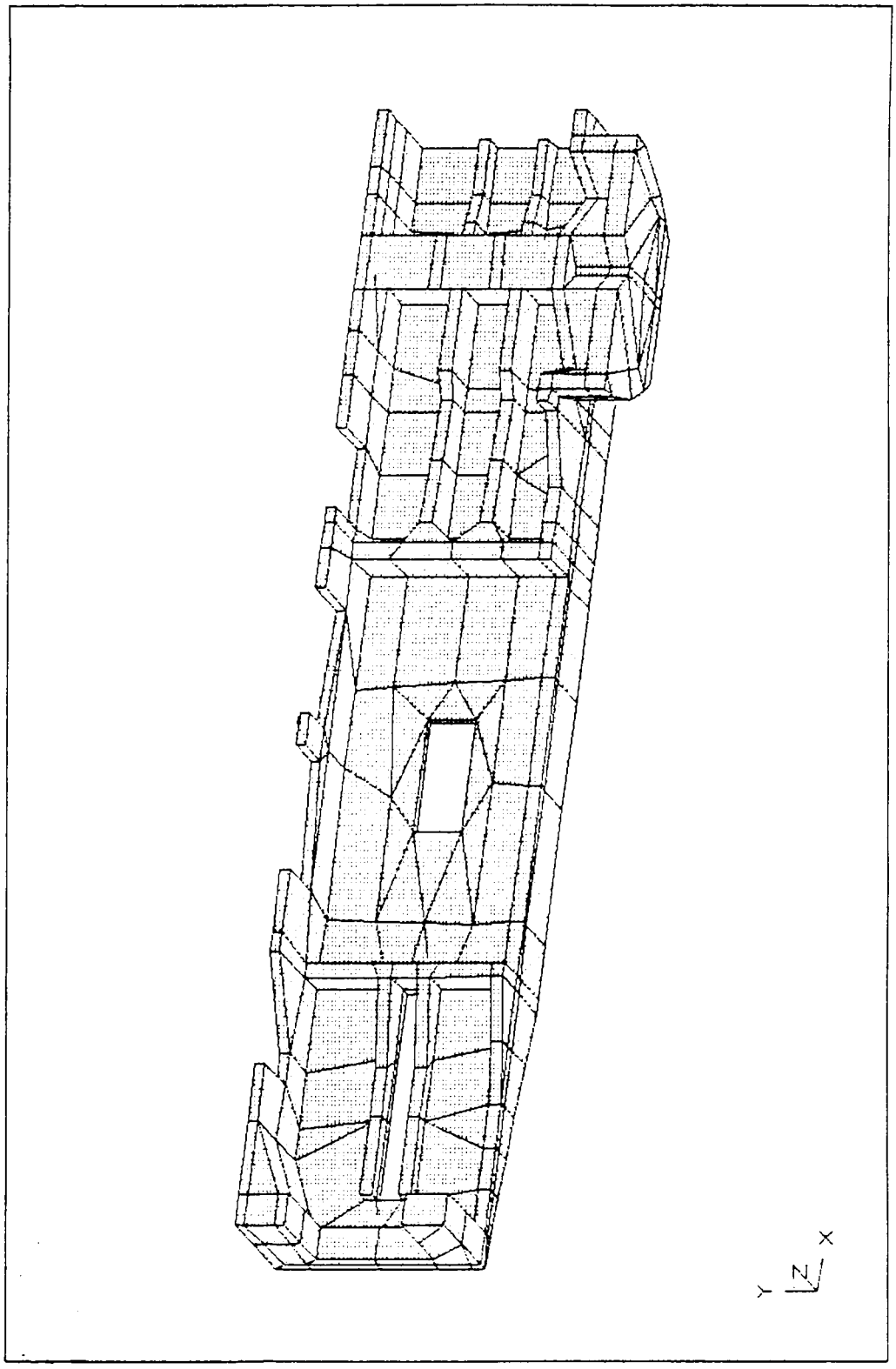

Figure 19. First Redesigned Model (Side View).

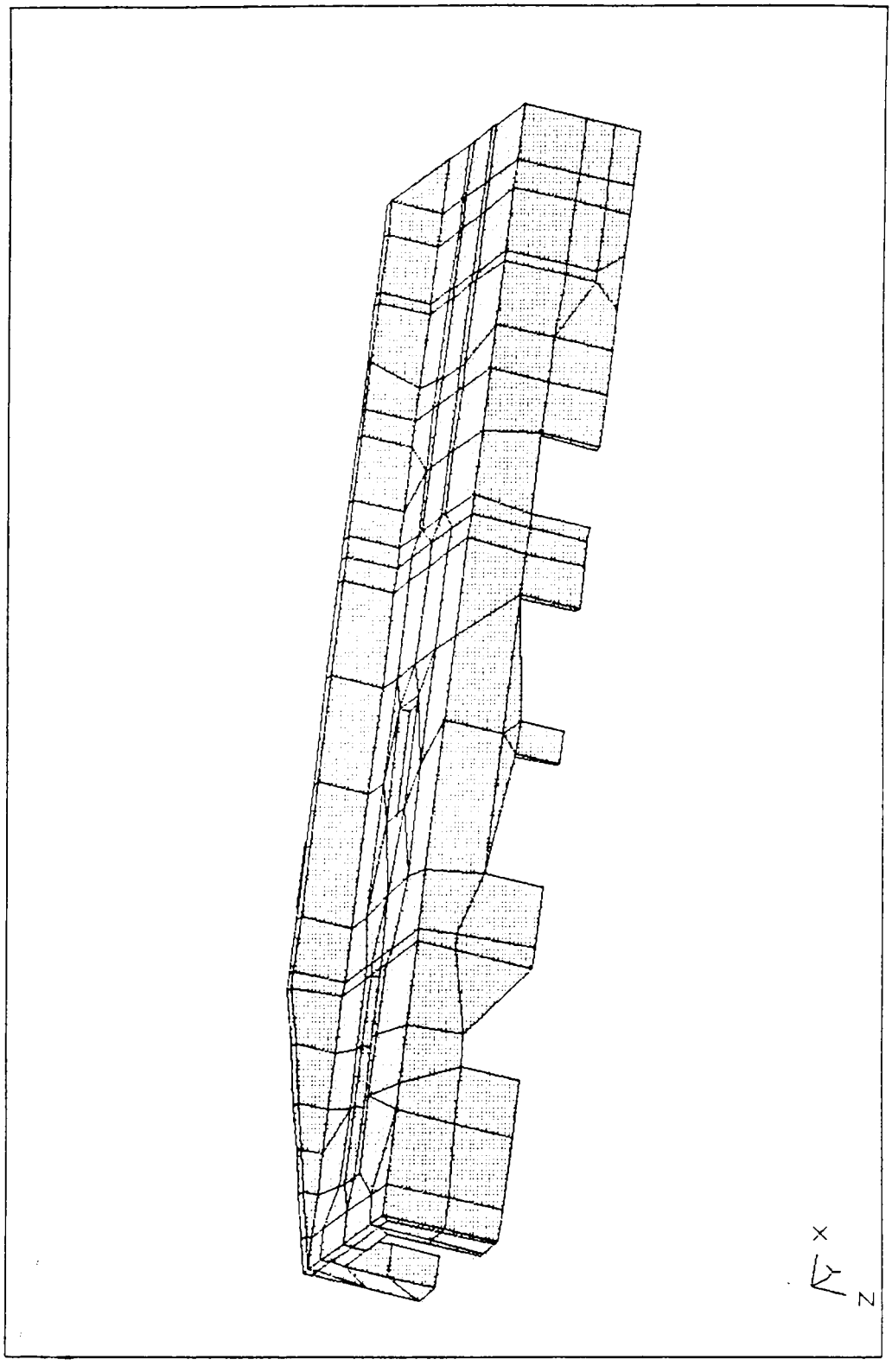

Figure 20. First Redesigned Model (Top View).

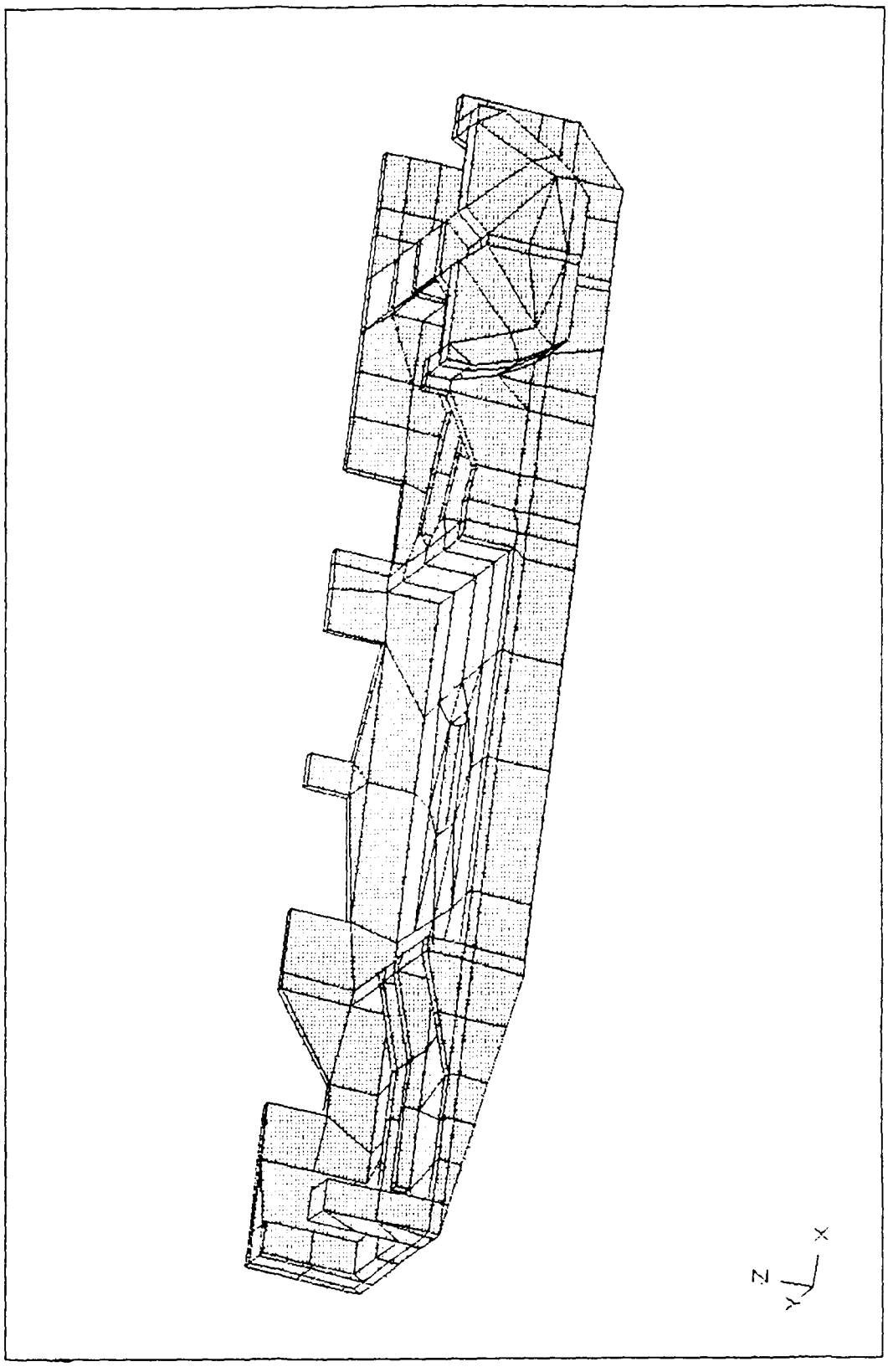

Figure 21. First Redesigned Model (Bottom View).

Chapter 7

Second and Final Analysis Iteration

Having completed and analyzed the original and first iterative models, a third model was created to move towards two major objectives. The first being to make the finite element model of the draftsill as realistic as possible. The second was to correct any flaws in the redesigns done and move toward a lighter and more structurally efficient draftsill casting. Another separate study done after this final analysis iteration was a draftlug pressure redistribution study. Here the applied pressures were studied for a possible alternative loading form (if needed) that would be more effective in transmitting these applied loads to the draftsill casting.

7.1 Changes Made to the First Iterative Model

On this final finite element model there were many changes made. Most of these changes made were modifications in which the finite element model was redesigned to reduce the weight of the draftsill without increasing the internal stresses of the casting by a substantial amount. The follow-

ing is a listing of the modifications made to create the final design of the draftsill. These changes were dictated by the stress results obtained from the first iterative model:

- The rear vertical wall located perpendicular to the sidewalls and above the centerplate was removed from the top of the draftsill to the top of the lower rib behind the rear draftlug.

- The two rear ribs behind the rear draftlugs were tapered into the sidewall. The taper started at the point where these ribs began to curve toward the center of the casting and tapered linearly to a point inside the sidewall where the sidewall and vertical wall, in which the center post is attached, formed a corner. For a more detailed visualization see Appendix A.

- All rear ribs that perpendiculary stuck out of the sidewall behind the center post vertical wall were deleted. That is, the draftsill was modified to eliminate all ribs behind the center post.

- The rear top hole, which was located slightly behind the rear draftlugs, was found to have an increased stress value when analyzed in the last model. Because of this, its increase in size was reduced to the size of the hole specified in the blueprints.

- Because of the low stress values found around the front top hole, which is located above the keyslot area, it was enlarged to be slightly bigger (2 times) than was originally designed.

- A number of elements were added to the top of the finite element model in a position directly above the rear center post area. This was done to accurately model load case 3 (Vertical Load), which until now had produced low stress values even when modeled as a uniform displacement. The elements were added to represent the cover plate and bolster beam members that rest on the top of the draftsill. See Figure 16 on page 48 in Chapter 5 for this application.

- To make this model reflect as much of the draftsill's true environment as possible, the application of load case 3 (Vertical Load) was applied simultaneously with each of the other applied load cases. This was done due to the fact that load case 3 was a constant load that realistically

represented the hopper car weight. This weight, which was transmitted through the bolster beam and coverplate, was applied on top of the draftsill above the centerpost.

- The applied pressure on the front draftlug (load case 1) was removed from the lower part of the draftlug to more accurately represent the loading area between it and the draftgear. The applied pressure was increased from 11,030 psi to 11,860 psi(76 MPa to 82 MPa) to keep the same specified load magnitude.

The above modifications in the finite element model were made and then analyzed using both linear and parabolic elements. This new model is shown in Figure 22, Figure 23 and Figure 24 which show all of these discussed changes. The results obtained from this model are shown in the next chapter and are presented in such a manner that all modeling results can be reviewed and compared simultaneously.

7.2 Pressure Redistribution Study

Once the entire finite element model had been analyzed and redesigned, a more specific study involving the applied pressures to the draftlugs was done. The purpose of this study was to try to create a possible alternative to the existing mating surface between the draftlug and draftgear. This possible alternative should have theoretically redistributed the stresses created from the draftlug load cases such that they were distributed closer to the sidewall of the draftsill casting. This would reduce the localized high stresses occuring on the ribs both in front and back of the front and rear draftlugs respectively.

The pressures were redistributed and studied specifically on the front draftlug due to the fact that this load case needed modification already. In addition to the already discussed changes for this iterative model, there were three different pressure load situations applied. The specific applications

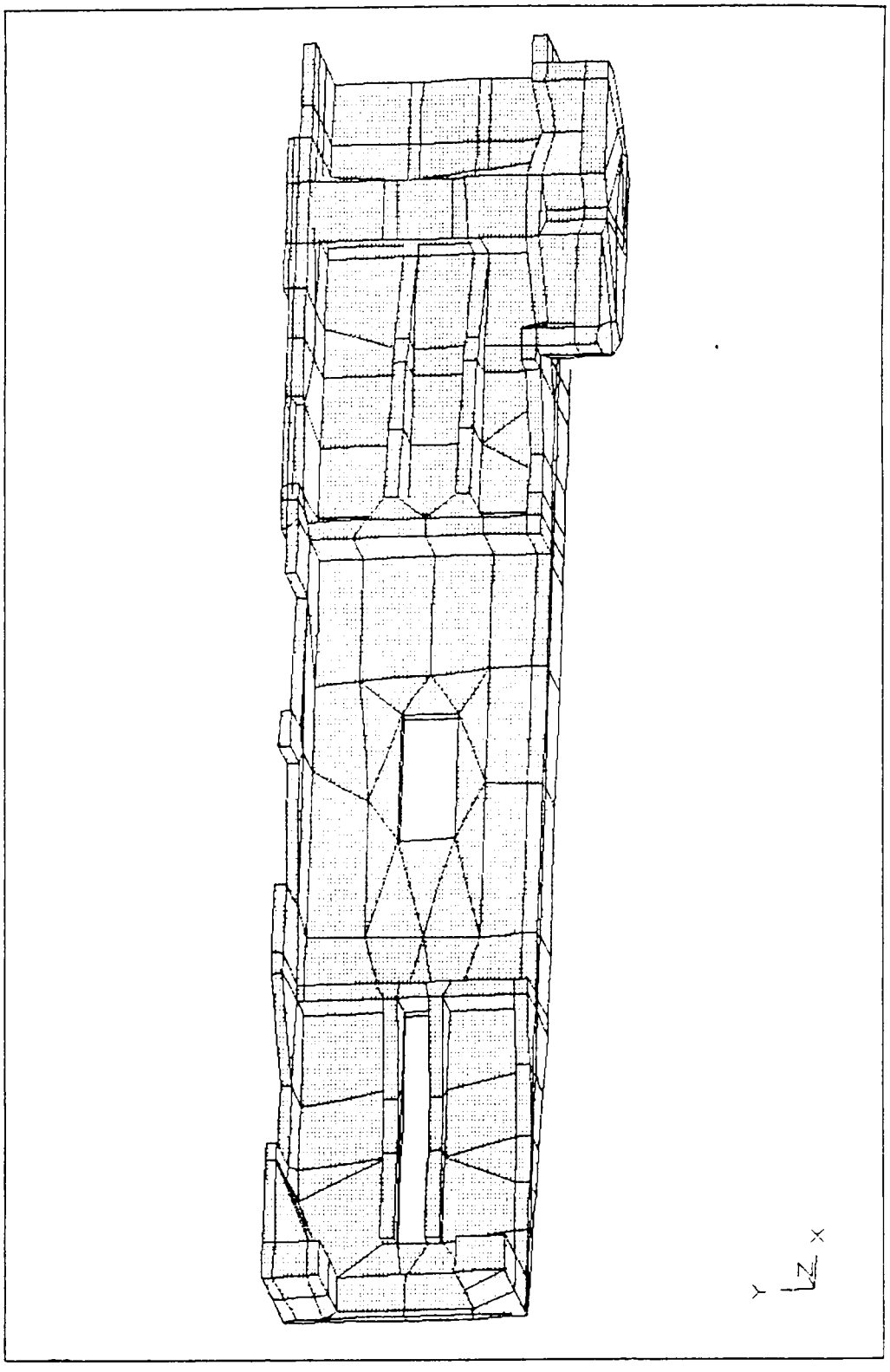

Figure 22. Final Draftsill Model (Side View).

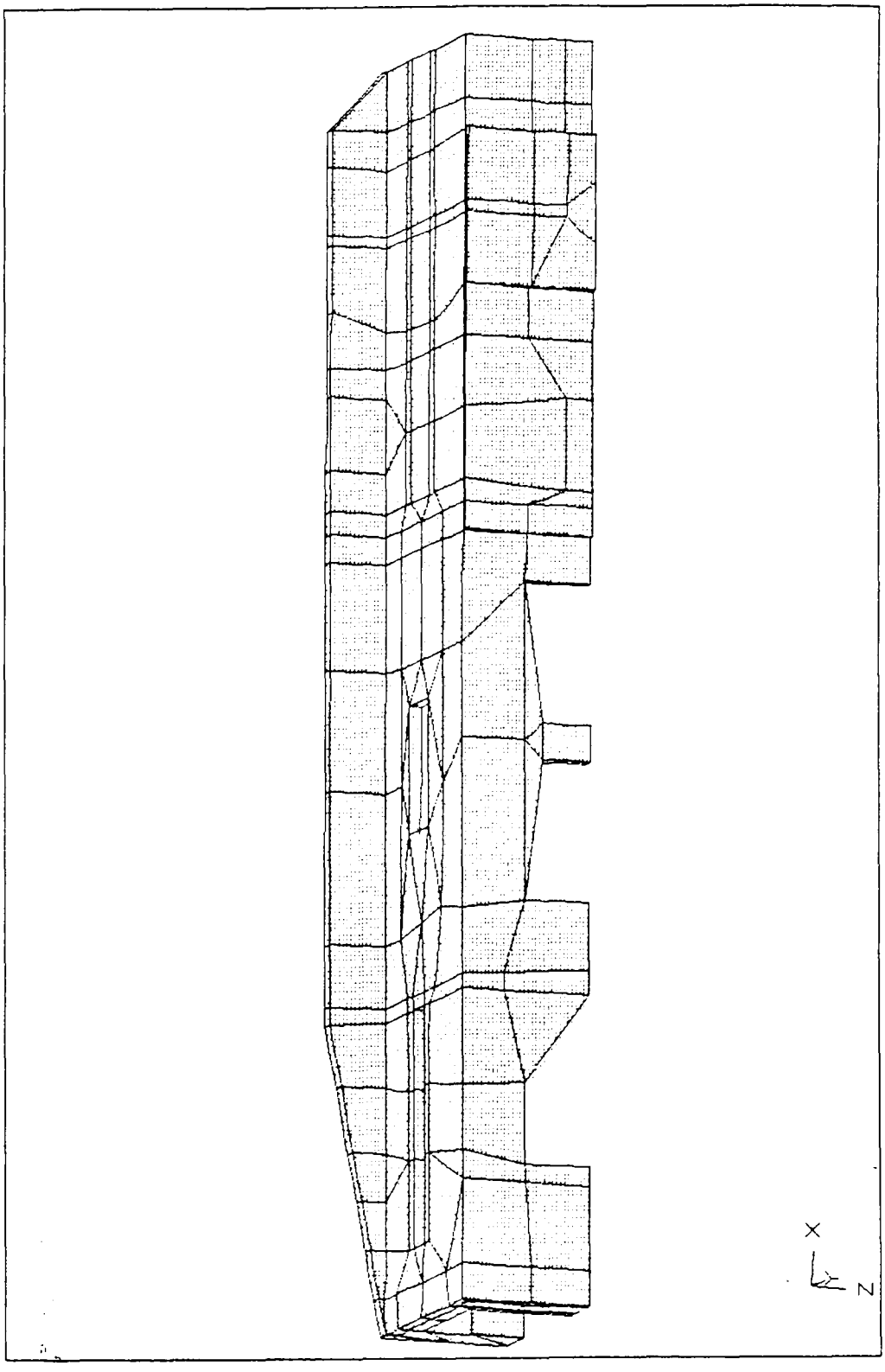

Figure 23. Final Draftsill Model (Top View).

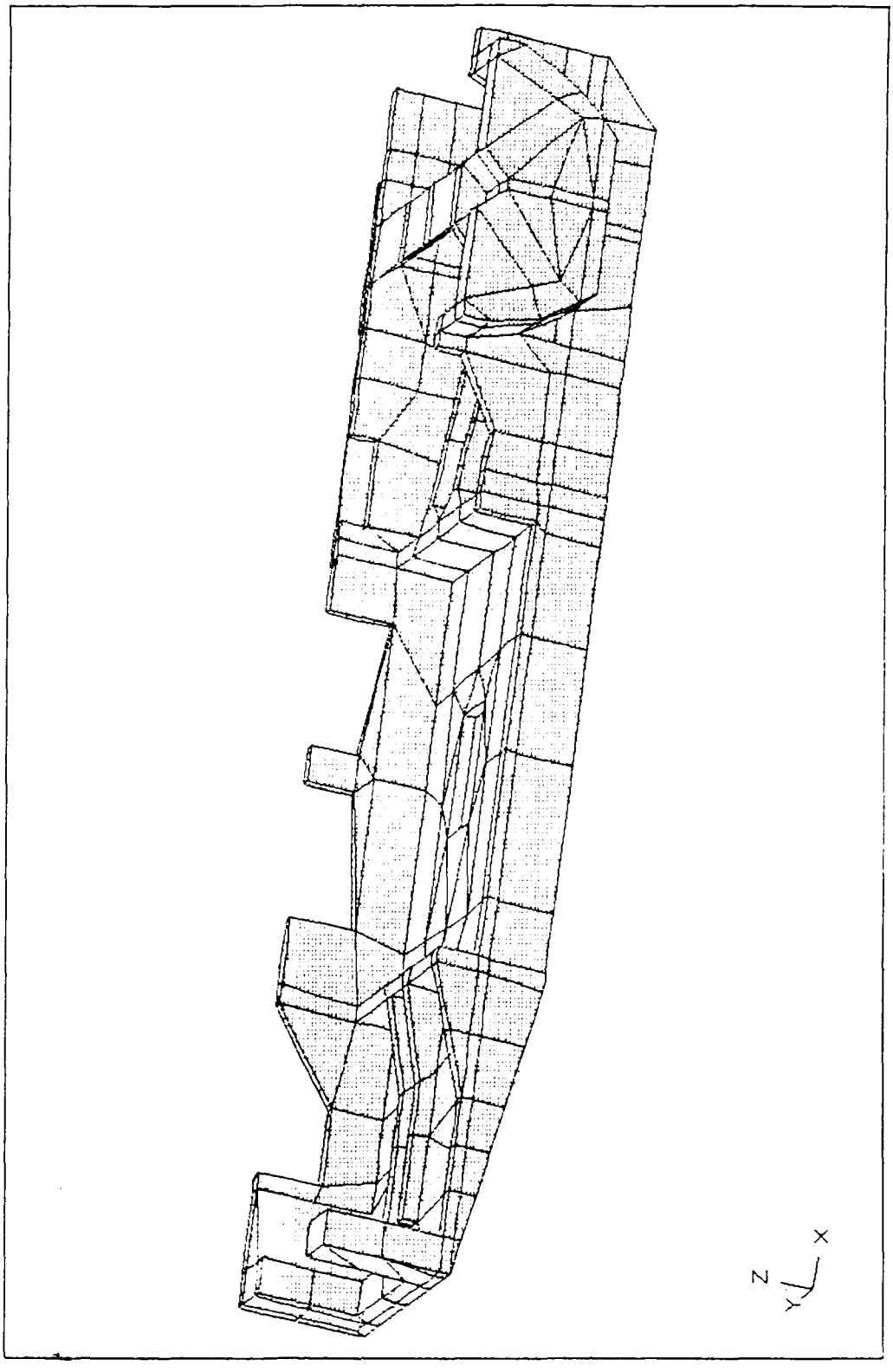

Figure 24. Final Draftsill Model (Bottom View).

of this load study are shown in the next chapter as well as any other results and recommendations for a more effective load distribution at the draftlug-draftgear interface.

7.3 Other Changes Studied

Once the project had come to a near finish there were some ideas that were generated that needed to be considered, but due to the time constraints put on this research project they could only be looked at briefly. These ideas and their findings were:

1. To release the vertical (Y - direction) restraints that were applied at the centersill connection. This was thought to be a more representative constraint criteria especially for the vertical loading situations. This change was made and the final model was analyzed only to find that this restraint change generated no difference from the previous solutions obtained. It is worth noting at this point that if the draftsill encounters any motion which causes the centerplate to loose contact with the truck unit, i.e., a rocking motion, the draftsill might generate high stresses in the area of the centerplate due to the concentration of the vertical load, but this is not conclusive.

2. Stresses due to the hopper car rocking from side to side. For this part a brief look at the centerplate was done by releasing the restrained nodes on the centerplate that appeared to be pulling away from the truck unit under load. This was done for each of the load cases, but there was no apparent large change in results.

3. A large load was applied to the striker face to simulate impact of the draftgear on this area. The load applied was 1,000,000 lbs(4450 kN). The resulting stress values were disastrously high indicating that if this type of load is generated the draftsill will fail.

Chapter 8

Results and Conclusions

Having completed all discussions of the modifications and steps made to reach a final redesign model of the draftsill, it is now appropriate to show all of the important results and data obtained while analyzing these models. It is hoped that by using this format the reader will be able to get more of an understanding as to the continuity of the whole iterative process used in this research.

In this research project a final redesign model of a draftsill casting was created. This final design incorporated a total weight reduction of 106 lbs(472 N), per draftsill casting, while remaining structurally sound. The design created is based upon the original draftsill design, but particular areas, considered to be overdesigned, were removed or modified to increase the efficiency of the casting. Also included in this work was a detailed study of the applied draftlug loading situations. This analysis found that tapering the draftlugs 0.025 - 0.050 in.(0.0635 - 0.127 cm), where they contact the draftgear, would distribute the load more effectively throughout the casting.

In this chapter a variety of topics will be discussed and presented. The major topics are the comparision of the composite plot data of the original and final draftsill designs, the weight reductions made in the draftsill casting, the modeling results for each model, the pressure redistrib-

utions recommended, and a justification of the results obtained. All of this will then be followed by a brief conclusive description of the project.

8.1 Composite Stress Plots and Results

During the course of this research, there was a need for a way to present simultaneously the results of the multiple applied load cases relative to each other. To do this a computer code was written to extract from the multiple case solution stress data the highest stress values for each node (see Appendix B). This was done via the following procedure:

1. The stress values for each node (σ_x, σ_y, σ_z, τ_{xy}, τ_{yz}, τ_{xz}) of each element corresponding to each load case were read into the program.

2. These nodal stress values from connected elements were then averaged for each separate load case and then stored.

3. The average stress values (σ_{xav}, σ_{yav}, σ_{zav}, τ_{xyav}, τ_{yzav}, τ_{xzav}) at each node for each load case were then used to compute five Von Mises stress values for that node as it occured in each of the load cases. The highest Von Mises value was then selected and the corresponding stresses that represent that value were stored.

4. All of the stored nodal stress values were then treated as one load case and presented as a COMPOSITE STRESS PLOT. This Composite Stress Plot is a combination of the highest stress levels seen by each node for any load case.

Figures 25 through 36 show the composite plots for the original and final draftsill designs. These plots use only three contour levels so as not to clutter the figure. The intention is that these stress

plots show areas of possible concern so the stress levels shown begin at values of 50,000 psi(345 MPa).

Figures 25 through 27 and 31 through 33 show specifically the high stresses generated in the draftlug regions for both the original and final draftsill models. In general this region is where the maximum values were consistantly occuring. Note that in both models the critical regions appear in the support ribs which connect to the draftlugs. Also note the high stresses generated in the lower corners between the draftlugs and the lower ribs.

Figures 28 and 34 present the top views of the original and final models. Here the important areas to notice are the outer flange just behind the rear draftlug and the front of the keyslot where it meets the sidewall.

Figures 29 and 30, 35 and 36 show an unexpected result. There is an area of high stress located where the centerplate meets the lower surface of the draftsill approximately 45 degrees off center. This is shown to be a result of load cases 4 and 5 which are discussed in more detail in a later section of this chapter.

Note that when comparing the original and final designs of the draftsill, the stress plots show similar contours which indicates that the stress levels in the draftsill do not change by a significant amount due to the design changes made. This then justifies the conclusion that the general integrity of the draftsill has not been compromised. It must be noted at this point that if the draftsill is exposed to the design load magnitudes used for this research, then the draftsill will most definitely have some local yielding in the high stressed regions.

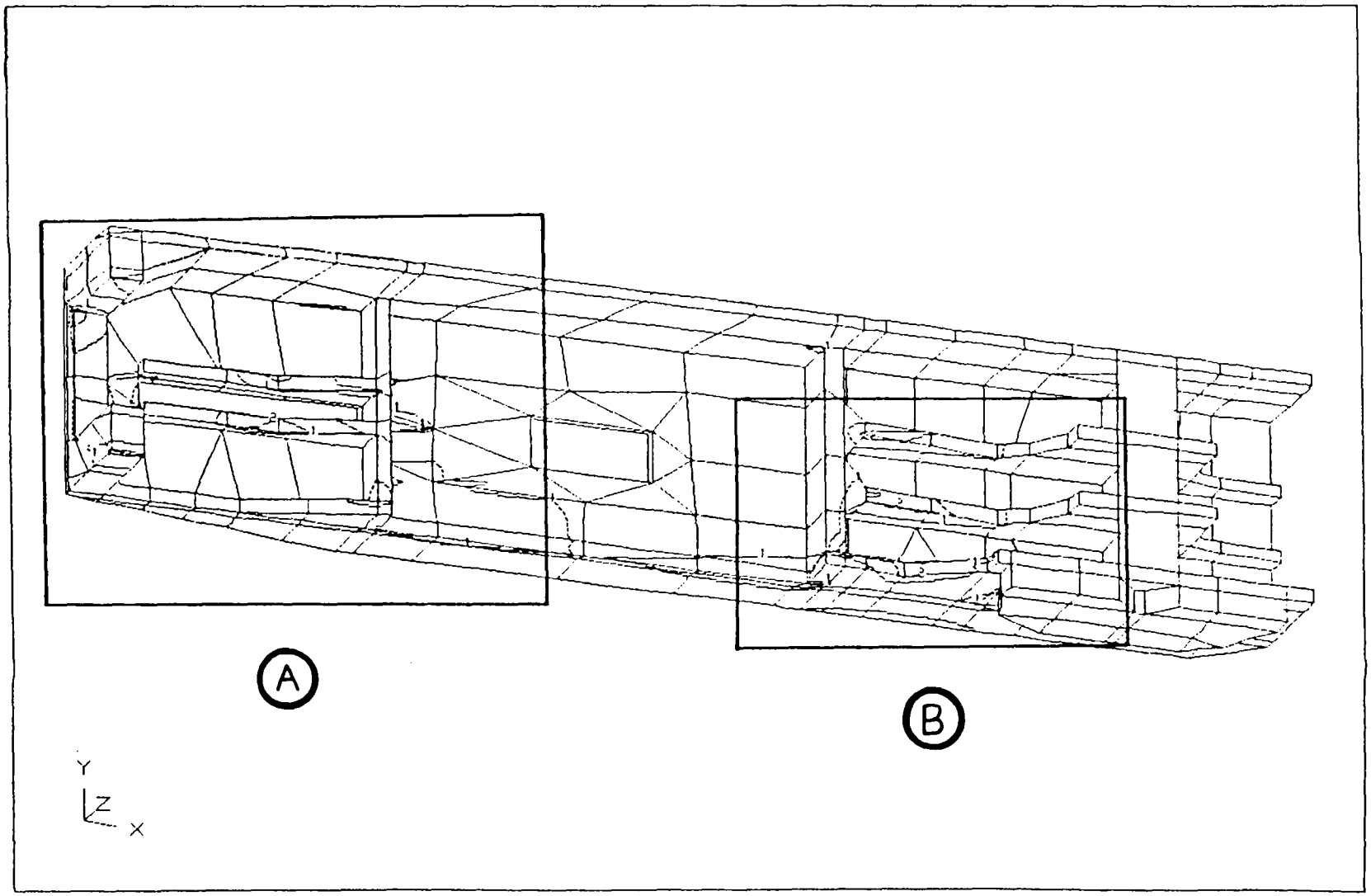

Figure 25. Composite Stress Plot for Original Draftsill Model (side view).

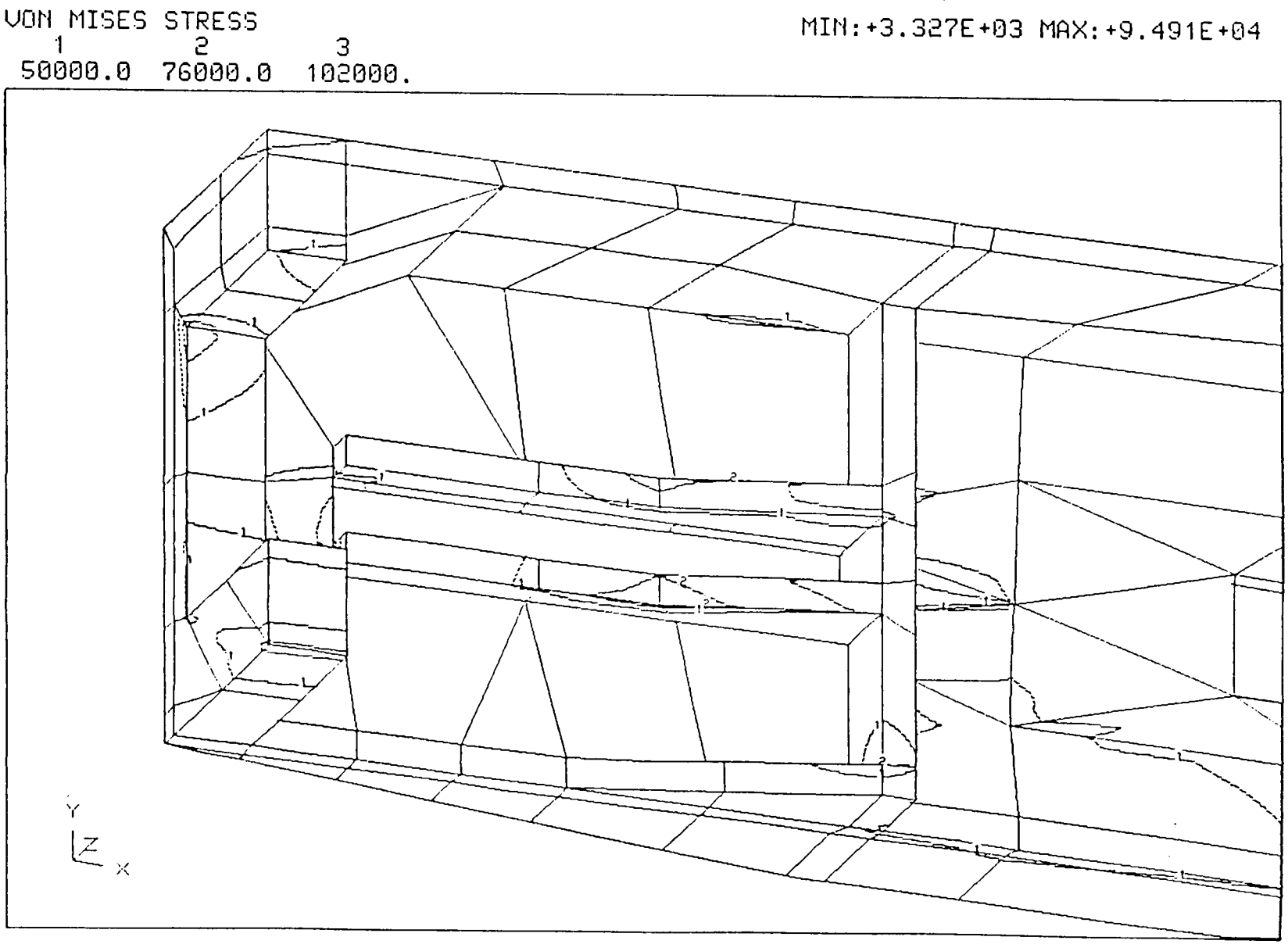

Figure 26. Composite Stress Plot for Original Draftsill Model Detail A (side).

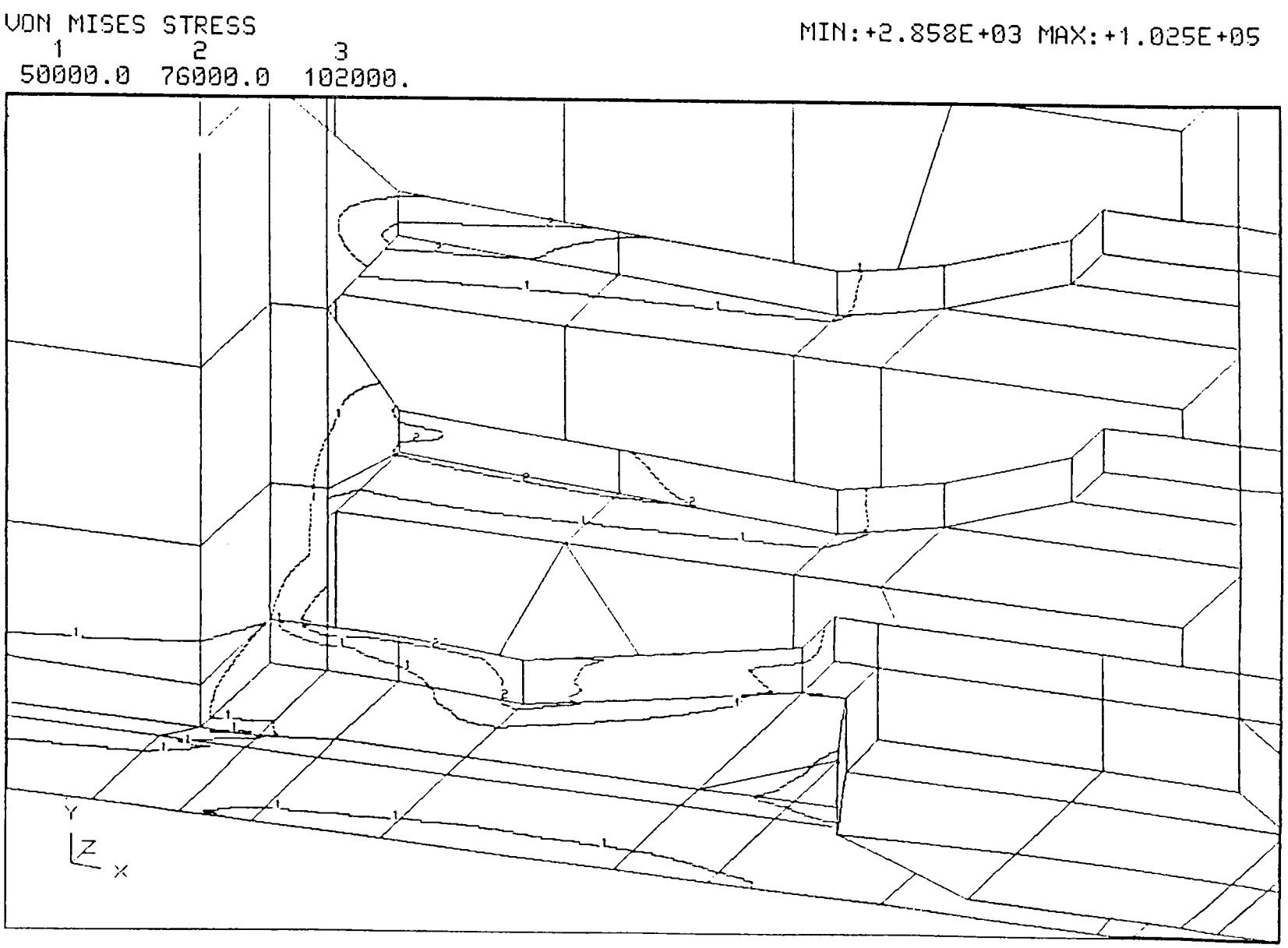

Figure 27. Composite Stress Plot for Original Draftsill Model Detail B (side).

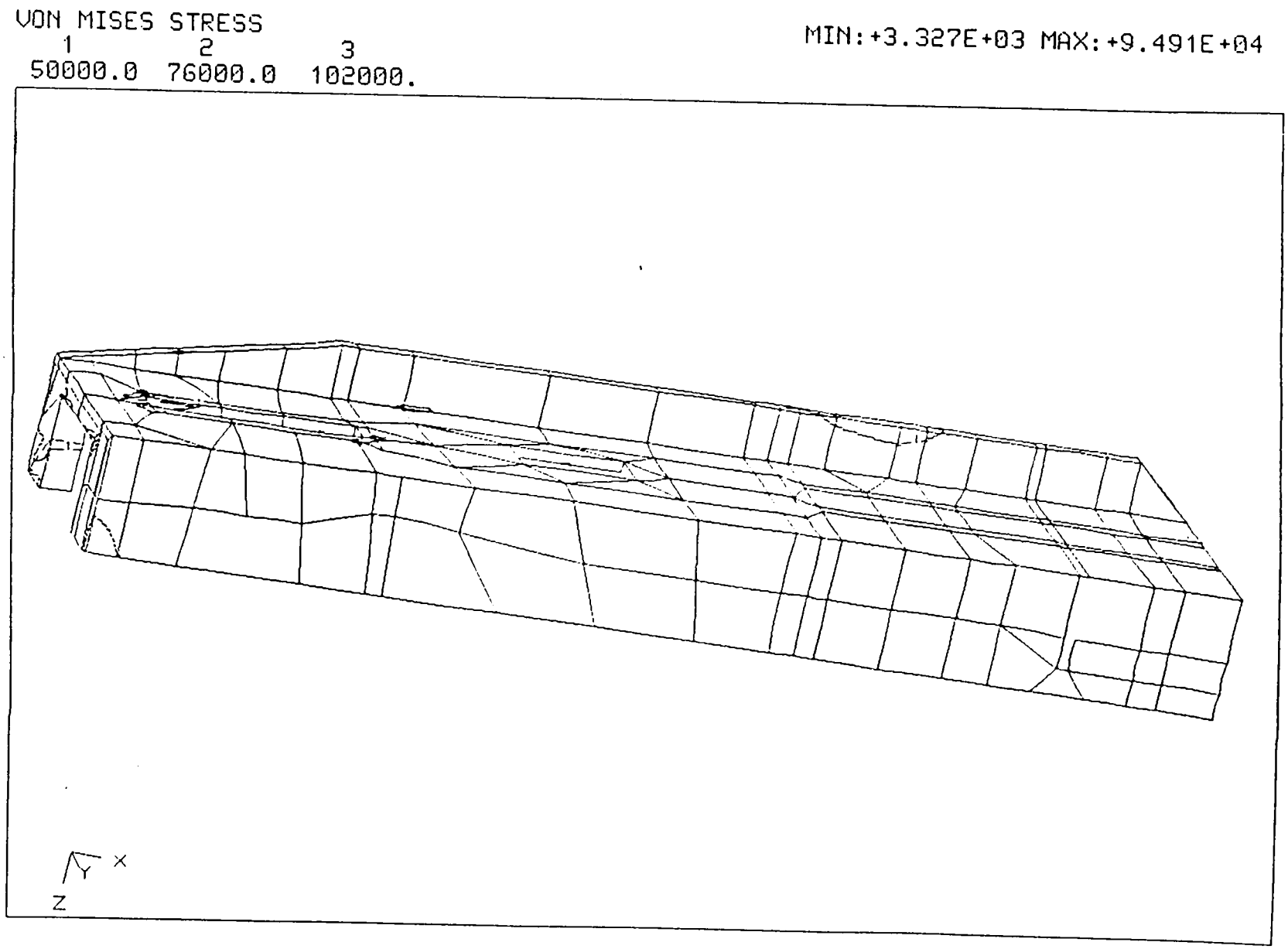

Figure 28. Composite Stress Plot for Original Draftsill Model (top view).

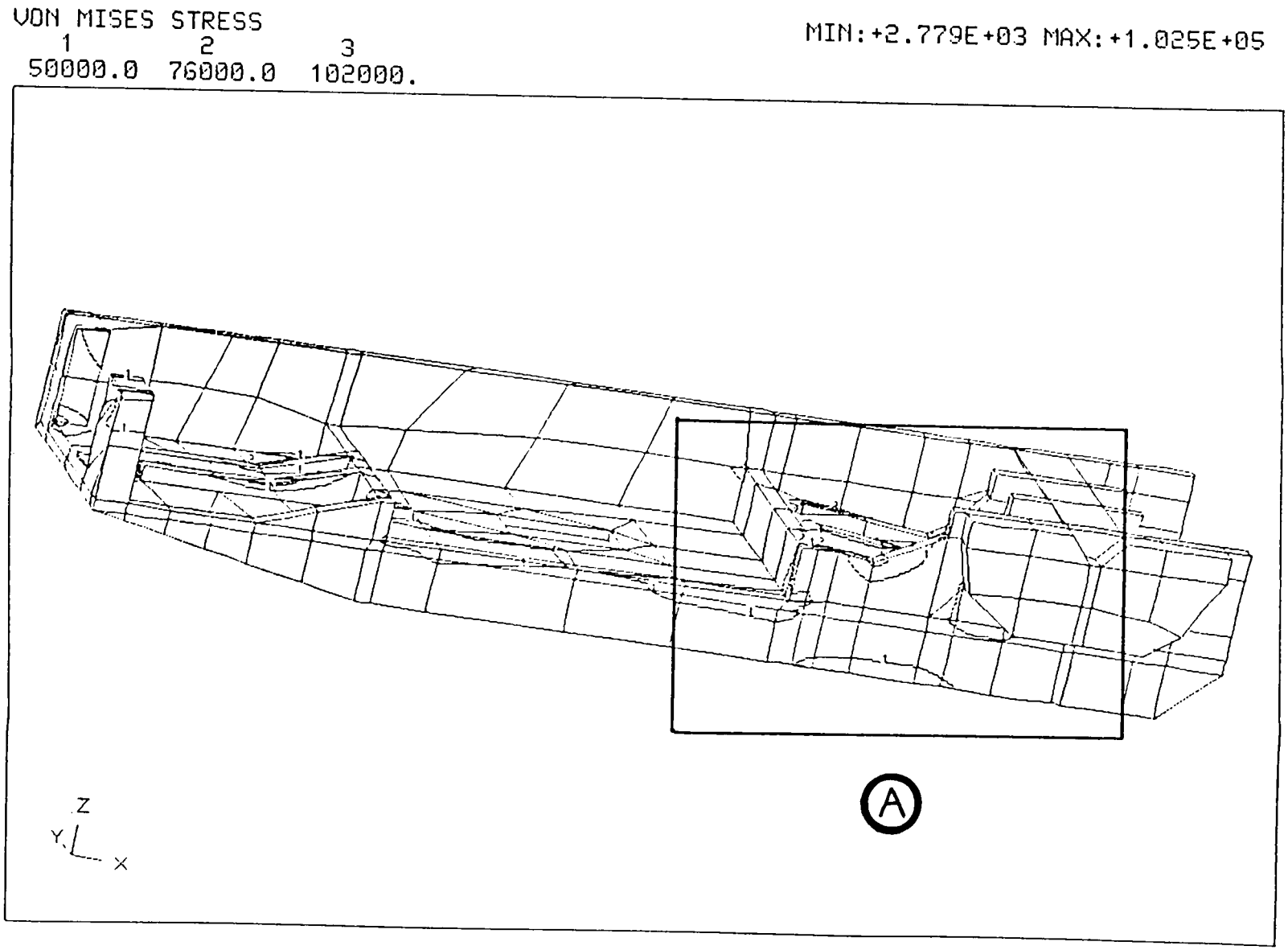

Figure 29. Composite Stress Plot for Original Draftsill Model (bottom view).

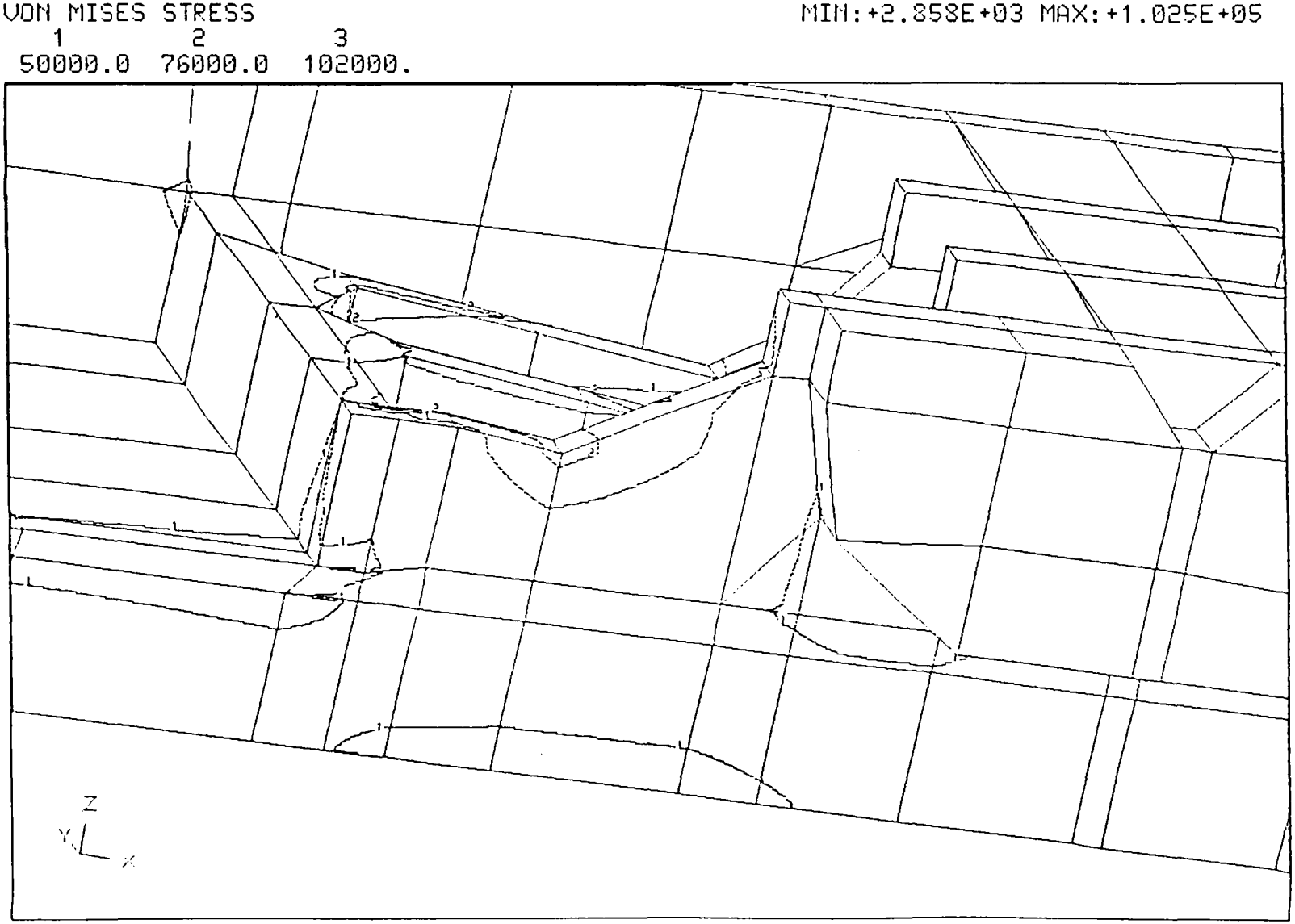

Figure 30. Composite Stress Plot for Original Draftsill Model Detail A (bottom).

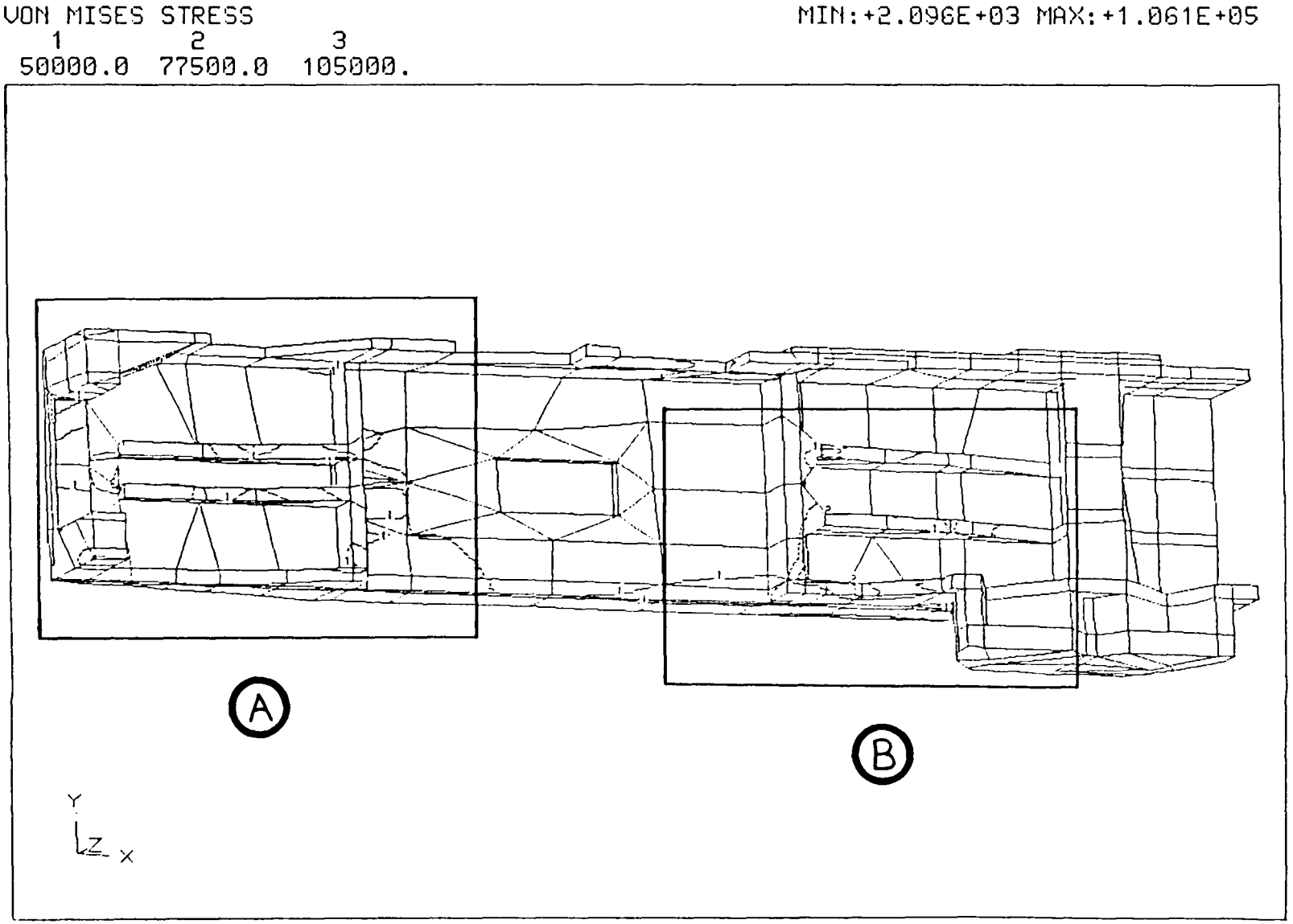

Figure 31. Composite Stress Plot for Final Draftsill Model (side view).

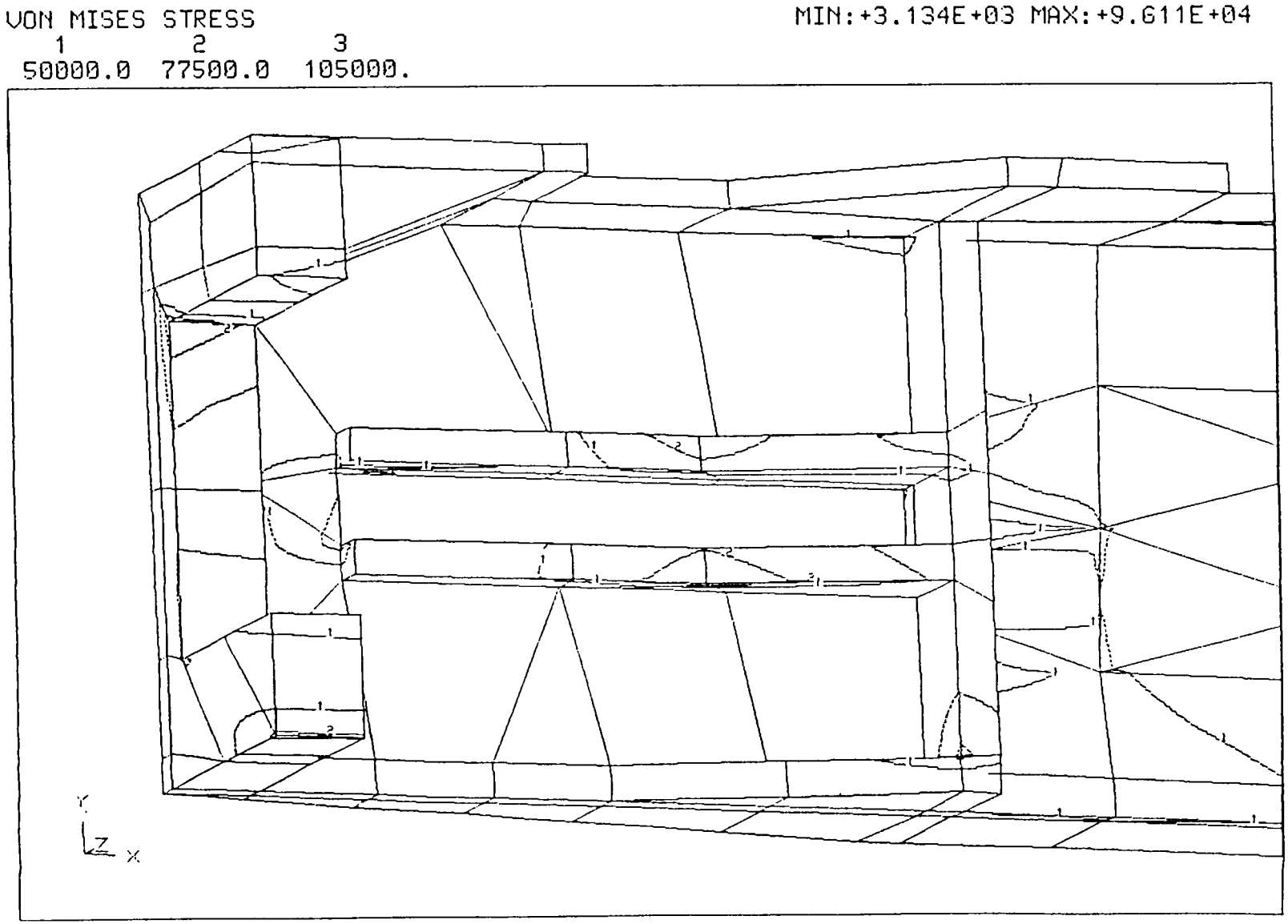

Figure 32. Composite Stress Plot for Final Draftsill Model Detail A (side).

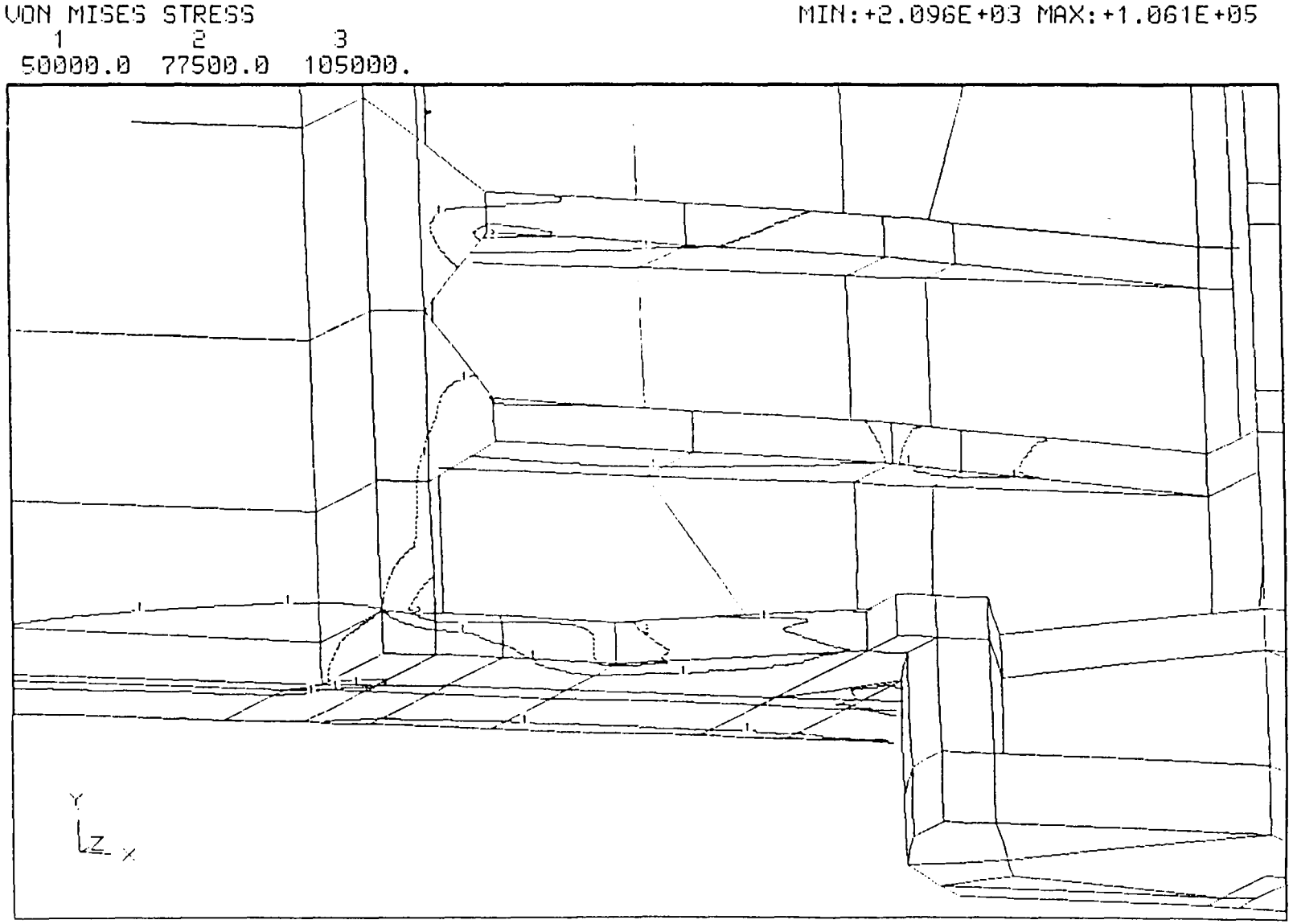

Figure 33. Composite Stress Plot for Final Draftsill Model Detail B (side).

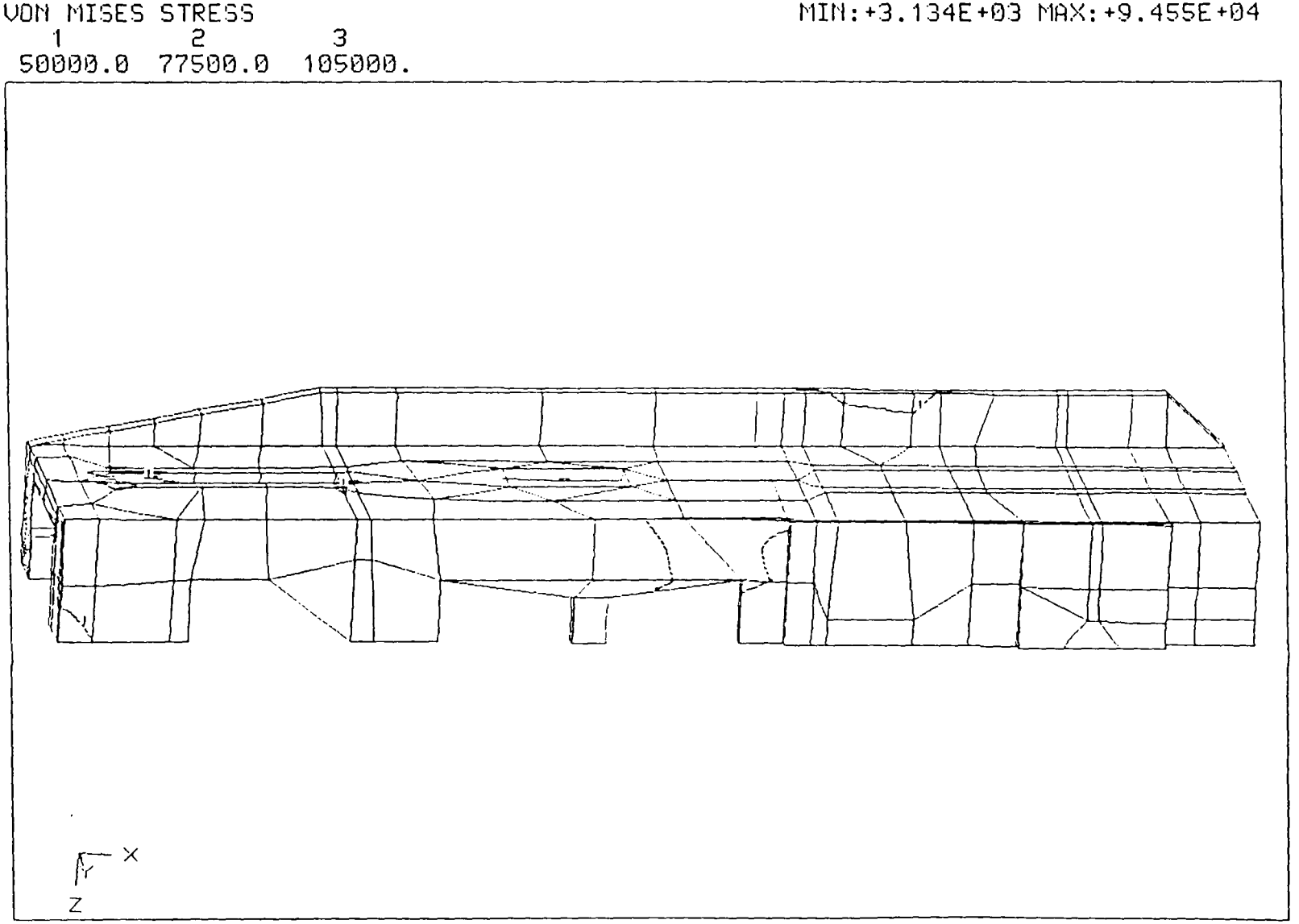

Figure 34. Composite Stress Plot for Final Draftsill Model (top view).

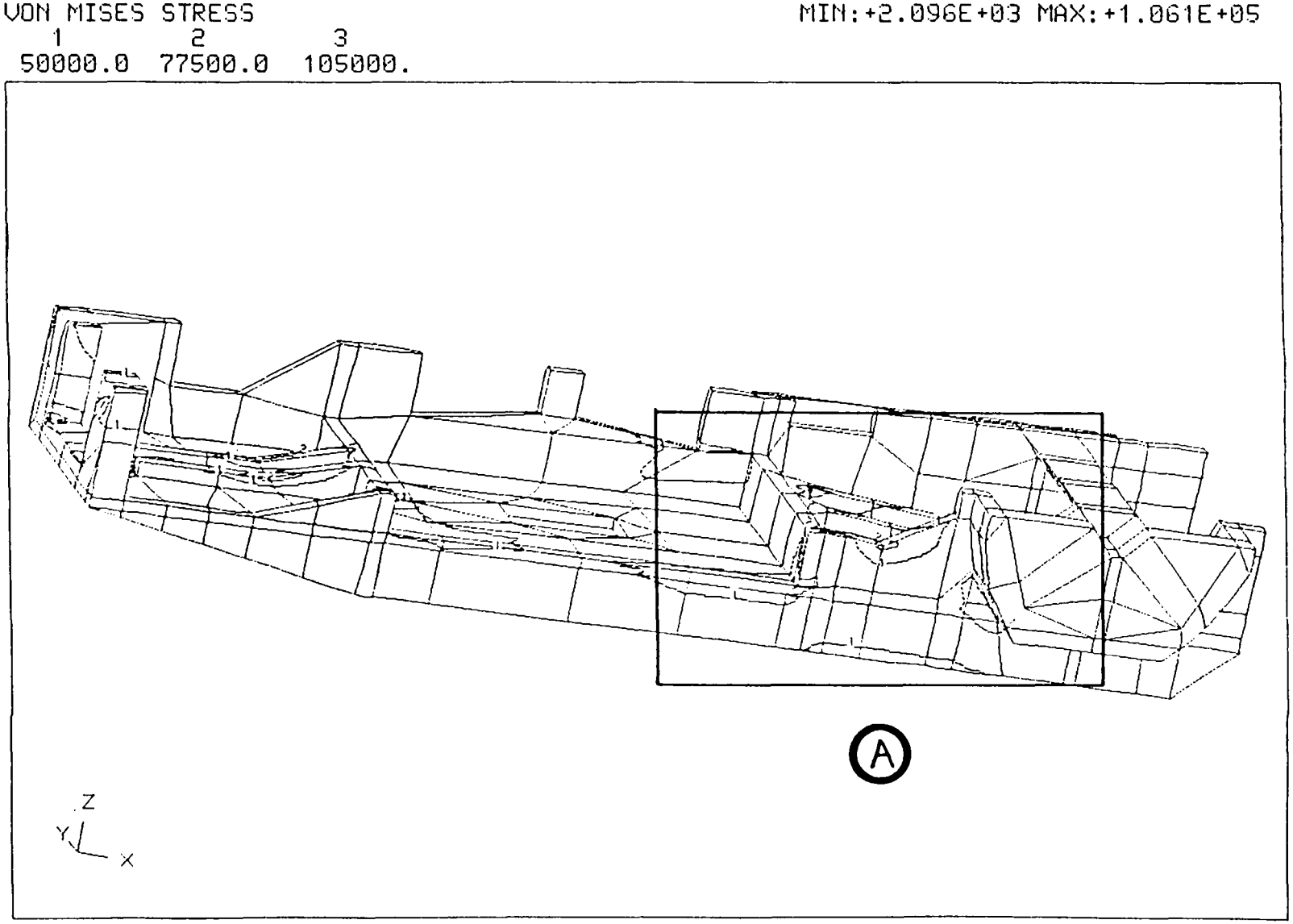

Figure 35. Composite Stress Plot for Final Draftsill Model (bottom view).

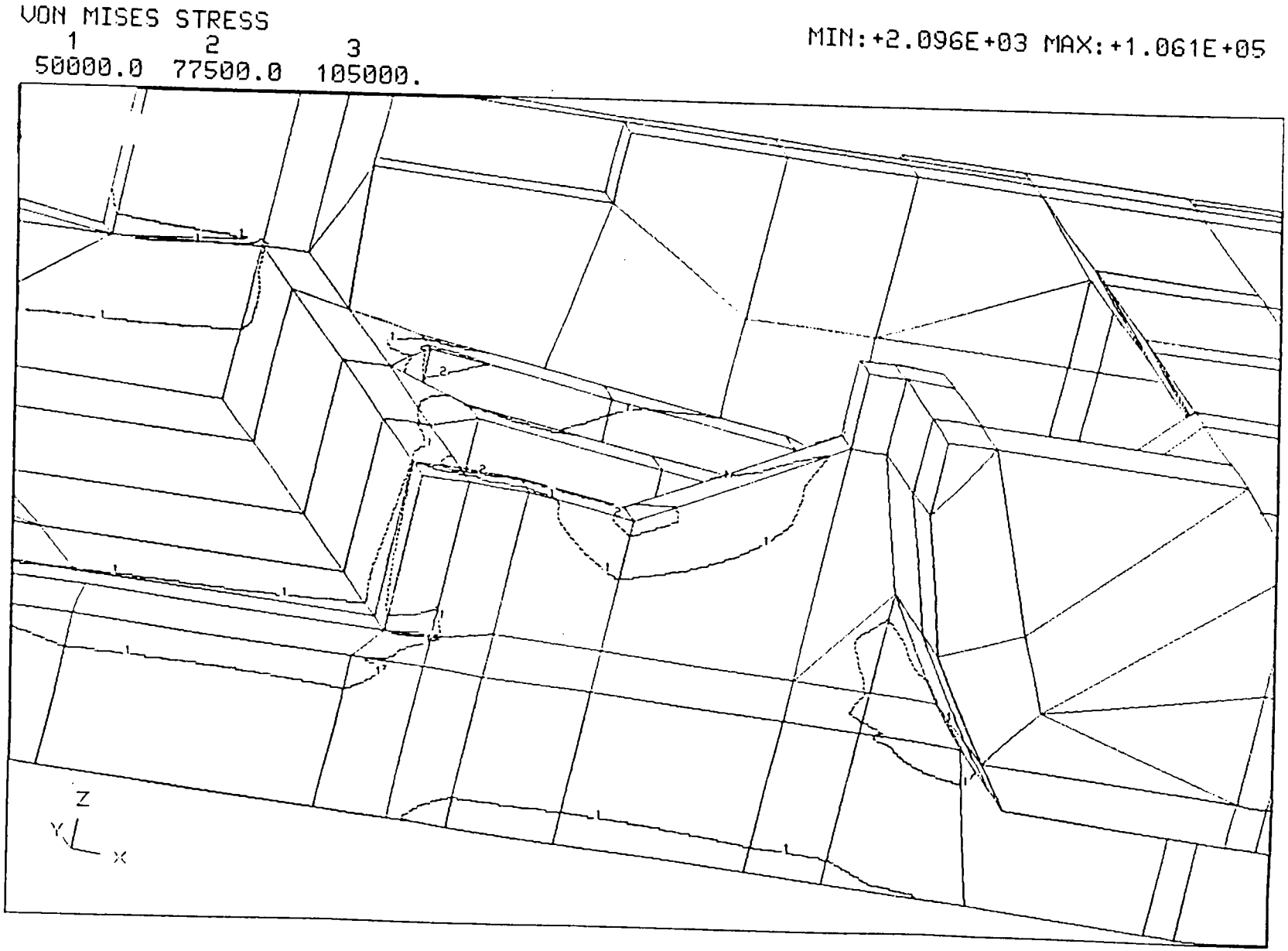

Figure 36. Composite Stress Plot for Final Draftsill Model Detail A (bottom).

8.2 *Weight Reduction Results*

One of the major goals of this analysis and redesign procedure was to create a redesigned draftsill that was lower in weight without compromising the current stability of the structure. The actual draftsill casting weighs approximately 1,100 lbs(4892.8 N) so reduction of any weight from this member would be of substantial importance because there are two draftsill castings on each hopper car. If a train is made up of a large number of cars, the reduction in weight could add up to a large figure, which in turn would translate into larger load-carrying capability.

Table 1 presents the calculated weights for each of the iterative steps done in this research. Note that the weight of the parabolic models is the same as that of a linear model since there had been no change in the element construction. The total reduction in weight is approximately 106 lbs(471.5 N) for a whole draftsill casting. This value is a 9.6 percent reduction from the original draftsill weight and may seem small but, as an example, take a 50 car train and subtract off this weight and one finds that the train can now carry an additional 5 tons(4536 kg).

Table 1. Calculated Weights of Models in Pounds (Newtons).

Model Type	Original	Redesign I	Redesign II
1) Symmetrical Models	463 (2060)	438 (1950)	410 (1820)
2) Whole Models	926 (4120)	876 (3900)	820 (3650)
Total Weight Reduction = 106 (472)			

8.3 *Modeling Results*

In this section all of the critically stressed areas of the finite element models analyzed will be compared sequentially to show continuity and convergence. All of the data is presented in tabular form showing for each load case the stress levels for certain described locations on the draftsill. The stress values studied were Von Mises stresses and were selected as the output type because they take into account all three dimensions of stress. Since the models studied were three dimensional, using Von Mises stresses made for a clearer representation as to what was actually happening within the draftsill models. Another reason for selecting this theory was that it is the best failure theory for ductile metals and will indicate the initiation of yielding (10). Mathematically the Von Mises stresses were calculated as follows (10):

$$\{\sigma_{vm}\} \equiv \text{VON MISES STRESS}$$

$$\{\sigma_{vm}\} = \sqrt{\frac{(\sigma_1 - \sigma_2)^2 + (\sigma_2 - \sigma_3)^2 + (\sigma_3 - \sigma_1)^2}{2}} \qquad [8.1]$$

where:

$$\sigma_1, \sigma_2, \sigma_3 \equiv \text{Principal Stresses}$$

When using the Von Mises stresses for output one must realize that their value is a scalar quantity and, as such, it has no directional properties. For this reason, particular stress directions will not be discussed in this work.

8.3.1 Load Case One Results

Table 2 describes the results of load case one, the simulated pulling of the hopper car. There were seven positions on the models that consistantly showed higher stress values. Of all these positions listed, there appear to be only two that showed a large break from solution convergence. They were positions 1 and 3. An explaination for these high stress levels, as seen on the final model and the first model, is that they occurred only when parabolic elements were used and were also restricted to very small areas when seen. This would tend to indicate that some local yielding and/or stress concentration was occurring. Figure 37, Figure 38 and Figure 39 show these locations and stresses as they occurred in the last model analyzed (the final redesigned model).

The results of this load case were produced using the loading situation discussed in Chapter 5 which was the basis for a pressure redistribution study that is shown in a later section of this chapter.

Table 2. Load Case One Results, Stresses in kpsi (MPa).

Position on the F.E. Model	Original Linear	Original Parabolic	Redesign I Linear	Redesign II Linear	Redesign II Parabolic
1) Keyslot ribs on the striker face side of the front draftlug, where the ribs change to a flat slope	34 (234)	91 (627)	35 (241)	31 (213)	96 (661)
2) Mating corner edge of the sidewall and outer flange in the draft pocket (inner edge)	34 (234)	50 (344)	35 (241)	31 (213)	45 (310)
3) Bottom inside corner between the front draftlug and sidewall (in draft pocket)	41 (282)	90 (620)	42 (289)	37 (255)	80 (551)
4) Vertical center of the front draftlug toward the outer edge of its face	34 (234)	35 (241)	35 (241)	31 (213)	33 (227)
5) Top surface of the draftsill near the top holes which are above the draft pocket	25 (172)	30 (206)	28 (193)	31 (213)	33 (227)
6) Outer edge area of the outer flange at a position behind the rear draftlug	34 (234)	40 (275)	35 (241)	31 (213)	35 (241)
7) The diagonal area in the sidewall located between the hole and bottom corner of the front draftlug (in the draft pocket)	41 (282)	60-90 (620)	42 (289)	37 (255)	50 (344)

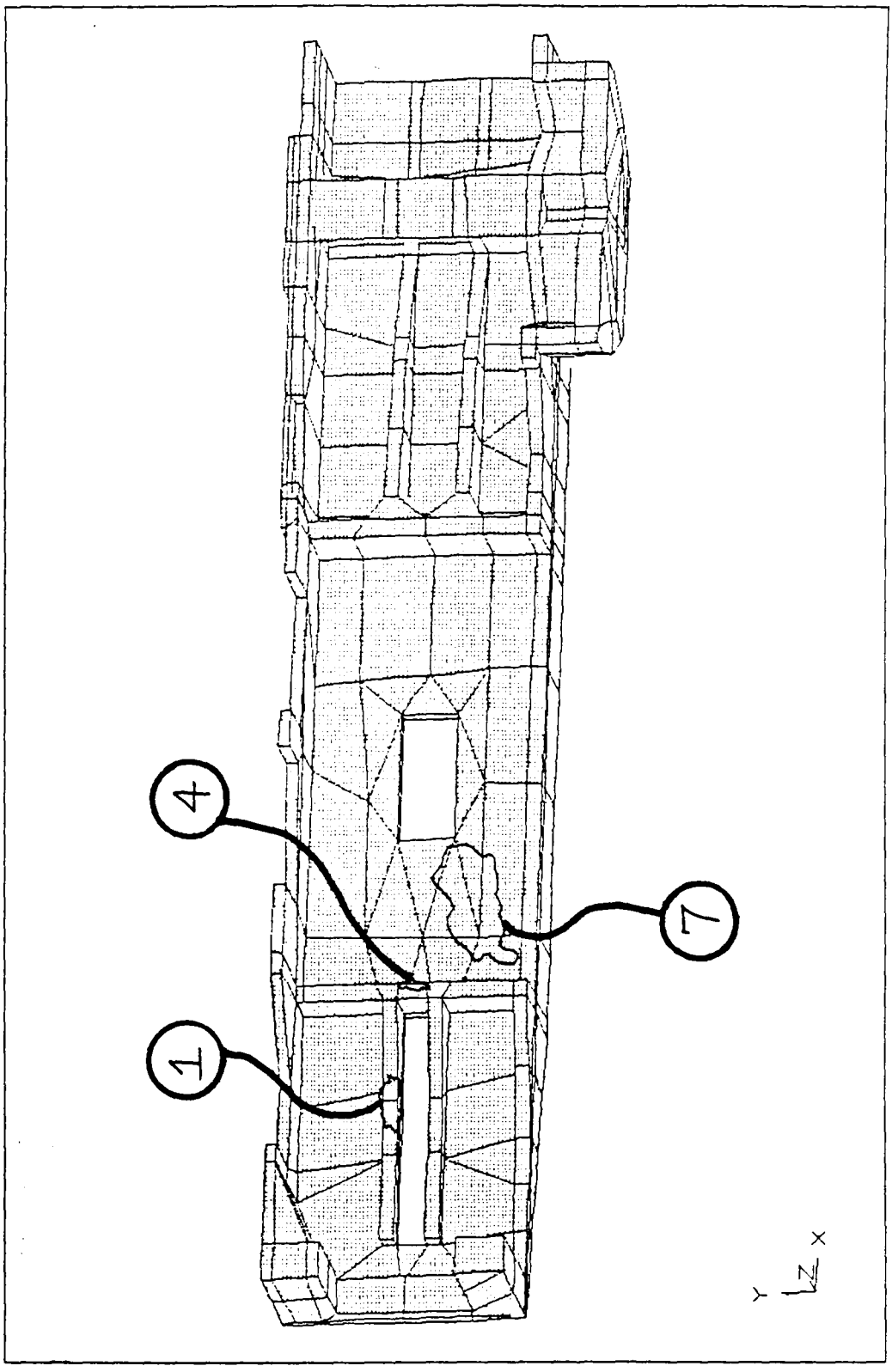

Figure 37. Positions On Draftsill Corresponding To Table 2 (Side View).

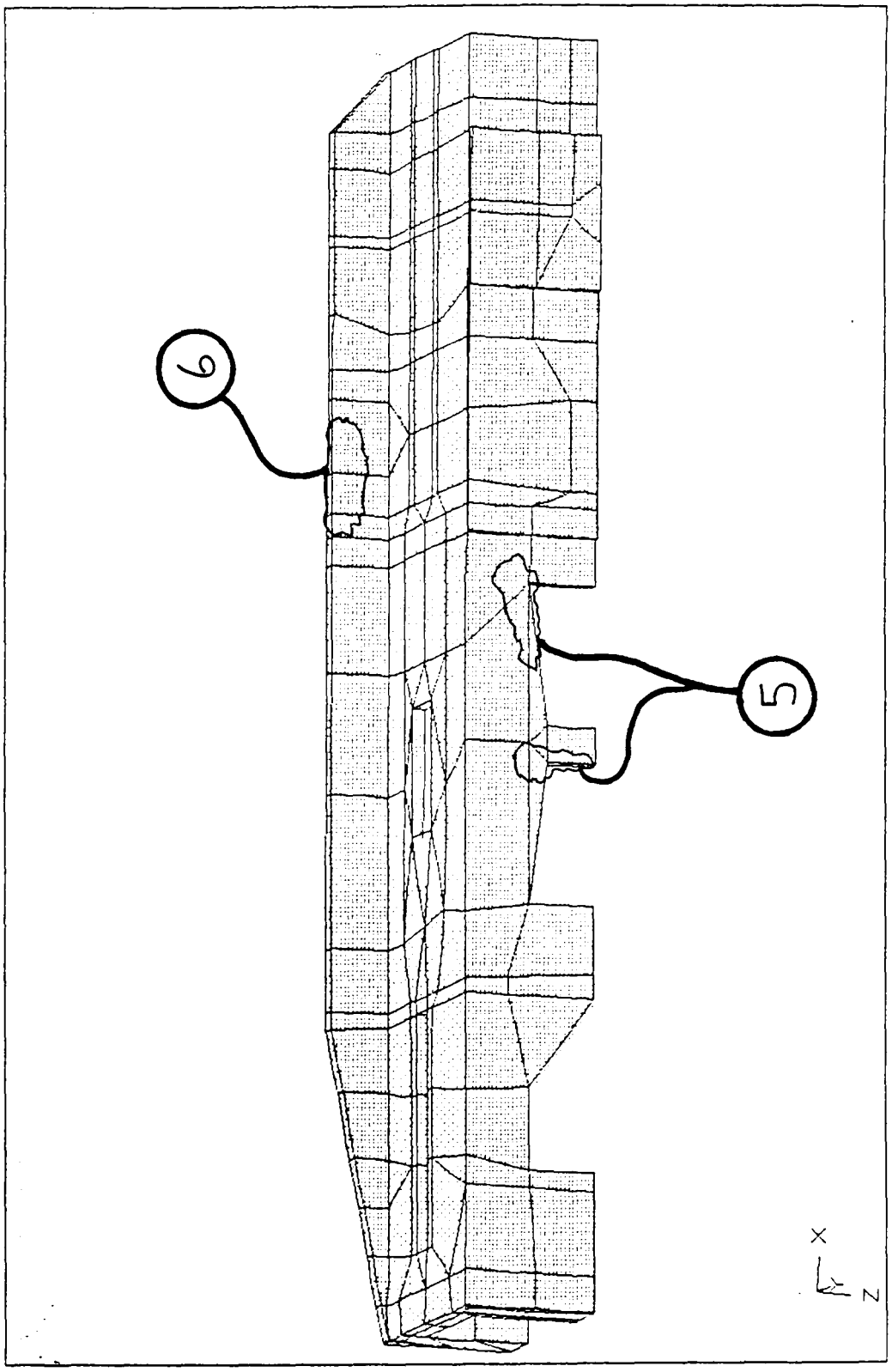

Figure 38. Positions On Draftsill Corresponding To Table 2 (Top View).

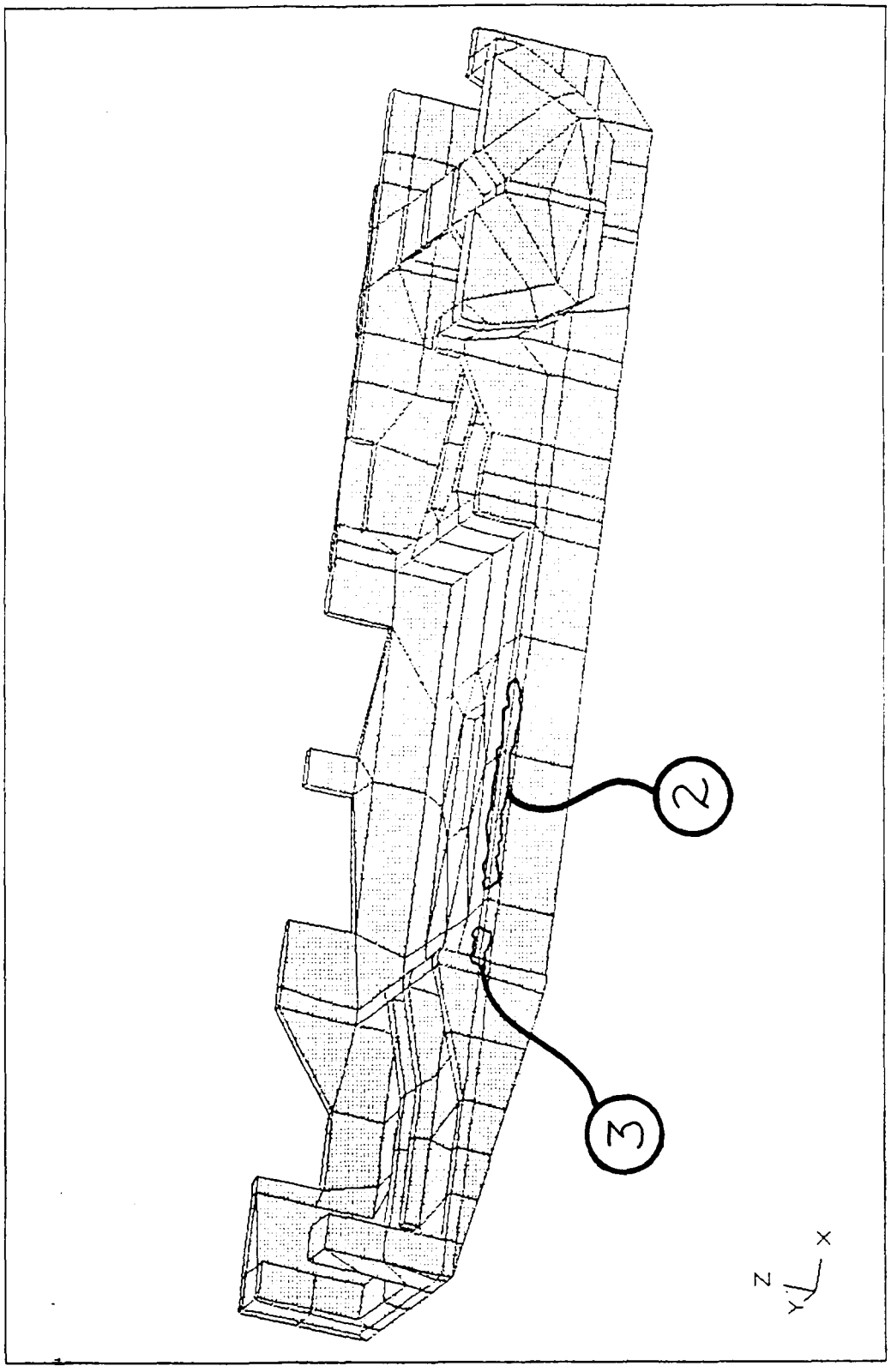

Figure 39. Positions On Draftsill Corresponding To Table 2 (Bottom View).

8.3.2 Load Case Two Results

Recall that in this load case the draftsill was being loaded to represent the hopper car being pushed by another car. The stresses generated were shown to remain very localized. Table 3 displays the three areas where the stress was concentrated and the levels to which it rose in each model. It should be noted that this load case generated the highest stress values of all the applied loads. The stress values obtained were extremely high which would tend to indicate localized yielding or failure in the rear ribs. Since this has not shown to be a problem area in the past, it must hold true that the draftsill casting does not actually encounter this magnitude of loading and, if it does, then only local yielding must be taking place. A more detailed visual understanding of the locations of these high stresses is shown in Figure 40, Figure 41 and Figure 42 which show the positions of the tabulated Von Mises stresses as they were generated on the final redesign model of the draftsill.

Table 3. Load Case Two Results, Stresses in kpsi (MPa).

Position on the F.E. Model	Original Linear	Original Parabolic	Redesign I Linear	Redesign II Linear	Redesign II Parabolic
1) The two rear ribs in the sidewall behind the rear draftlug.					
top rib-----	61 (420)	99 (682)	60 (413)	63 (434)	80 (551)
bottom rib-----	61 (420)	99 (682)	60 (413)	53 (365)	80 (551)
2) Bottom rib at a position just behind the rear draftlug	61 (420)	99 (682)	60 (413)	64 (441)	100 (689)
3) Area in the rear side wall where the sidewall and the perpendicular wall going to the centerpost meet	30 (206)	28 (193)	30 (206)	32 (220)	35 (241)

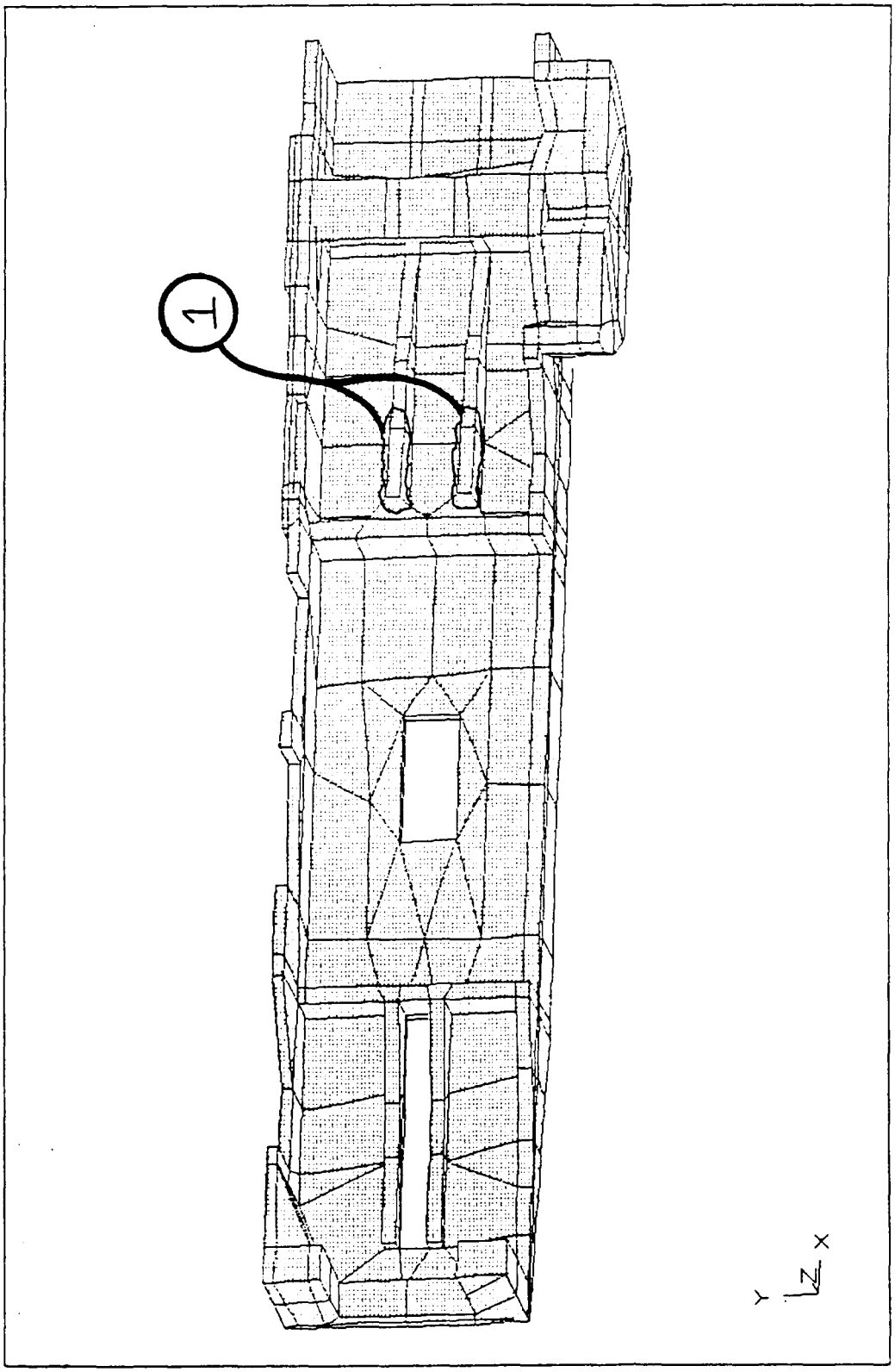

Figure 40. Positions On Draftsill Corresponding To Table 3 (Side View).

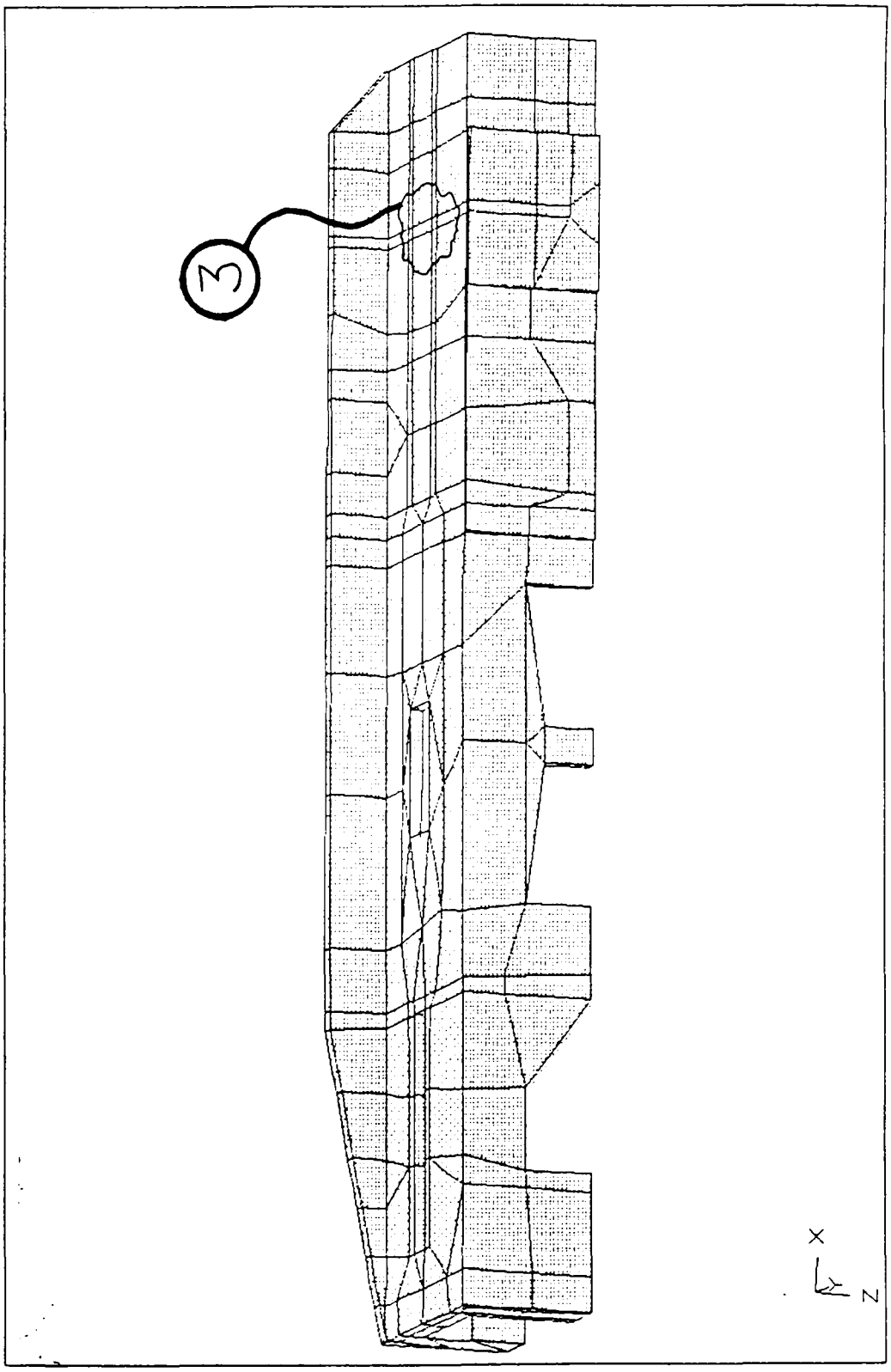

Figure 41. Positions On Draftsill Corresponding To Table 3 (Top View).

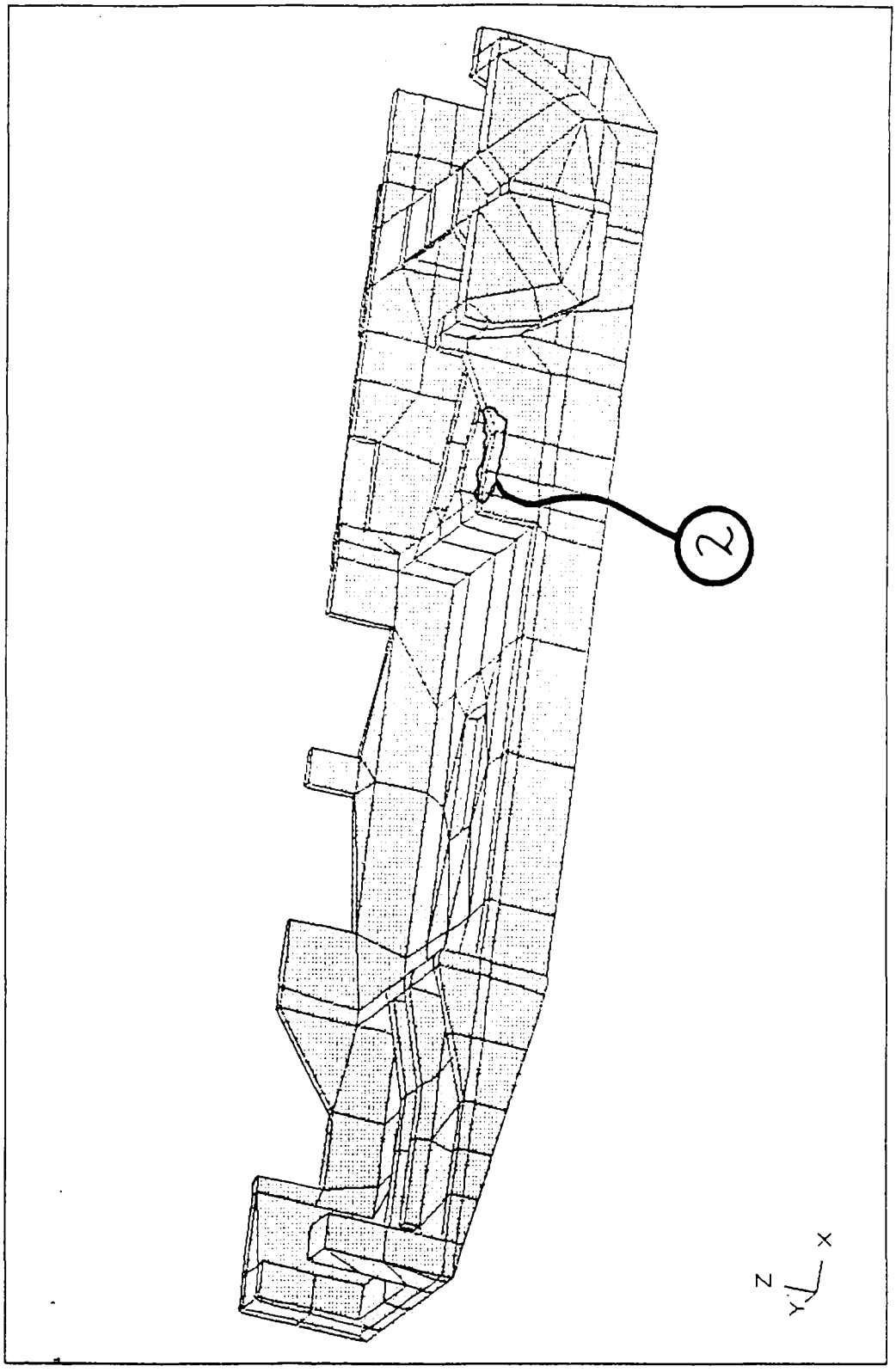

Figure 42. Positions On Draftsill Corresponding To Table 3 (Bottom View).

8.3.3 Load Case Three Results

Since this load case was superimposed onto all load cases for the last models created, it is no longer studied as an independent loading. Its effect is now accounted for in the results shown for Redesign II models listed in the tables of this section. This loading is not an applied load that is best analyzed independently because it is a constant loading situation as discussed before.

When looking at the stress magnitudes found from analysis of this loading as an independent load case the maximum stress levels were between 10,000 psi(69 MPa) and 18,000 psi(124 MPa). When compared to the stress magnitudes produced in the other load cases this load case showed low stress values. The technique used to produce these results was the application of a uniform displacement to the upper surface of the draftsill where the bolster beam and coverplate make contact.

8.3.4 Load Case Four Results

Here the draftsill was loaded to represent the hopper car being lifted by the coupler. In this load case the draftsill appeared to react like a beam and as such the majority of high stresses produced were at positions furthest from the centroid of the cross-section. Other regions of high stress were produced locally in areas where the loads were actually applied. Figure 43, Figure 44 and Figure 45 show the positions of interest in Table 4 as they correspond to the final draftsill model. Note here that there is a high stress region generated at the outer edge of the centerplate (position 2). This region of high stress may partially account for some of the failures that have occured in the past in this area of the draftsill.

Table 4. Load Case Four Results, Stresses in kpsi (MPa).

Position on the F.E. Model	Original Linear	Original Parabolic	Redesign I Linear	Redesign II Linear	Redesign II Parabolic
1) Top surface of the draftsill above and behind the rear draftlug(near the top hole)	44 (303)	39 (268)	61 (420)	34 (234)	39 (268)
2) Rear bottom of the draftsill near the centerplate and toward the sidewall on the frontend of the centerplate (45 degrees off center)	44 (303)	65 (448)	51 (351)	50 (344)	78 (537)
3) Bottom edge of the draft pocket where the rear draftlug, sidewall and outer flange meet	55 (381)	65 (448)	52 (358)	50 (344)	65 (448)
4) Lower rear rib at the center of its curvature	66 (455)	68 (468)	61 (420)	50 (344)	52 (358)
5) Upper corner where the striker face meets the vertical sidewall	55 (381)	78 (537)	51 (351)	50 (344)	78 (537)
6) Outer edge area of the outer flange at a position behind the rear draftlug	44 (306)	55 (379)	42 (289)	42 (289)	54 (372)
7) Mating outer edge between the sidewall and outer side flange at the rear of the draft pocket (on the outside surface)	44 (303)	52 (358)	42 (289)	42 (289)	53 (365)
8) Top surface of the draftsill above the draft pocket (near top holes)	34 (234)	39 (268)	41-51 (351)	42-50 (344)	60 (413)
9) Front of keyslot in the sidewall	30 (206)	78 (537)	32 (220)	34 (234)	78 (537)

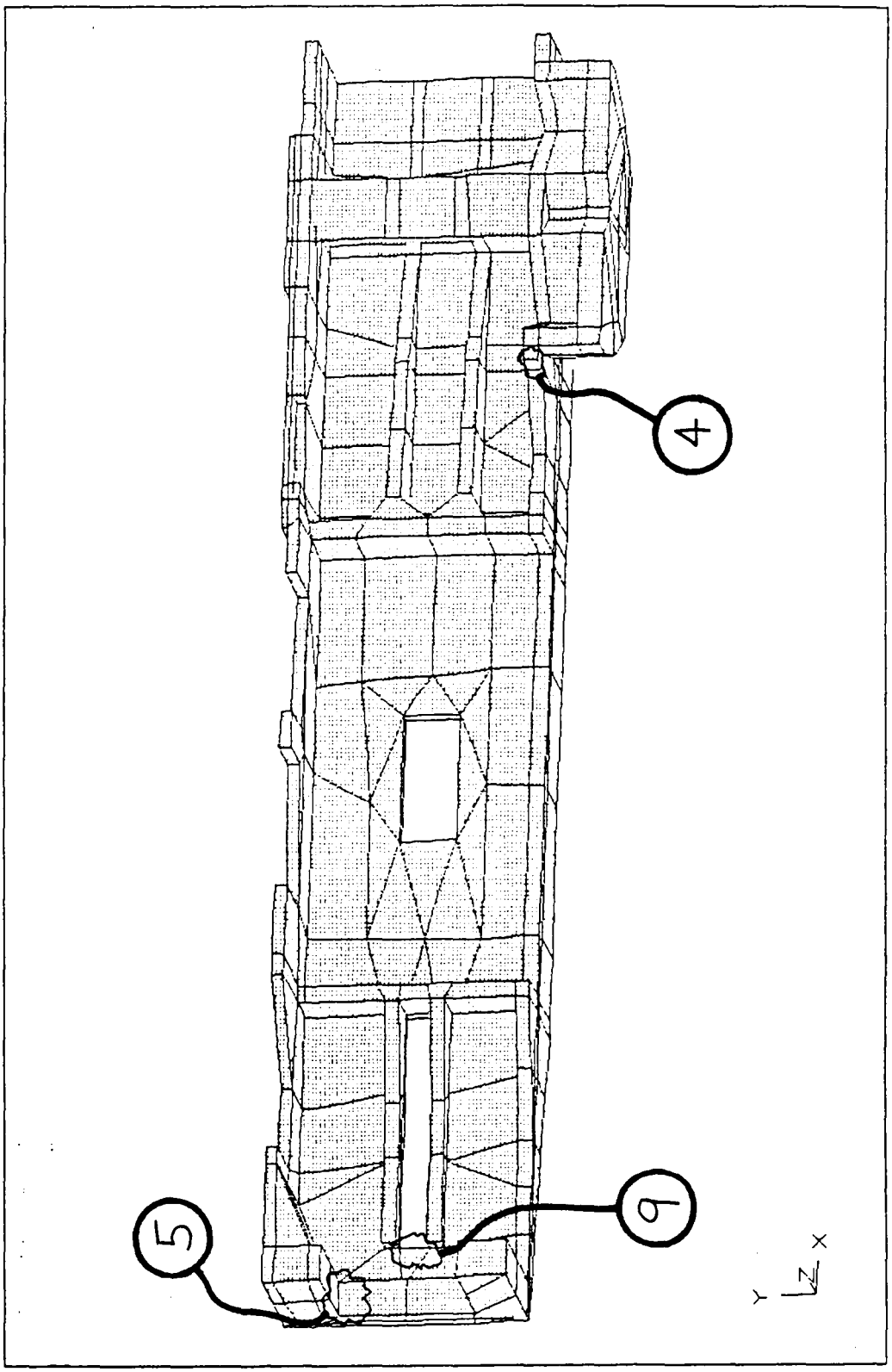

Figure 43. Positions On Draftsill Corresponding To Table 4 (Side View).

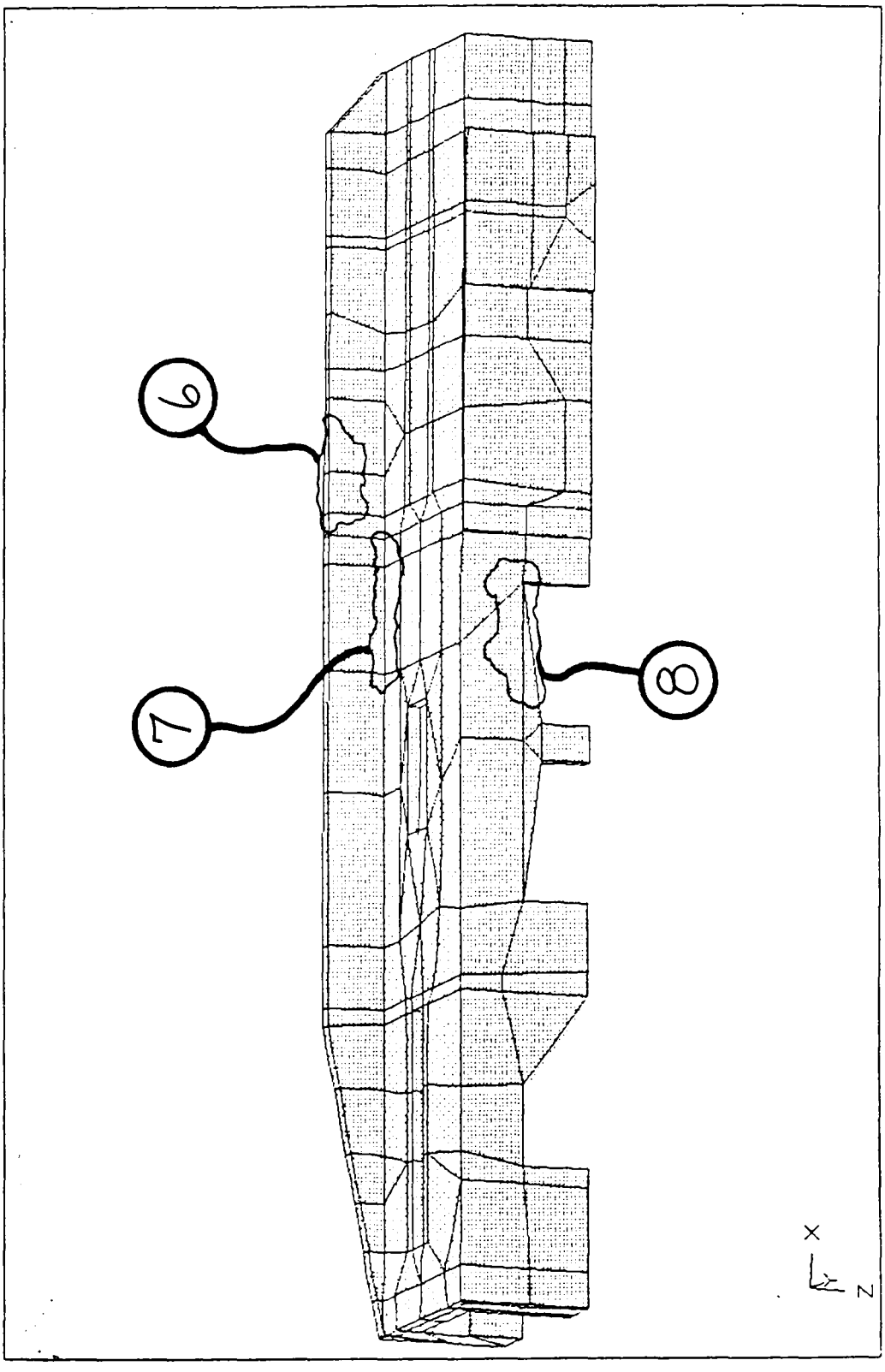

Figure 44. Positions On Draftsill Corresponding To Table 4 (Top View).

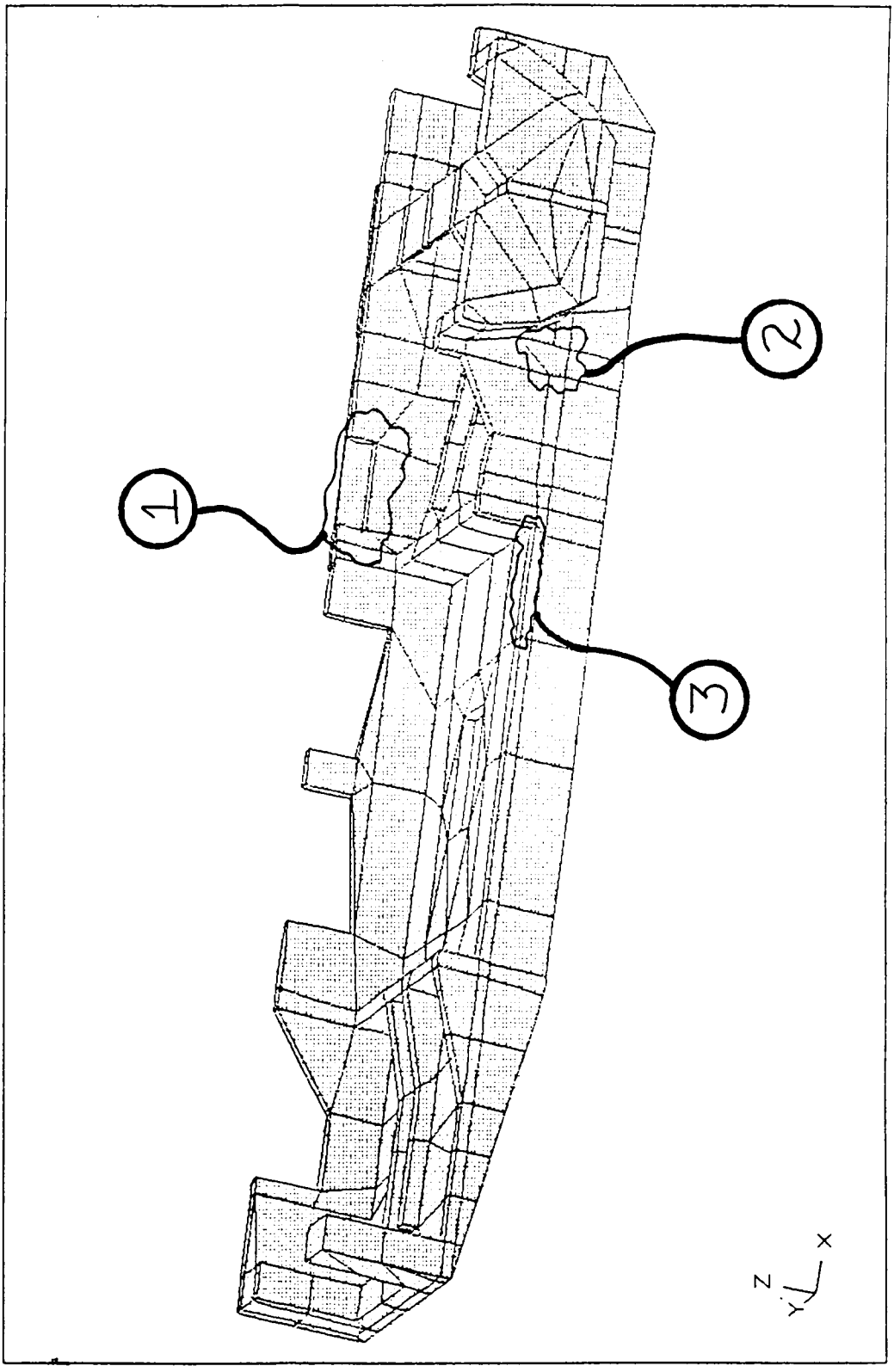

Figure 45. Positions On Draftsill Corresponding To Table 4 (Bottom View).

8.3.5 Load Case Five Results

Recall that in this loading situation the draftsill was being loaded with a downward vertical load to represent a large force applied to the coupler. The stress results were relatively low and consistant. They showed good convergence with all models and produce only small areas of high stress. Figure 46, Figure 47 and Figure 48 present the positions described in Table 5 as they apply to the final draftsill model. Note that positions 5 and 9 show the highest stresses, but note also that these are the positions of the load application and as such one would expect a high localized stress region, especially since the specified load magnitudes are so large.

Table 5. Load Case Five Results, Stresses in kpsi (MPa).

Position on the F.E. Model	Original Linear	Original Parabolic	Redesign I Linear	Redesign II Linear	Redesign II Parabolic
1) Top surface of the draftsill above and behind the rear draftlug(near the top hole)	25 (172)	25 (172)	35 (241)	18 (124)	27 (186)
2) Rear bottom of the draftsill near the centerplate and toward the sidewall on the frontend of the centerplate (45 degrees off center)	25 (172)	30 (206)	30 (206)	29 (199)	45 (310)
3) Bottom edge of the draft pocket where the rear draftlug, sidewall and outer flange meet	31 (213)	35 (241)	35 (241)	29 (199)	35 (241)
4) Lower rear rib at the center of its curvature	37 (255)	30 (206)	35 (241)	35 (241)	27 (186)
5) Lower mating surface of the striker and draftgear (place of load application)	31 (213)	80 (551)	30 (206)	29 (199)	81 (558)
6) Outer edge area of the outer flange at a position behind the rear draftlug	25 (172)	35 (241)	29 (199)	24 (165)	35 (241)
7) Mating outer edge between the sidewall and outer side flange at the rear of the draft pocket (on the outside surface)	25 (172)	30 (206)	29 (199)	29 (199)	35 (241)
8) Top surface of the draftsill above the draft pocket (near top holes)	24 (165)	25 (172)	27 (186)	29 (199)	35 (241)
9) Front of keyslot in the sidewall	30 (206)	65 (448)	29 (199)	29 (199)	58 (399)

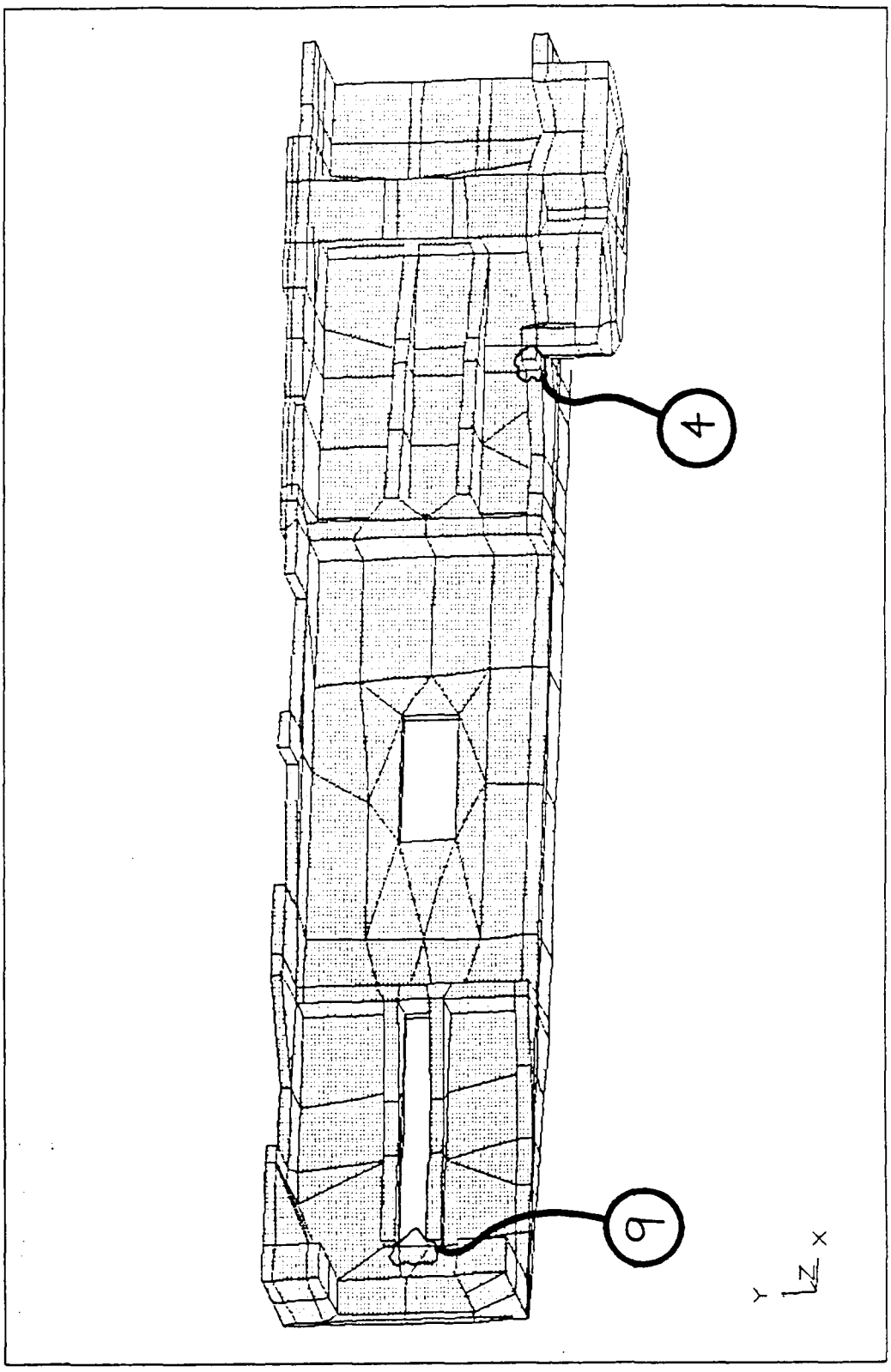

Figure 46. Positions On Draftsill Corresponding To Table 5 (Side View).

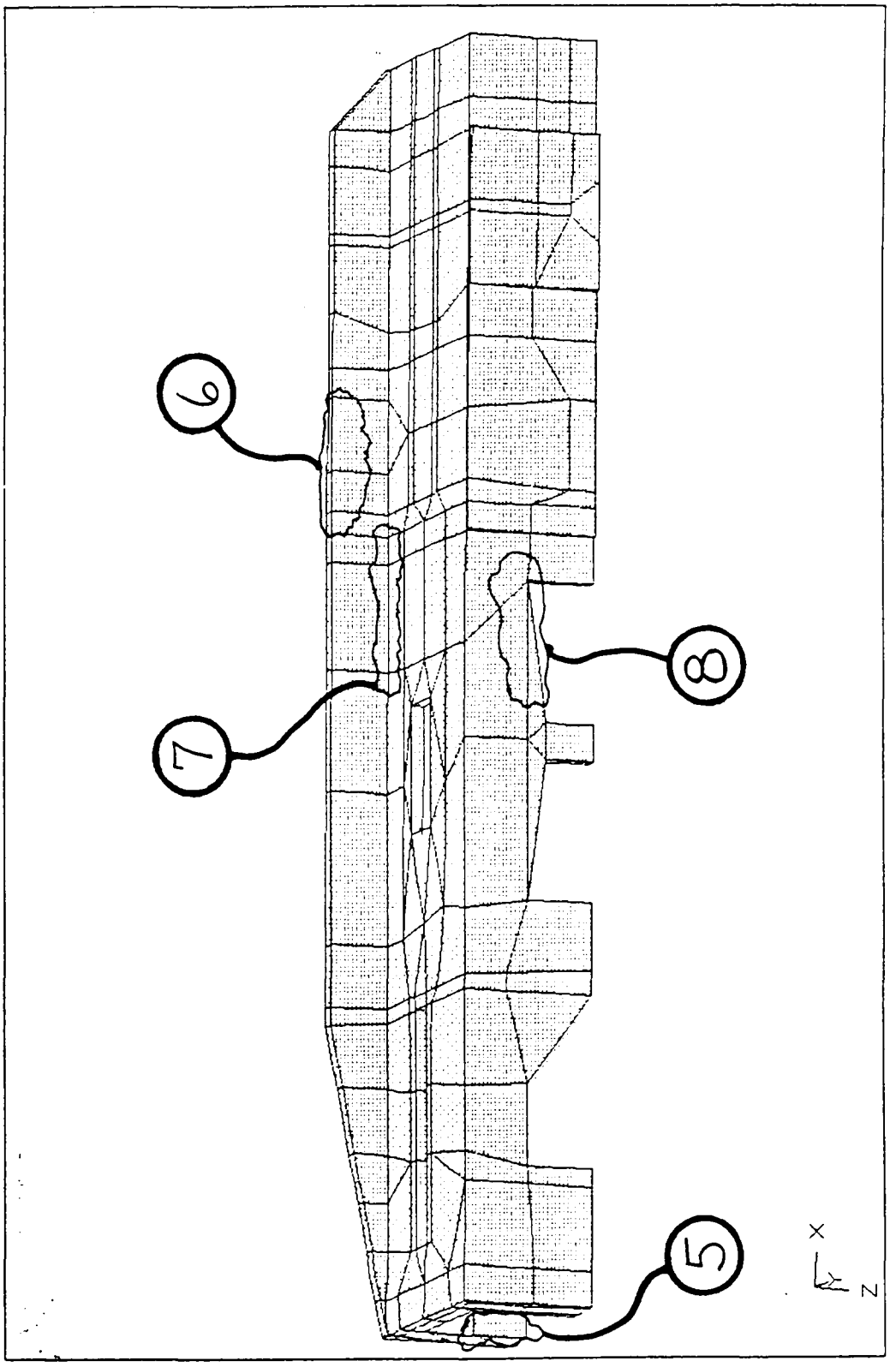

Figure 47. Positions On Draftsill Corresponding To Table 5 (Top View).

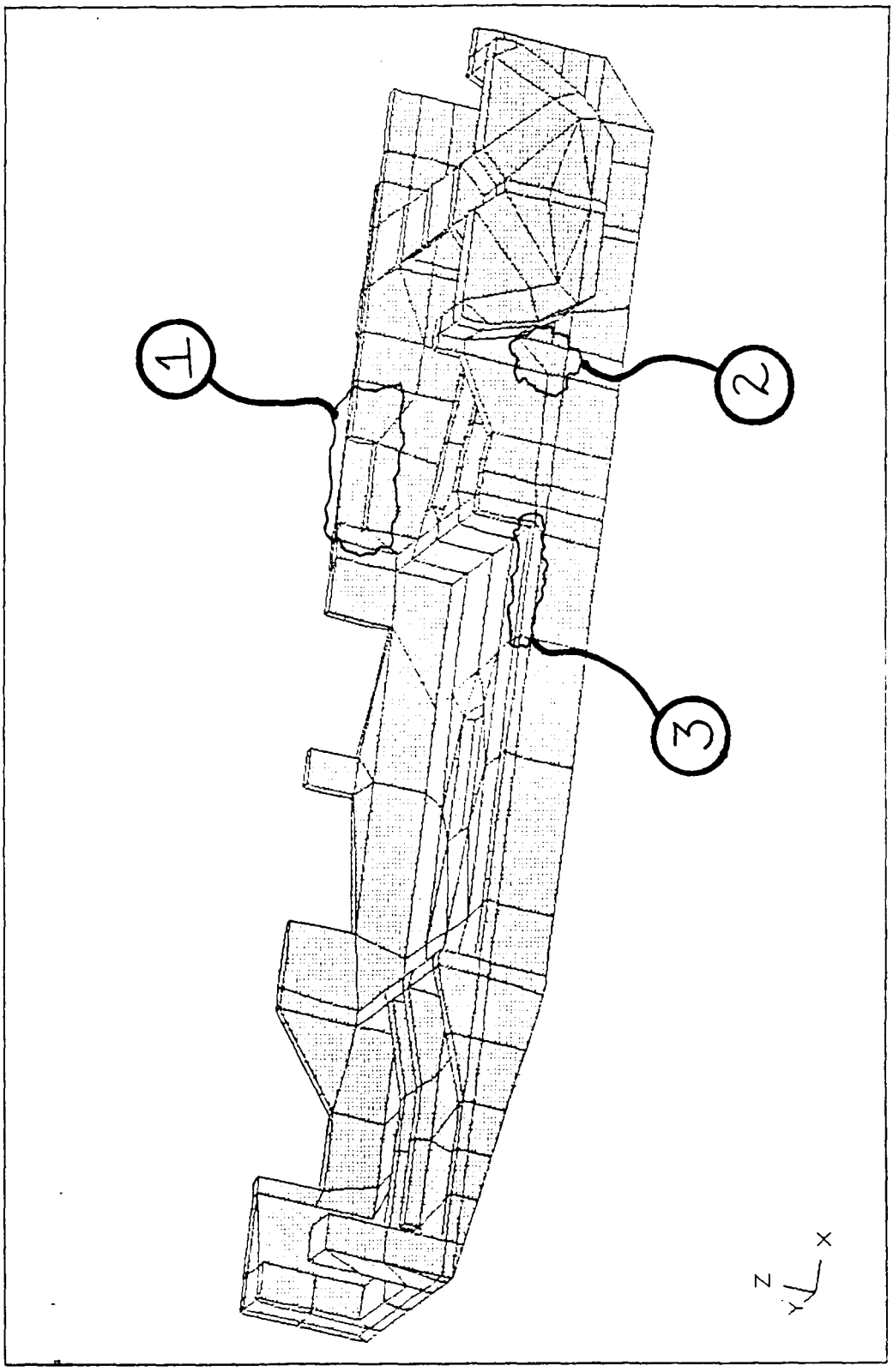

Figure 48. Positions On Draftsill Corresponding To Table 5 (Bottom View).

8.4 *Pressure Redistribution Analysis*

Once the complete draftsill casting had been analyzed, attention was turned to the pressure distributions applied in the draftlug load cases. The purpose of this part of the research was to determine if an alternative distribution of the pressure caused by the follower block, on the draftlug, was warranted. In developing the recommended taper suggested, three alternative pressure loadings were applied to the front draftlug. Each of the redistributions studied were done using the parabolic finite element models so the pressures could be controlled more accurately via the midside nodes. These clearly presented an indication that if the center of the applied load pressure could be moved toward the sidewall of the draftsill casting then the high stress levels could be reduced by a significant amount. The different loadings applied were as follows:

1. The original application of uniform pressure was changed to no longer cover the bottom element face of the draftlug to more nearly match the follower block contact area. For this application the load pressure was increased, but still remained constant over the area of application.

2. The applied pressure distribution was changed to parabolic from the center of the draftlug to its outer edge (the edge not connected to the sidewall), while the segment of the loading from the center to the sidewall remained a constant pressure. This choice of application was made to follow up on the idea that a possible taper of the draftlug face would redistribute the current high stresses.

3. The third and last loading was a triangular pressure distribution sloping from the sidewall to a magnitude of zero at the outer edge of the draftlug. (the outer edge being the edge not connected to the sidewall)

The application of these three loading distributions are shown in Figure 51. This figure shows the approximate pressure center for each of these situations along with the pressure magnitudes applied to the draftlug. Note that the original and first redistribution produce the same load center because of their parabolic application, but their load magnitudes differ because the second removes the pressure on the bottom element of the draftlug.

By moving the load center closer to the sidewall of the draftsill, the Von Mises stresses created were reduced by 20 percent or more throughout the high stressed region. This is shown more clearly in Table 6 on page 104 which presents a comparison of the stress levels obtained for each redistribution and their respective positions on the draftsill (refer to Figures 49 and 50) to the original application of load case one.

It is recommended that the draftlug face be tapered. The technique used to calculate the recommended taper was as follows:

1. The follower block was analyzed as a two dimensional finite element model from which its deflections were found.

2. From the analysis of the third redistribution (the triangular loading), the deflections for the draftlug were calculated.

3. The difference between the slope of the follower block and the draftlug was then taken to be the amount of taper needed to create a triangular pressure distribution.

Following these listed steps, the value calculated for a taper was 0.013 in.(0.033 cm). This is an unrealistic number in terms of actual application to the draftsill, so the alternative recommendation is to relieve the draftlug face by 0.025 - 0.050 inches(0.0635 - 0.127 cm) from the face center outward. These calculations and applications are more clearly seen in Figure 52 on page 108 which displays the specific deflections and recommended taper values obtained.

Table 6. Pressure Redistribution Stress Levels in kpsi (MPa).

Position on Final F.E. Model	Original Parabolic	Redist. 1 Parabolic	Redist. 2 Parabolic	Redist. 3 Parabolic	%Diff, Orig. vs. Redist3
1) Keyslot ribs	91 (627)	96 (661)	85 (586)	71 (489)	22
2) Mating edge of sidewall and outer flange	50 (344)	45 (310)	43 (296)	40 (275)	20
3) Bottom corner between draftlug and sidewall	90 (620)	80 (551)	56 (386)	60 (413)	33
4) Center of the front draftlug	35 (241)	33 (227)	28 (193)	24 (165)	31
5) Top of the draftsill near the top holes	30 (206)	33 (227)	28 (193)	23 (158)	23
6) Outer area of the outer flange	40 (275)	35 (241)	35 (241)	40 (275)	0
7) Diagonal area between the sidewall hole and draftlug	60-90 (620)	50 (344)	28-50 (344)	35-55 (379)	40

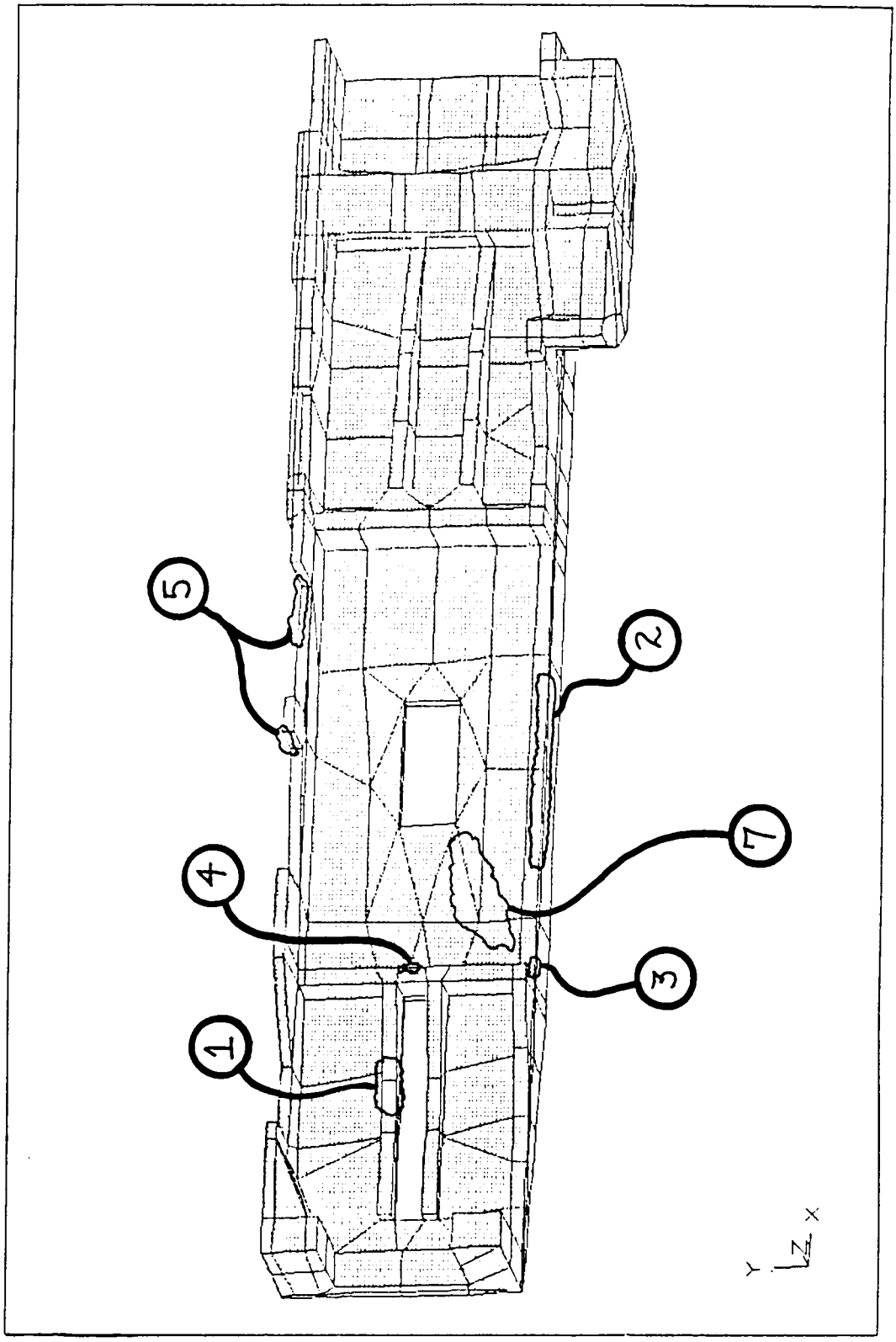

Figure 49. Positions On Draftsill Corresponding To Table 6 (Side View)

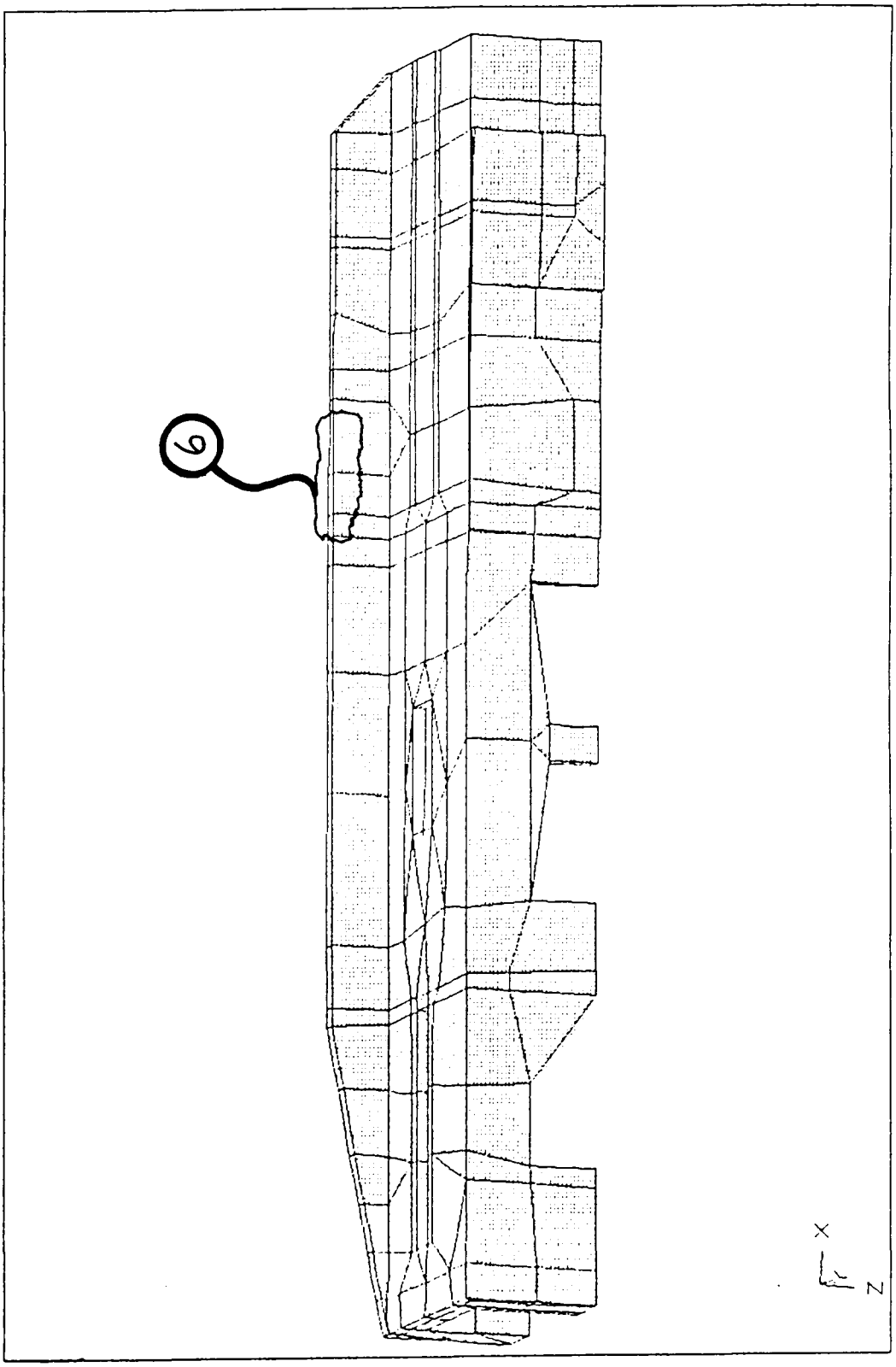

Figure 50. Positions On Draftsill Corresponding To Table 6 (Top View).

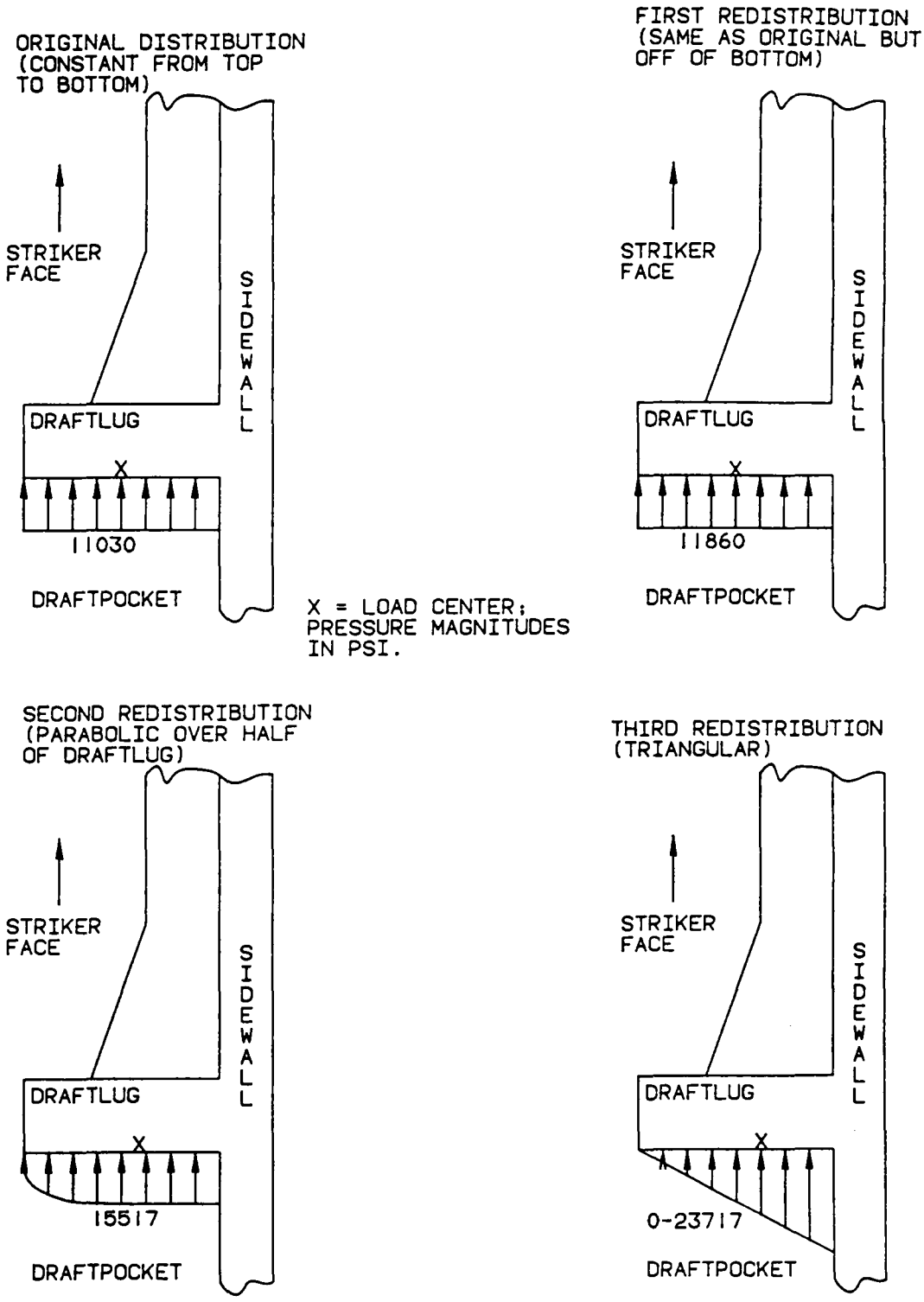

Figure 51. Pressure Redistributions on Front Draftlug (top view).

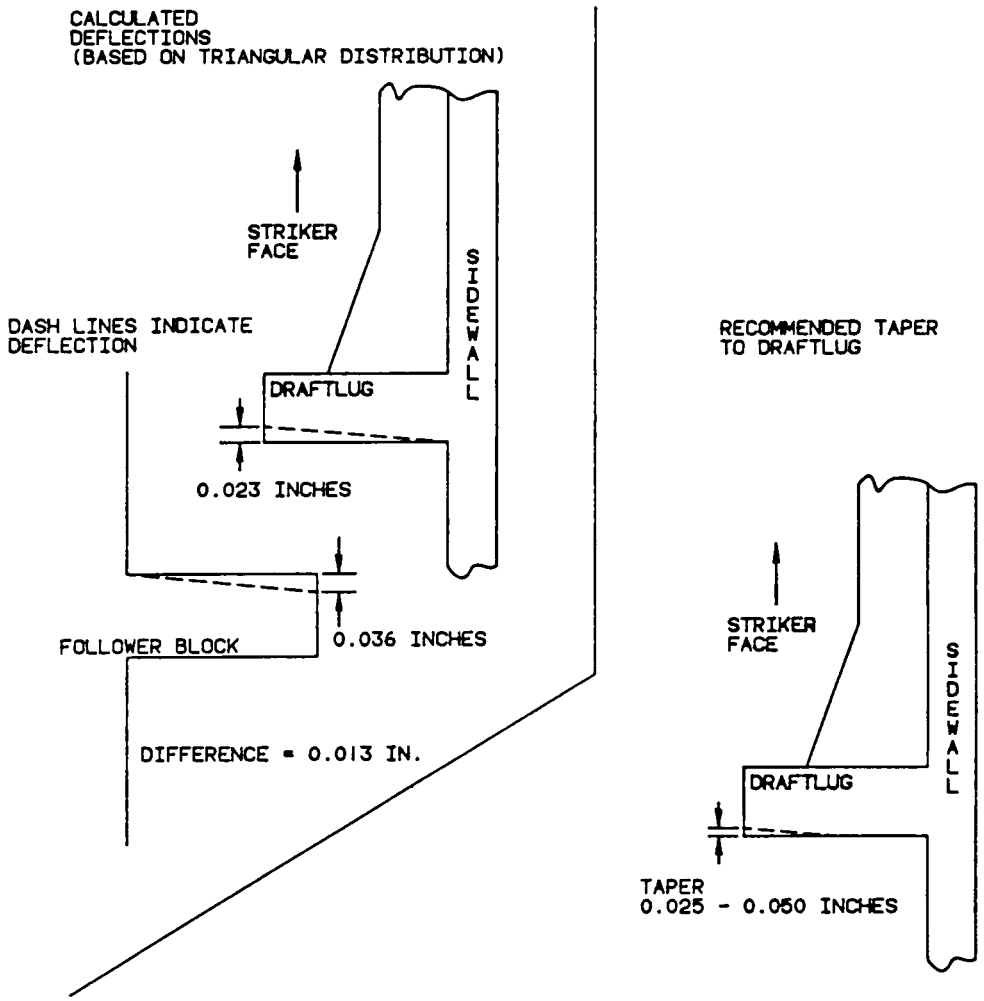

Figure 52. Draftlug Taper Calculations and Recommendations.

8.5 *Sample Calculations*

Having generated results, one must determine if those results are to be considered valid. For this reason an engineer must do sample calculations to find out if the finite element solutions are in the right magnitude and range of the actual solution. Because of the complexity of the draftsill structure one cannot directly find a mathematical solution, but doing sample calculations produces a way to justify the computer solution magnitudes.

The sample calculations used for the draftsill were done based on load case 4 (Carbody Lift) because it could most realistically be simplified to a mathematical model. Both deflections and stress calculations were made. These calculations were based on classical beam theory in which the draftsill's cross section (Figure 53) was assumed to be constant along the length of the beam. This was a valid assumption since the draftsill in reality has a rather constant cross section when looking specifically at its outerwalls. All data for the cross section of the beam, i.e., moment of inertia were calculated using CADAM's beam analysis features (11). The calculated results indicated that the generated finite element solution, based on the original parabolic model, were in reasonable agreement with the values produced using beam theory. This is shown more clearly in Table 7 which displays both the finite element solution values and the sample calculation values obtained.

Table 7. Sample Calculations As Compared To Finite Element Results.

Calculation Type	Deflections	Bending Stress
1) Finite Element Solution From Original Model.	0.4 in. (1 cm)	45-47 kpsi (324065 kPa)
2) Sample Calculations Based On Beam Theory(Appendix C)	0.6 in. (1.5 cm)	51 kpsi (350 MPa)

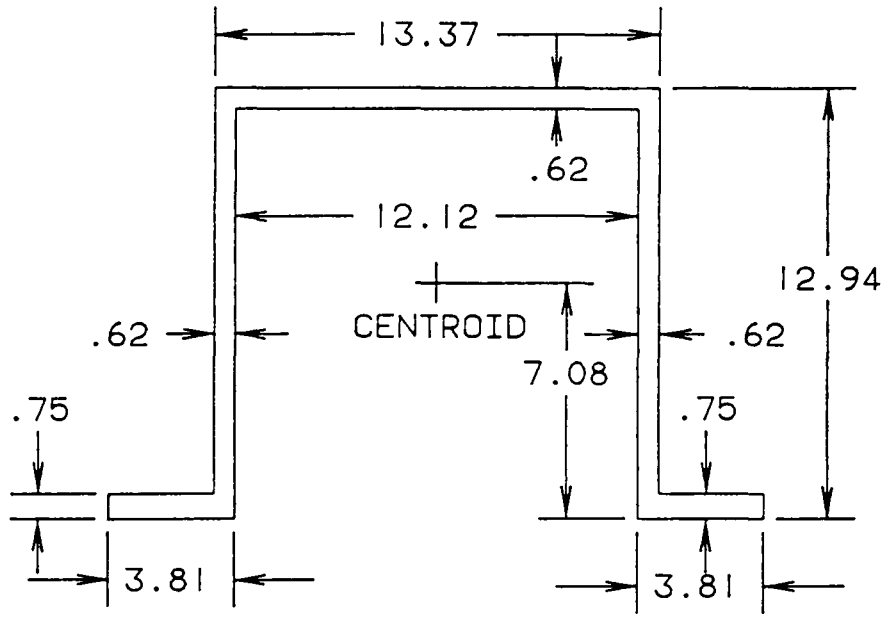

AREA = 28.5306

I X-X= 679.959

I Y-Y= 1082.514

Figure 53. Cross Section And Properties Of Beam Used In Sample Calculations.

Specifically, the values for deflection were calculated at the striker face end of the draftsill while the stress values were calculated on the lower surface of the outer flange in line with the rear draftlugs. A more detailed presentation of the sample calculations made is shown in Appendix C.

Since these results produced good agreement with the finite element solution a confidence could be justified in the solutions obtained provided they met the convergence criteria.

8.6 Conclusions and Recommendations

In presenting the results of this finite element analysis and redesign, this author has tried to show a justification that the values obtained were generated with confidence and not just results assumed be correct. By using model checking, sample calculations and convergence studies it is felt that the values generated are accurate and sound. This is not to say that the obtained results are exact because the method of finite elements is a mathematical approximation technique and therefore produces only relatively close approximations of the true reaction of the draftsill to the prescribed loading conditions. These results show that as well as redesigning the draftsill for a reduction in weight (106 lbs(472 N)) the work done was carried further to a point which also indicated that tapering the front draftlug (0.025 - 0.050 in.(0.0635 - 0.127 cm)) would relieve some of the high stresses generated in the draftsill. These final design changes and recommendations are shown specifically in the modified draftsill blueprints in Appendix A.

Some alternative ideas that involved the creation of a whole new finite element model might have been incorporated had a 3-D mesh generator been available. Since this was not the case, these ideas must be mentioned as possible alternatives for future study. The following is such a listing of ideas:

1. Move the rear sidewalls, which are located behind the rear draftlugs, inward to the load center of the rear draftlugs.

2. Similarly, move the front sidewalls, which are located infront of the front draftlugs, inward to the load center of the front draftlugs. Although these ideas involve modification of other components of the draftsill-draftgear assembly, they are ideas that could possibly make a very significant difference in the draftsill-draftgear system's effectiveness.

3. Another idea for future study is to consider the possibility of reducing all wall thicknesses by a small amount. It is this type of change that makes the quickest difference in weight and volume reduction.

4. Also, a closer analysis of the keyslot ribs might show an alternative design to reduce out the high localized stresses that are occuring in the current design.

5. Investigate the possibly of using a three-dimensional shape optimizer as design tool.

6. Examine the possibility of removing the outer side flange.

References

1. McNally, G. S., S. H. Lee, and J.L. Dehner. "The Impact of Finite Element Analysis on the Railroad Industry." *Intersociety Conference on Transportation.* 4th Annual. Proceedings. New York: A.S.M.E., July 18-23, 1976.

2. Robinson. *Understanding Finite Element Stress Analysis.* England: Robinson and Associates.

3. Imam, M. H. "Minimum Weight Design of 3-D Solid Components." *2nd International Computers in Engineering Conference.* San Diego, California, Vol.2, pp.210-215, 1982.

4. Sussman, and Bathe. "Studies of Finite Element Procedures--On Mesh Selection." *Computers and Structures.* Vol. 21, No. 1/2, pp. 257-264, 1985.

5. Cook, R. D. *Concepts and Applications of Finite Element Analysis.* 2nd Edition. New York: John Wiley and Sons, 1981.

6. *Superb User Manual 6.0.* Structural Dynamics Research Corporation, 1983.

7. Zienkiewicz, O. C. *The Finite Element Method.* 3rd Edition. New York: McGraw-Hill Book Company, 1977.

8. Knight, C. E. *M. E. 4980 Class Notes.* Virginia Polytechnic Institute & State University, Fall 1986.

9. Newton, R. E. "Degeneration of Brick-Type Isoparametric Elements." *IJNME,* Vol. 7, No. 4, 1973, pp. 579-581.

10. Shigley, and Mitchell. *Mechanical Engineering Design.* 4th Edition. New York: McGraw-Hill Book Company, 1983.

11. *IBM CADAM SOFTWARE.* 1986 Release.

Appendix A

Detailed Drawings

Included in this section are the following:

1. Blueprint of the original draftsill casting.

2. Blueprint of the original draftsill casting showing the final design changes made.

   X -- Indicates material that is to be removed.

3. Blueprint showing a cross-section of the draftgear assembly as it fits into the draftsill.

4. Overall drawing showing how the draftsill fits into the hopper car.

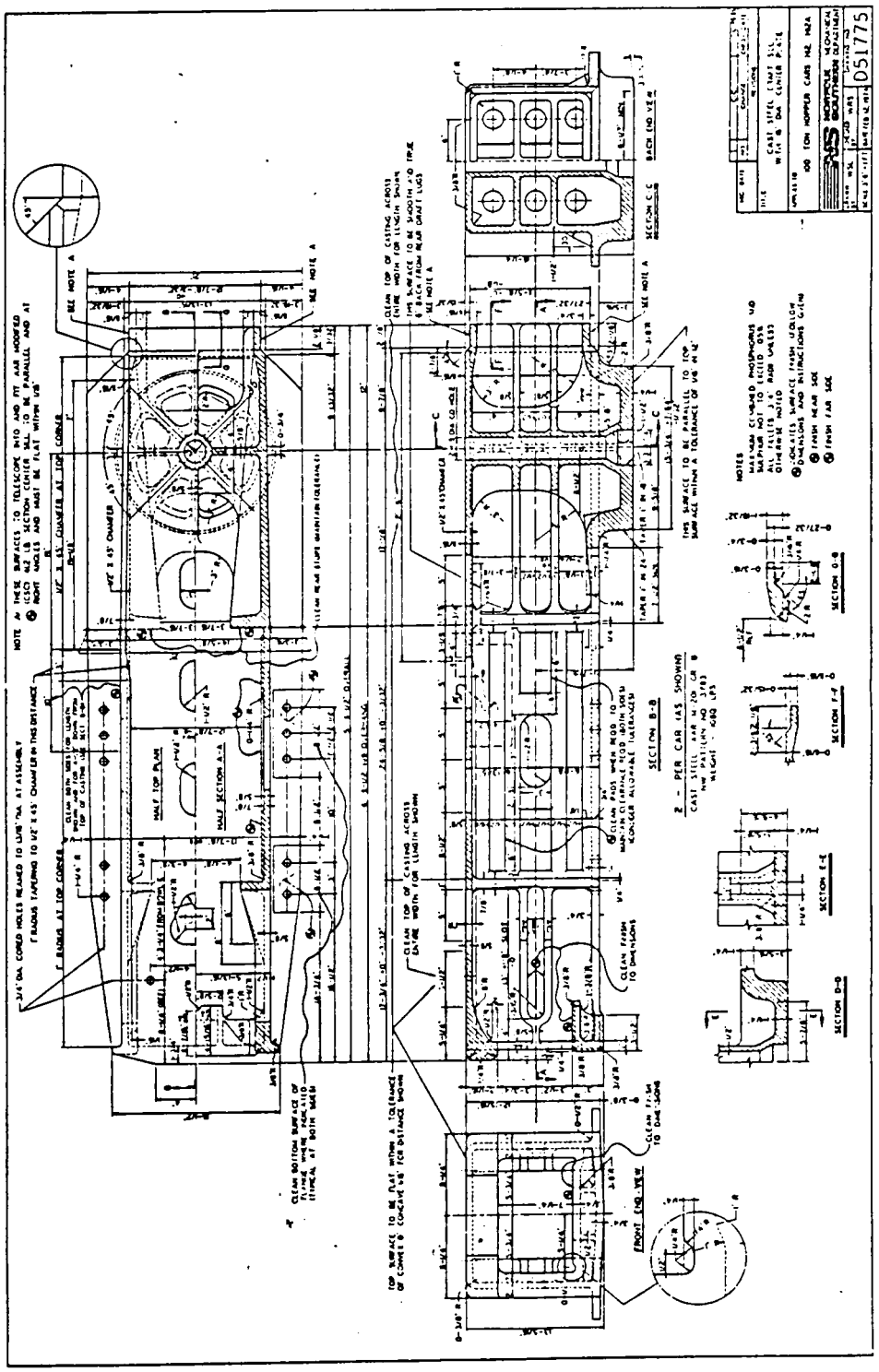

1. Blueprint of the original draftsill casting.

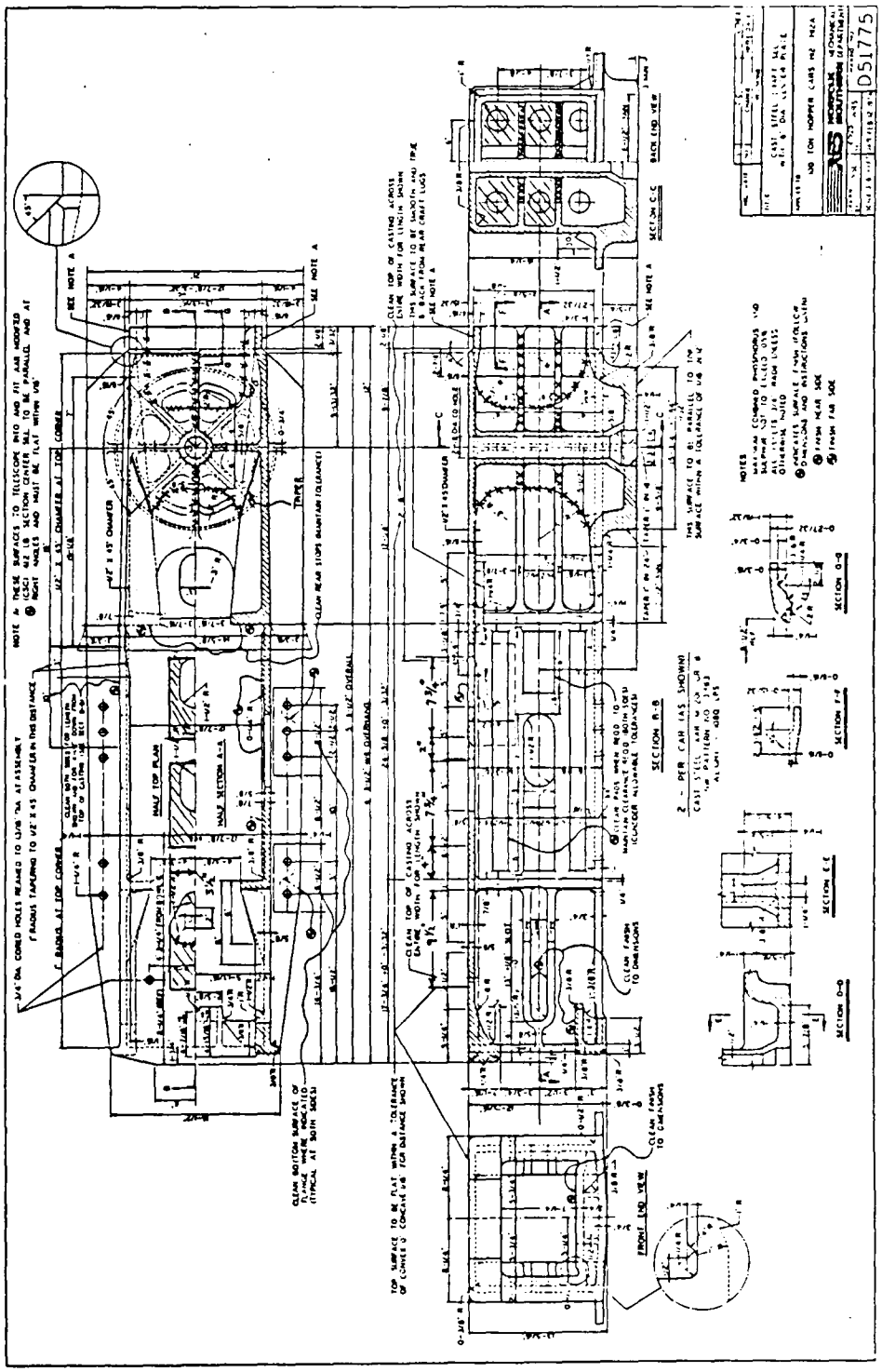

2. Blueprint of the original draftsill casting showing the final design changes made.

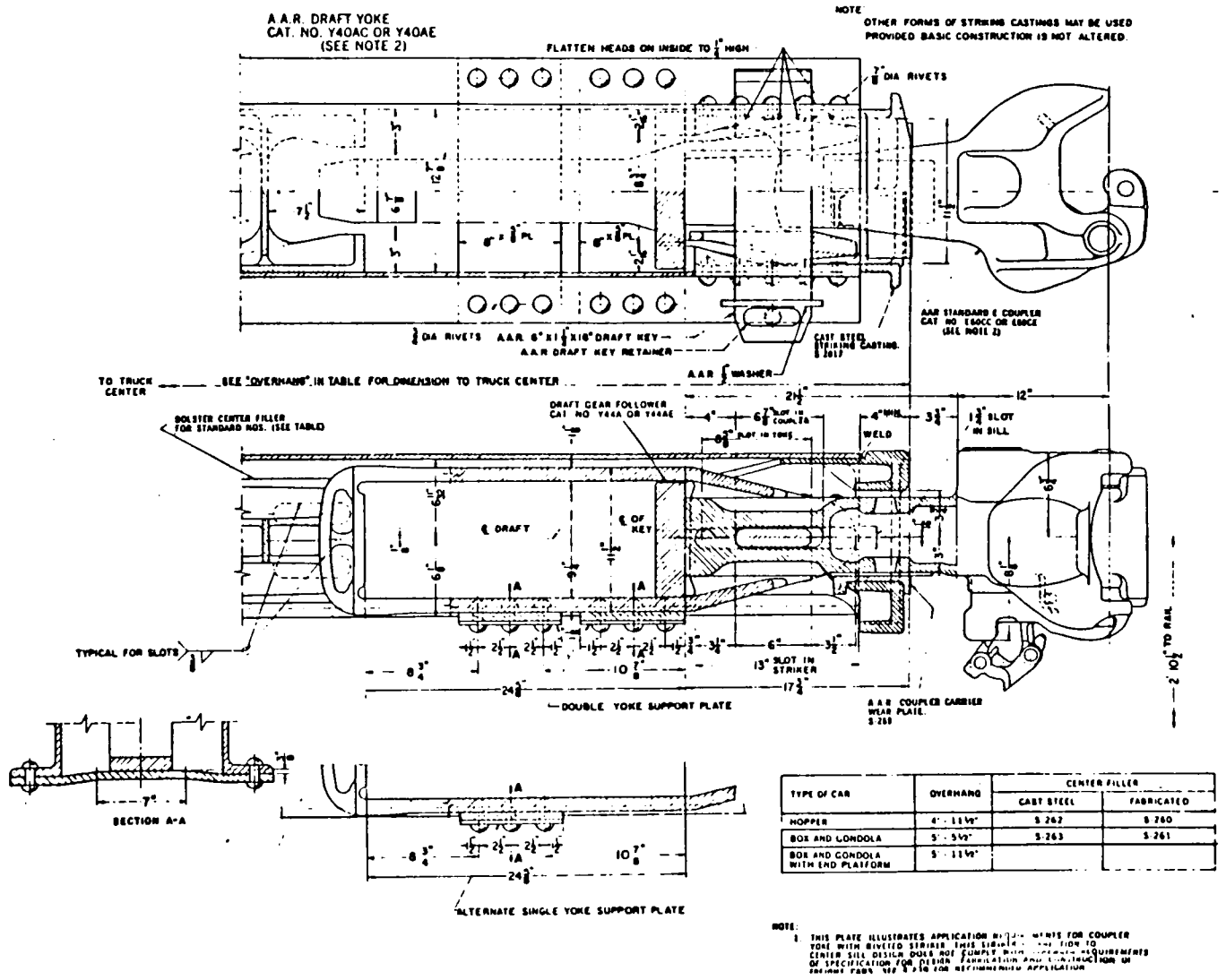

3. Blueprint showing a cross-section of the draftgear assembly as it fits into the draftsill.

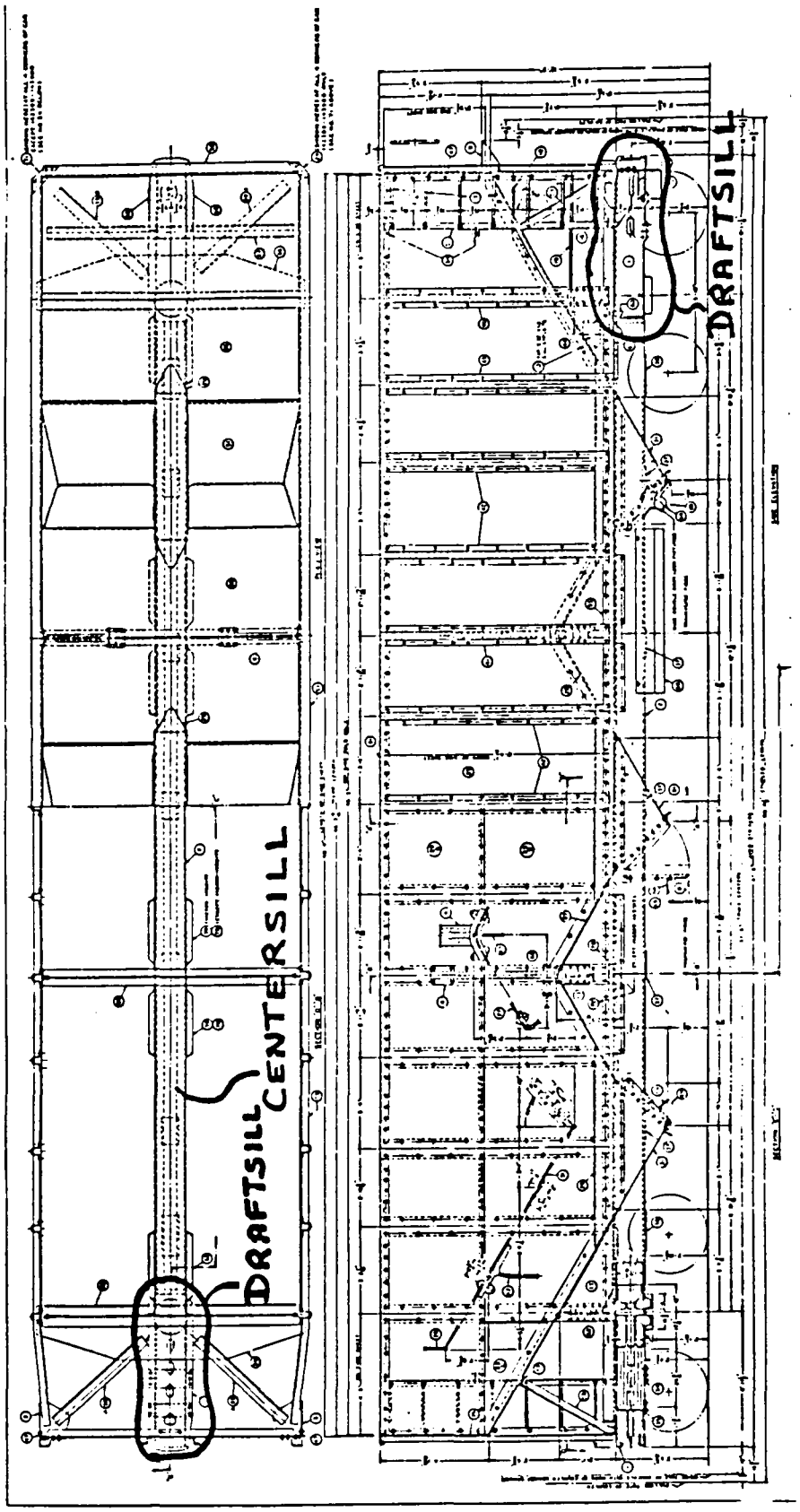

4. Overall drawing showing how the draftsill fits into the hopper car.

Appendix B

Composite and Restraint Creations Codes

Presented in this section are the actual codes discussed in the previous chapters of this work. There are two codes shown:

1. COMPOSITE STRESS PLOT code.

2. RESTRAINT CREATION code.

These codes are documented for easy understanding as to what is occuring as the code operates.

COMPOSITE STRESS PLOT code.

```
C234567
CCCCCCCCCCCCCCCCCCCCCCCCCCCCCCCCCCCCCCCCCCCCCCCCCCCCCCCCCCCCCCCCCCCC
C
C
C  THE PURPOSE OF THIS PROGRAM IS TO IDENTIFY THE AVERAGE
C  STRESS AT EACH NODE FOR EACH OF THE FIVE LOAD CASES.
C  THEN FIND THE VON MISES STRESSES FOR THAT NODE FOR
C  EACH OF THE FIVE LOAD CASES. THE HIGHEST OF THE VON MISES
C  STRESS VALUES DICTATES WHICH NODAL STRESSES ARE THEN
C  TO BE READ INTO I-DEAS.
C
C
CCCCCCCCCCCCCCCCCCCCCCCCCCCCCCCCCCCCCCCCCCCCCCCCCCCCCCCCCCCCCCCCCCCC
C
C
C   DIMENSIONING ARRAYS

      DIMENSION ICON(500,50),IEL(500),STRESS(4000,6)
      DIMENSION STRESSNODE(4000,6),INODE(4000),STRESSNODE1(4000,6)
      DIMENSION STRESSNODE2(4000,6),STRESSNODE3(4000,6)
      DIMENSION STRESSNODE4(4000,6),STRESSNODE5(4000,6)
      DIMENSION STRESSNEW(4000,6)
      DIMENSION IELNO(500)

C
C DEFINING THE INPUT/OUTPUT CODES
C
      IO=30
      IN=20


C
C READING FROM THE SCREEN NO. OF EL,NO.OF NODES, NO. OF LOAD CASES
C (THIS WILL READ ALL ELEMENTS IN THE UNV. FILE AND WILL
C  EXCLUDE THE EL. NO. EXCLUDED IN THE UNIVERSAL FILE
C  CREATION. THE ELEMENTS THAT ARE SPRING ELEMENTS ARE NOT COUNTED
C  IN THE TOTAL NUMBER OF ELEMENTS.)
C

      WRITE(6,*)' ENTER THE NO. OF ELEMENTS IN MODEL: '
      READ(5,*)NUMEL

      WRITE(6,*)
      WRITE(6,*)
      WRITE(6,*)'ENTER THE NO. OF NODES IN THE MODEL: '
      READ(5,*)NUMNODE

      WRITE(6,*)
      WRITE(6,*)
      WRITE(6,*)' ENTER THE NO. OF LOAD CASES TO BE CONDENSED: '
      READ(5,*)NLOAD


C
C
C  READING ELEMENT CONNECTIVITY
C
C
```

```
      DO 100 I=1,NUMEL

      READ(IN,*)NOEL,IFL1,IFL2,IMAT,IFL3,IFL4,NODE
      IELNO(I)=NOEL

      IF(NODE.EQ.20)GO TO 50
      IF(NODE.EQ.8)GO TO 48
      IF(NODE.EQ.6)GO TO 45

      READ(IN,*)(ICON(NOEL,J),J=1,8)
      READ(IN,*)(ICON(NOEL,J),J=9,15)
      IEL(NOEL)=NODE

      GO TO 100

   45 CONTINUE

      READ(IN,*)(ICON(NOEL,J),J=1,6)
      IEL(NOEL)=NODE

      GO TO 100

   48 CONTINUE

      READ(IN,*)(ICON(NOEL,J),J=1,8)
      IEL(NOEL)=NODE

      GO TO 100

   50 CONTINUE

      READ(IN,*)(ICON(NOEL,J),J=1,8)
      READ(IN,*)(ICON(NOEL,J),J=9,16)
      READ(IN,*)(ICON(NOEL,J),J=17,20)
      IEL(NOEL)=NODE

  100 CONTINUE

C
C  LOAD LOOP FOR EACH LOAD CASE
C

      DO 500 K=1,NLOAD



C
C ZEROING STRESSNODE ARRAY
C
      DO 150 I=1,NUMNODE
      DO 160 J=1,6

      STRESSNODE(I,J)=0.0

  160 CONTINUE
  150 CONTINUE

C
C  READING STRESSES
C
```

```
      DO 200 I=1,NUMEL

      READ(IN,*)NOEL,IFL1,NODE,IFL2

      DO 220 I1=1,NODE

      READ(IN,*)(STRESS(ICON(NOEL,I1),J),J=1,6)

      DO 230 J1=1,6

      STRESSNODE(ICON(NOEL,I1),J1)=STRESSNODE(ICON(NOEL,I1),J1)
     ++STRESS(ICON(NOEL,I1),J1)

  230 CONTINUE
  220 CONTINUE
  200 CONTINUE


C
C  DEFINING THE NO. OF TIMES EACH NODE IS USED BY AN ELEMENT
C
      IF(K.GT.1)GO TO 390


      DO 300 I=1,NUMEL
      L=IELNO(I)

      DO 320 J=1,20

      KTEMP=ICON(L,J)
      IF(KTEMP.EQ.0)GO TO 300

      INODE(KTEMP)=INODE(KTEMP)+1

  320 CONTINUE
  300 CONTINUE
  390 CONTINUE

C
C AVERAGING THE STRESSES AT EACH NODE
C

      DO 400 I=1,NUMNODE

      DO 410 J=1,6

      IF(INODE(I).EQ.0)WRITE(6,*)I
      IF(INODE(I).EQ.0)GO TO 400


      STRESSAV=STRESSNODE(I,J)/FLOAT(INODE(I))

      GO TO(420,430,440,450,460)K

  420 CONTINUE

      STRESSNODE1(I,J)=STRESSAV

  430 CONTINUE
```

```
      STRESSNODE2(I,J)=STRESSAV

  440 CONTINUE

      STRESSNODE3(I,J)=STRESSAV

  450 CONTINUE

      STRESSNODE4(I,J)=STRESSAV

  460 CONTINUE

      STRESSNODE5(I,J)=STRESSAV

  410 CONTINUE
  400 CONTINUE

C
C  NEW LOAD VALUE
C
  500 CONTINUE

C
C DEFINING THE STRESSES AT EACH NODE FOR EACH LOAD CASE
C TO BE USED IN THE VON MISES CALCULATIONS.
C

      DO 600 I=1,NUMNODE


      S11=STRESSNODE1(I,1)
      S12=STRESSNODE1(I,2)
      S13=STRESSNODE1(I,3)
      S14=STRESSNODE1(I,4)
      S15=STRESSNODE1(I,5)
      S16=STRESSNODE1(I,6)

      S21=STRESSNODE2(I,1)
      S22=STRESSNODE2(I,2)
      S23=STRESSNODE2(I,3)
      S24=STRESSNODE2(I,4)
      S25=STRESSNODE2(I,5)
      S26=STRESSNODE2(I,6)

      S31=STRESSNODE3(I,1)
      S32=STRESSNODE3(I,2)
      S33=STRESSNODE3(I,3)
      S34=STRESSNODE3(I,4)
      S35=STRESSNODE3(I,5)
      S36=STRESSNODE3(I,6)

      S41=STRESSNODE4(I,1)
      S42=STRESSNODE4(I,2)
      S43=STRESSNODE4(I,3)
      S44=STRESSNODE4(I,4)
      S45=STRESSNODE4(I,5)
      S46=STRESSNODE4(I,6)

      S51=STRESSNODE5(I,1)
```

```
      S52=STRESSNODE5(I,2)
      S53=STRESSNODE5(I,3)
      S54=STRESSNODE5(I,4)
      S55=STRESSNODE5(I,5)
      S56=STRESSNODE5(I,6)

C
C CALCULATION OF THE VON MISES STRESSES FOR EACH OF
C THE THE 5 LOAD CASES. THIS CALCULATION CORRESPONDS
C TO ONLY ONE NODE.
C


      VM1=SQRT(((S11-S12)**2+(S12-S13)**2+(S13-S11)**2
     ++6*((S14**2)+(S15**2)+(S16**2)))/2)

      VM2=SQRT(((S21-S22)**2+(S22-S23)**2+(S23-S21)**2
     ++6*((S24**2)+(S25**2)+(S26**2)))/2)

      VM3=SQRT(((S31-S32)**2+(S32-S33)**2+(S33-S31)**2
     ++6*((S34**2)+(S35**2)+(S36**2)))/2)

      VM4=SQRT(((S41-S42)**2+(S42-S43)**2+(S43-S41)**2
     ++6*((S44**2)+(S45**2)+(S46**2)))/2)

      VM5=SQRT(((S51-S52)**2+(S52-S53)**2+(S53-S51)**2
     ++6*((S54**2)+(S55**2)+(S56**2)))/2)


C
C COMPARISON TO FIND MAXIMUM VON MISES VALUE FOR NODE.
C

      KTEMP=1
      TEMP=VM1

      IF(ABS(VM2).GT.ABS(TEMP))THEN
      TEMP=VM2
      KTEMP=2
      ENDIF

      IF(ABS(VM3).GT.ABS(TEMP))THEN
      TEMP=VM3
      KTEMP=3
      ENDIF

      IF(ABS(VM4).GT.ABS(TEMP))THEN
      TEMP=VM4
      KTEMP=4
      ENDIF

      IF(ABS(VM5).GT.ABS(TEMP))THEN
      TEMP=VM5
      KTEMP=5
      ENDIF


C
C PUTTING NEW STRESS VALUES THAT CORRESPOND TO THE
C HIGHEST VON MISES STRESS IN THE STRESSNEW ARRAY.
```

```
C
      GO TO(621,622,623,624,625)KTEMP

  621 CONTINUE

      STRESSNEW(I,1)=S11
      STRESSNEW(I,2)=S12
      STRESSNEW(I,3)=S13
      STRESSNEW(I,4)=S14
      STRESSNEW(I,5)=S15
      STRESSNEW(I,6)=S16

      GO TO 626

  622 CONTINUE

      STRESSNEW(I,1)=S21
      STRESSNEW(I,2)=S22
      STRESSNEW(I,3)=S23
      STRESSNEW(I,4)=S24
      STRESSNEW(I,5)=S25
      STRESSNEW(I,6)=S26

      GO TO 626

  623 CONTINUE

      STRESSNEW(I,1)=S31
      STRESSNEW(I,2)=S32
      STRESSNEW(I,3)=S33
      STRESSNEW(I,4)=S34
      STRESSNEW(I,5)=S35
      STRESSNEW(I,6)=S36

      GO TO 626

  624 CONTINUE

      STRESSNEW(I,1)=S41
      STRESSNEW(I,2)=S42
      STRESSNEW(I,3)=S43
      STRESSNEW(I,4)=S44
      STRESSNEW(I,5)=S45
      STRESSNEW(I,6)=S46

      GO TO 626

  625 CONTINUE

      STRESSNEW(I,1)=S51
      STRESSNEW(I,2)=S52
      STRESSNEW(I,3)=S53
      STRESSNEW(I,4)=S54
      STRESSNEW(I,5)=S55
      STRESSNEW(I,6)=S56

  626 CONTINUE
  600 CONTINUE
```

```
C
C WRITING BACK OUT TO FOR030.DAT
C

      OPEN(UNIT=30,STATUS='NEW')

      DO 700 I=1,NUMEL

      WRITE(IO,720)IELNO(I),1,IEL(IELNO(I)),6
  720 FORMAT(7X,I3,9X,I1,8X,I2,9X,I1)

      DO 710 J=1,IEL(IELNO(I))

      WRITE(IO,730)(STRESSNEW(ICON(IELNO(I),J),J1),J1=1,6)
  730 FORMAT(1X,6(E12.5,1X))

  710 CONTINUE
  700 CONTINUE

      WRITE(IO,*)'   -1'

      CLOSE(UNIT=30)

      STOP
      END
```

RESTRAINT CREATION code.

```
C234567
CCCCCCCCCCCCCCCCCCCCCCCCCCCCCCCCCCCCCCCCCCCCCCCCCCCCCCCCCCCCCCCCCC
C
C  THE PURPOSE OF THIS PROGRAM IS TO SCAN THE NODE
C  NODE COORDINATES FOR THOSE THAT HAVE VALUES
C  ON THE RESTRAINT PLANES. THESE NODES WILL THEN BE
C  STORED AND THEIR VALUES WILL BE ASSOCIATED WITH
C  THE APPROPRIATE SUPPORT RESTRAINT CONDITION
C  NEEDED FOR USE IN THE SUPERB ANALYZER.
C
CCCCCCCCCCCCCCCCCCCCCCCCCCCCCCCCCCCCCCCCCCCCCCCCCCCCCCCCCCCCCCCCCC
C
C
C
C DEFINING THE ARRAYS TO STORE THE COORDINATES AND
C DEFINED RESTRAINTS
C
      DIMENSION  XC(5000),YC(5000),ZC(5000),IREST(5000,3)
C
C OPENING THE COORDINATE FILE
C
      OPEN(UNIT=35,STATUS='OLD')

C
C USING A LOOP TO READ THE NODAL COORDINATES
C
      DO 100 I=1,5000

      READ(35,*)NO,XC(I),YC(I),ZC(I),J
      IF(NO.EQ.-1)GO TO 101
      N1=NO

  100 CONTINUE
  101 CONTINUE

C
C CHECKING EACH NODAL COORDINATE TO SEE IF ITS
C VALUE IS ON ONE OF THE RESTRAINT PLANES
C
      DO 200 I1=1,N1

      IF(XC(I1).GE.(25.531))IREST(I1,1)=1
      IF(XC(I1).GE.(25.531))IREST(I1,2)=2
      IF(XC(I1).GE.(25.531))IREST(I1,3)=3
      IF(YC(I1).LE.(-3.312))IREST(I1,2)=2
      IF(YC(I1).GE.(17.9))IREST(I1,1)=1
      IF(YC(I1).GE.(17.9))IREST(I1,2)=2
      IF(YC(I1).GE.(17.9))IREST(I1,3)=3
      IF(ZC(I1).GE.(6.68))IREST(I1,3)=3

  200 CONTINUE

C
C OPENING FILE FOR SUPPORT DATA TO BE WRITTEN
C
      OPEN(UNIT=36,STATUS='NEW')

      J1=0
      J2=0
      J3=0
```

```
      WRITE(36,*)'SUPPORTS'

      DO 300 I2=1,N1

C
C CALCULATING THE NUMBER OF TIMES EACH RESTRAINT DIRECTION
C IS IDENTIFIED
C
      IF(IREST(I2,1).NE.0.0)J1=J1+1
      IF(IREST(I2,2).NE.0.0)J2=J2+1
      IF(IREST(I2,3).NE.0.0)J3=J3+1

C
C CREATING SUPPORTS FOR THE SUPERB INPUT FILE
C BASED ON THE CALCULATED RESTRAINT NODES
C
      IF(IREST(I2,1).NE.(0.0))WRITE(36,*)I2,IREST(I2,1)
      IF(IREST(I2,2).NE.(0.0))WRITE(36,*)I2,IREST(I2,2)
      IF(IREST(I2,3).NE.(0.0))WRITE(36,*)I2,IREST(I2,3)

  300 CONTINUE
      WRITE(36,*)' X-RESTRAINTS=  ',J1
      WRITE(36,*)' Y-RESTRAINTS=  ',J2
      WRITE(36,*)' Z-RESTRAINTS=  ',J3
      J4=J1+J2+J3
      WRITE(36,*)' TOT. REST. =   ',J4



      CLOSE(UNIT=36)
      STOP
      END
```

Appendix C

Sample Calculations

This section presents the calculations made to arrive at the values shown in Chapter 8. There were two major calculations done, a deflection calculation and a bending stress calculation. All of the calculations done were based on standard beam theory and/or the principle of superposition.

Before doing any calculations, it had to be decided what type of calculation would represent the draftsill best in such a way that a hand calculation could be done with some confidence. It was decided that load case 4 (Carbody Lift) would represent the draftsill as a beam and as such allow it to take on beam theory calculations. The following diagrams show the procedure used and the results obtained for the individual calculations done.

DEFLECTION CALCULATIONS

BEAM MODEL

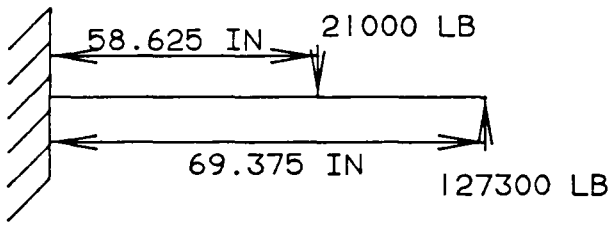

USING SUPERPOSITION

BEAM A

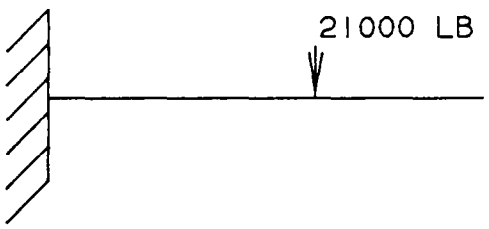

BEAM B

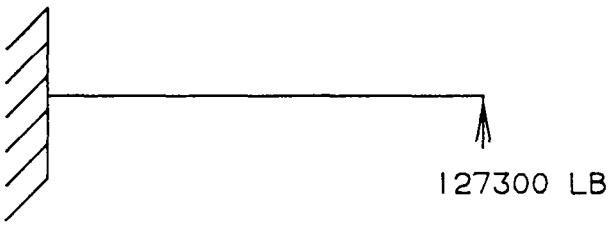

CALCULATIONS FOR BEAM A (AT END OF BEAM)

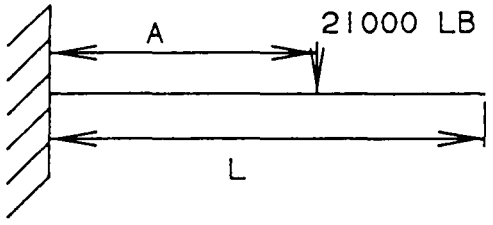

$$YMAX_A = \frac{FA^2 (A-3L)}{6EI}$$

$$= \frac{(21000)(58.625)^2}{6(30E6)(679.97)} \; X$$

$$(58.625-3(69.375))$$

$$= -0.08816 \text{ IN.}$$

CALCULATIONS FOR BEAM B (AT END OF BEAM)

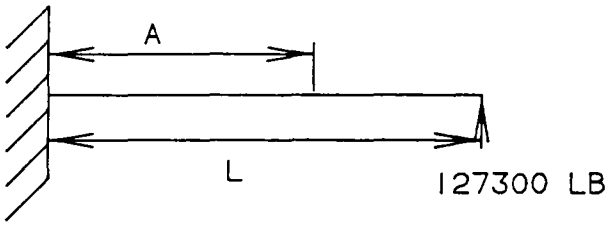

$$YMAX_B = \frac{FL^3}{3EI}$$

$$= \frac{(127300)(69.375)^3}{3(30E6)(679.97)}$$

$$= 0.6945 \text{ IN.}$$

$$YTOTAL = YMAX_A + YMAX_B$$

$$= -0.08816 + 0.6945$$

$$= 0.606 \text{ IN.}$$

APPROXIMATE DEFLECTION FROM ORIGINAL MODEL OUTPUT = 0.4 IN.

STRESS CALCULATIONS

BEAM MODEL

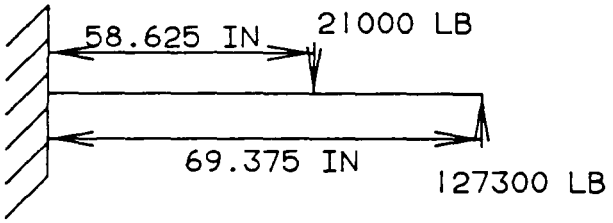

FREE BODY DIAGRAM

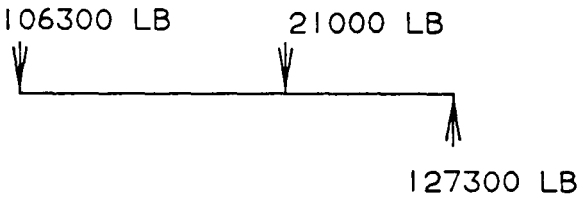

SHEAR DIAGRAM

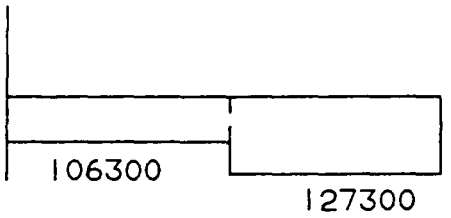

MOMENT DIAGRAM

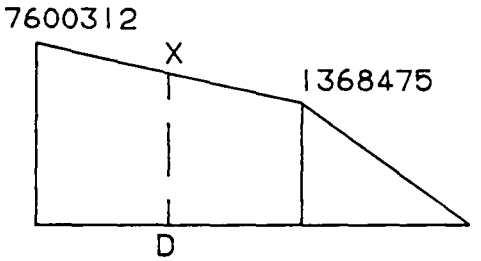

LOCATED AT 25.5 INCHES ON DRAFTSILL

INTERPOLATING TO FIND THE VALUE OF X FROM THE MOMENT DIAGRAM

$$\frac{7600312-X}{0-25.5} = \frac{7600312-1368475}{0-58.625}$$

X = 4886367.2 LB IN

NOW APPLYING THE BENDING STRESS EQUATION

$$\text{BENDING STRESS} = \frac{M\ Y}{I}$$

WHERE: Y-OUTTER FIBER DISTANCE

I-MOMENT OF INERTIA

M-MOMENT AT DISTANCE OF 25.5

$$\text{BENDING STRESS} = \frac{(488636.2)(7.08)}{(679.97)}$$

BENDING
STRESS = 50877 PSI

FROM DATA OF ORIGINAL MODEL

BENDING
STRESS = 45-47000 PSI

NOTE HERE THAT BOTH APPROXIMATIONS ARE IN GOOD AGREEMENT

The vita has been removed from the scanned document